UNIVERSITÀ DEGLI STUDI DI PADOVA
FACOLTÀ DI INGEGNERIA
—
DIPARTIMENTO DI INGEGNERIA DELL'INFORMAZIONE
—
TESI DI LAUREA SPECIALISTICA IN BIOINGEGNERIA

CEREBRAL BLOOD FLOW ESTIMATION FROM ARTERIAL SPIN LABELING MRI WITH LOOK-LOCKER READOUT: A BAYESIAN APPROACH

RELATORE: CH.MA PROF.SSA ALESSANDRA BERTOLDO
CORRELATORE: ING. MARCO CASTELLARO

LAUREANDO: MARCO BATTISTON

ANNO ACCADEMICO 2012-2013

Contents

Chapter 1

Introduction

1.1 Brain perfusion and hemodynamic parameters

Perfusion refers to the delivery of oxygen and nutrients to a capillary bed in the tissue by means of blood flow and is one of the most fundamental physiological process. Abnormalities or disruption in this process can have heavy effects, especially in brain which is a particulary highly perfused organ, receiving large portion of cardiac output (about 20% under normal conditions [1]). Adequate levels of cerebral perfusion are therefore essential to brain's functioning, making perfusion measurament an important tool in the assesment of brain tissue's health and activity. Infact many pathological conditions (including stroke, brain tumor, neurodegenerative diseases and epilepsy) are associated with disorders of perfusion whose accurate evaluation can provide useful diagnostic informations and aid the monitoring of treatment for some of those pathologies. Perfusion also serves as biomarker for a wider range of physiological functions due to the close coupling (whose precise mechanisms are still not completely understood) between tissue blood supply and glucose metabolism, which allows regional brain activity to be assessed through measurements of cerebral perfusion.

Perfusion is a complicated phenomenon that can be characterized by numerous parameters, each one sensitive to different aspects of the perfusion state of tissue (see [**?**] for a complete revision).

Cerebral blood flow

Cerebral blood flow (**CBF**) represents the most common measure of

perfusion state of brain. Adoptiong a general notation, it is given by:

$$P = \frac{F}{W} = CBF$$

where F is the blood flow rate in milliliters of blood per minute $\left[\frac{mL}{min}\right]$, W is the tissue mass in $10^2 g$ $[100g]$, and P is the quantity "perfusion", called CBF in brain context. Thus CBF is the volume of arterial blood delivered to 100g of tissue per minute, with $\left[\frac{mL}{100g\,min}\right]$ as nominal unit. A typical value is $CBF = 60\frac{mL}{100g\,min}$ for gray matter, and $CBF = 20\frac{mL}{100g\,min}$ for white matter.

In imaging applications, the most powerful way to accomplish perfusion quantfication, it is convenient to express CBF as flow delivered to a unit volume of tissue rather than a unit mass of tissue. With these techinques infact a signal is measured for a particolar volume, the imaging voxel, and the actual mass of tissue within that volume is not known, so it easier define CBF in terms of a volume of tissue. Always using a general notiation, we have:

$$f = \rho P = \rho \frac{F}{W}$$

where ρ is the tissue density in $\frac{10^2 g}{mL}$, and f, called sometimes perfusion rate, is expressed in milliliters of blood per millilter of tissue per minute (or second) $\left[\frac{mL}{mL\,min}\right]$($\left[\frac{mL}{mL\,s}\right]$). This voxel-based definition of CBF is the natural choice for imaged-based perfusion measurament and has the inverse time dimension as a rate costant. This dimensionality shows the primary role CBF plays in determining the delivery of metabolic substrate and the clearance of metabolic products: the rate of delivery to the tissue of any substrate is simply fC_b, where $C_b$is the arterial blood concentration of the substrate [2]. To express f in common CBF definition terms, it must be scaled by the local density of the voxel, remembering that the density of brain is close to $1\frac{g}{mL}$:

$$\frac{mL}{mL\,s} = 1\frac{g}{mL}\frac{mL}{100g\,min} = 1\frac{g}{mL}\frac{mL}{100g\,60s} = \frac{1}{6000}\frac{mL}{mL\,s} \Longrightarrow f = \frac{1}{6000}CBF \tag{1.1}$$

where the corretcting factor (including ρ and having its unit) from $\frac{mL}{100g\,min}$ to $\frac{mL}{mL\,s}$ is explicitated. Accepting a density value of $1\frac{g}{mL}$ as a good approximation in brain tissue, a typical value for human is $0.6\frac{mL}{mL\,min}$ or $0.01\frac{mL}{mL\,s}$. Beyond this amplitude correction, changing the localization of the process (voxel volume instead of mass of tissue) make the definition slightly different from the more usual because the quantity we now measure is the average flow to the voxel which is afflicted to

partial volume effects. That is, the average perfusion in the voxel is accurately measured, but the true flow per gram of tissue is unknown and dipends on which types of tissues are included in the voxel. However in this thesis both CBF and f refers the same perfusion quantity, keeping in mind the difference in unit and the consequent conversion equation (1.1).

Cerebral blood volume

In general blood volume V is defined as the subvolume occupied by blood whithin a volume of interest or in 100g of tissue. With the former definitions, the volume of interest is often chosen as the volume of a voxel V_0, allowing the blood volume to be expressed as a dimensionless factor q, called **CBV** in brain context

$$q = \frac{V}{V_0} = CBV$$

where V is the blood volume and V_0 is the voxel volume, both in $[mL]$. The cerebral blood volume is thus a dimensionless number (millilters of blood vessel per milliliters of tissue) that quantify the fraction of tissue volume occupied by blood vessels, and a typical value for the brain is CBV = 0.04 $\frac{mL}{mL}$. It can be furthermore subdivided in arterial (**aBV**), capillaries and venous volumes.

Mean transit time

Mean transit time (**MTT**) refers to the average time requires to a particle to pass through the tissue. It could be a few seconds if the particle remains in the vasculature, or much longer if the particles freely diffuse out of the capillary bed and fill the tissue space. A fundamental relation between MTT, CBV and CBF is described by central volume theorem:

$$MTT = \frac{V}{F} = \frac{CBV}{\rho CBF} = \frac{CBV}{f}$$

where MTT is in $[min]$ except in the last form where is in $[s]$.

1.1.1 The meaning of cerebral blood flow

Cerebral blood flow is often confused with blood velocity. Although CBF and blood velocity, together with CBV are all important aspects of perfusion state of tissue, they are distinct physiological quantities. Cerebral blood flow is mainly associated with the delivery of arterial blood to the tissue element and has no fixed relationship with either

the amount of blood present in the tissue volume (CBV) or the motion of blood within the tissue element (blood velocity). An increase in CBF (for example during brain activation) could occour through a number of different changes in blood volume or blood velocity. The only way to estabilish a connection between CBV and CBF is through the central volume principle: it is transit time, rather than blood velocity, that is directly connected to CBV and CBF.

It is difficult to make reliable measurament of CBF by looking at blood within a tissue element. An element of tissue, infact, could contain in larger arteries arterial blood that is just passing through, destinated for a capillary bed in another location, or venous blood passing through as it drains another tissue element. Also a measure of motion of the blood does not necessarly reflect CBF, the flow of arterial blood into capillary beds. For example, an element of tissue could have no change in CBF but shows increased blood motion if CBF increases in a distal tissue element with a corresponding increase in speed of the arteries and draining veins that pass through the first element.

The defining characteristic of CBF is not blood motion within the tissue element but rather delivery of arterial blood to the capillary bed [**?**]. For this reason, the most robust approaches to quantifying CBF are based on measuring the rate of delivery of an agent carried to the tissue by arterial blood flow. This is the case of Arterial Spin Labeling (ASL) technique which has the appealing property of measure perfusion in a completely non invasive way.

1.2 Goal and outline of the thesis

In this thesis approaches to CBF estimation from Arterial Spin Labeling data has been studied. In particular the work presented here can be summarized in two main steps:

- the standard model for ASL data, also knwon as Buxton model [3], was used to estimate CBF from datasets available. A new formulation was given to the estimation procedure typically adopted when parametric models,as standard model, are used in CBF estimation in which several assumption on parameters must be taken. Here a bayesian approach to soften this assumptions was proposed

- an improved version of standard model was considered to overcome a typical limitation of such model. In particular, a two component model [4] able to deal with the so called vascular artifacts

in the measured perfusion signal was proposed.

This thesis is structured as follows. In chapter 2 basic principles of ASL is given, along with some information about the particular ASL version used in this study. In chapter 3 fundamentals of ASL modeling, giving particular care to standard model, are reviwed. In chapter 4 data set used in this study is briefly described and methods apllied to data are presented. In chapter 5 results of the methods described in the previous chapter are shown. Finally, chapter 6 is dedicated to discuss some of the results achieved and problems encountered.

Chapter 2

Arterial Spin Labeling to measure perfusion

In this chapter Arterial Spin Labeling (ASL) technique is presented. This method can measure perfusion inside the brain and also in several other organs. The basic idea of ASL experiment, generalities and avandtages over other techniques are reviewed. ASL practical implementation are also given, with particular regard to those methods used to generate data analyzed in this work.

2.1 Basic principles of Arterial Spin Labeling

Arterial spin labeling (ASL, or arterial spin tagging AST) is a completely noninvasive technique that provides quantitative measures of cerebral blod flow (CBF). The general principle of ASL is to use protons of water molecules in the inflowing blood as an endogenous tracer to probe the blood supply to tissue. The tracer employed is constituted by a magnetic labeling of water molecules. This labeling is accomplish by manipulating blood water magnetization which is inverted at the location of the larger brain-feeding arteries (such as the internal carotid artery). The magnetization of those protons can serve as tracer for perfusion process since water transport across the blood brain barrier is relatively unrestricted, and water protons diffuses (although not as a freely diffusible tracer) from capillary to tissue with their labeling, allowing CBF to be measured.

In a typical ASL experiment, a radiofrequency (RF) inversion pulse is applied to flip the magnetization of arterial blood water before imaging region (a single slice or a volume) is reached. The water molecules, carrying the labeled magnetization, flow into each tissue element in

proportion to the local CBF. After a sufficient delay (typically denominated inversion time, TI) to allow the tagged blood to reach the region of interest, acquisition is made, creating the so-called tag image. Then the experiment is repeated without labeling the arterial blood to create the control image, in which no information about inflowing blood is observable. If the tag and control images are carefully adjusted so that the signal from the static spins is the same in both, then the difference of the two images (control and tag) gives rise to a signal (a magnetization difference signal Δ) proportional to the amount of blood delivered to each voxel, nothing else than the local CBF.

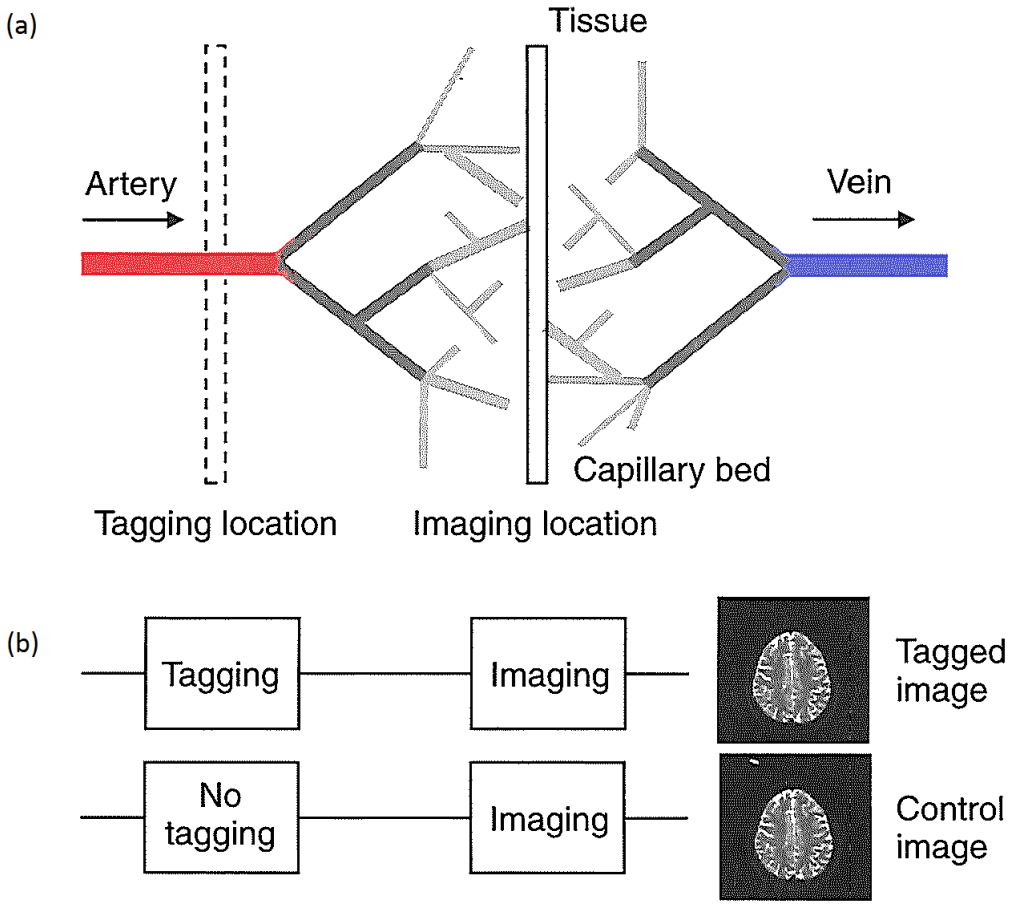

Figure 2.1: in panel (a) a schematic representation of the phenomenon that ASL measures is shown. Water in arterial blood is deliverd to tissue capillary bed by arterial flow, here it is exchanged with tissue water and then drained by venous flow. This process is magnetically detected by labeling arterial water at a location proximal to the tissue to image, and isolated by a proper image subtraction. The ASL protocol, based on tag and control subtraction, is conceptually shown in panel (b).

In each image (tag and control) the voxel signal is proportional to the longitudinal magnetization of the voxel at the time when image was acquired. If no arterial blood is delivered, the signal measured in tag and control images should be the same, and so difference image would be zero. But if arterial blood is delivered to a voxel, it will carry an inverted magnetization in the tag image and a fully relaxed magnetization in the control image, and so signal of blood will not cancel in the subtraction.

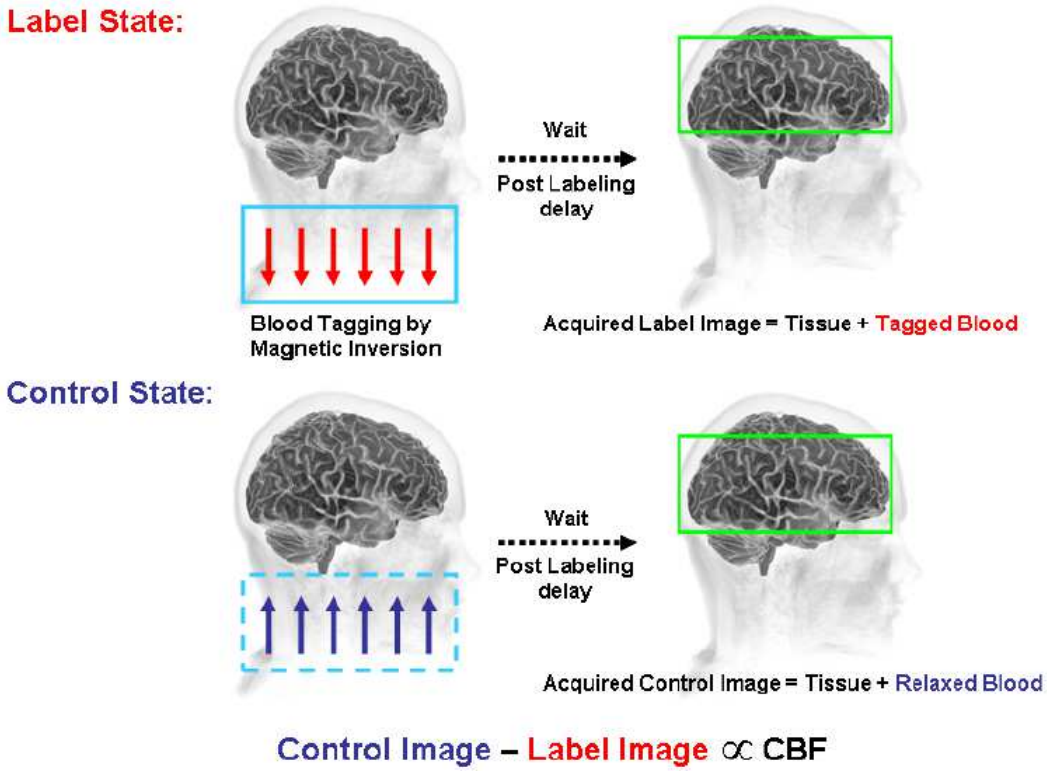

Figure 2.2: perfusion-weighted property of ASL images is the result of subtraction between tag (label) images and control images. The different magnetic state having the blood that reaches the tissue gives rise to a coeherent signal difference proportional to CBF, if it is holden the main assumption that magnetization of tissue (often named static spin magnetization) would remain the same in the two state of ASL experiment.

The major advantage of ASL comparing to other techniques used to measure CBF resides in its complete non invasive nature since it uses magnetically labeled water as tracer instead of requiring injection into blood stream of exogenous contrast agent or inalation of radioactive tracer (i.e. radioactive xenon studies). This confers to the technique a great versatility, making ASL applicable to human studies without

any restriction regarding age (even pediatric population) or pathological conditions (patient with kidney faliure can not undergo typical bouls tracking perfusion studies) of subjects examined, and also to measure perfusion in other tissues than brain. Moreover ASL opens the possibility of repeated perfusion measurements, that were not possible with older techniques based on the use of potentials harmful, costly tracer, including the widespread dynamic susceptibility contrast (DSC) MRI. These serial measurements could be useful in a number of applications, for example following perfusion changes after stroke or drug treatment, and for perfusion-based functional MRI.

Finally ASL technique traces a phenomenon directly related to perfusion. Especially, it provides a set of raw data, already showing a strong perfusion-weightening, from which quantitative measure of perfusion in absolute unit of $[\frac{mL}{100g\,min}]$ can be obtained.

The big issue of ASL is intrinsically connected to process that it aims to measure, and in the way it is intended to be measured. The signal change associated with tagged blood is small. It can be roughly estimated by considering how much tag water can enter the brain during the experiment. If f denoted local CBF in untis of $[\mathrm{s}^{-1}]$ (see section 1.1, f is simply CBF measured in mL of blood per mL of tissue per second), and the volume of voxel is V (mL), then the total rate of arterial flow into the voxel is fV (measured in $\frac{mL}{s}$), and the volume of arterial blood delivered during TI (time at which an ASL image is taken) is $fVTI$. Therefore the fraction of voxel volume that is replaced with the incoming arterial blood during the interval TI is $\frac{fVTI}{V} = fTI$. Since typical value for f and TI are respectively $0.01s^{-1}$ and $1s$, it results that the deliverd volume of arterial water is only about 1-2% of the volume of the voxel [**?**]. Moreover the magnetic label decay (with proprer rate costant) along time, making the measurements feasible only in a limited temporal extent.

Due to the relative small magnitude of ASL signal, every other factor potentially liable to cause even restreined signal variation must be avoided or compensated for. A common source of errors is the magnetization transfer (MT) effect (figure 2.3), which can cause signal loss substantially larger than the perfusion induced signal change, making fundamental adequate equalization of their effects between tagged and control images.

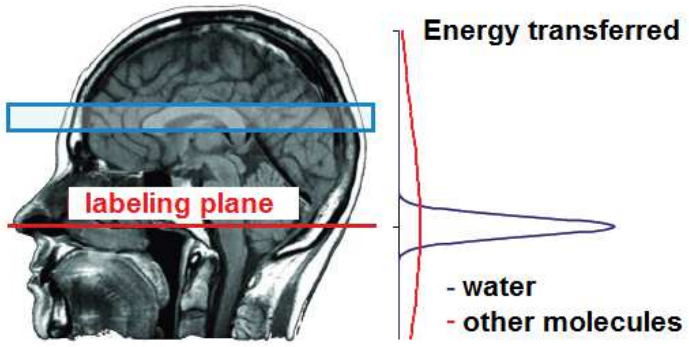

Figure 2.3: water protons in blood have a narrow frequency spectrum (plotted in blue). Frequency spectrum of macromolecules in brain tissue is much broader. Thus labeling pulses affect macromeluclar spin even when they are located at different position, and this magnetization can be trasnferred to the free water signal. If the total power of RF pulses in labell image differs from the control image, a net difference in magnetization will be created, and a subtraction errors will be shown in ASL images.

The small signal changes also makes perfusion very sensitive to random noise, necessitating signal averaging to increase signal-to-noise ratio (SNR). Tipically 20 to 40 pairs of subtracted control and label images are required to be averaged to get the desired SNR in the perfusion weighted maps. This inevitably lenghtening the acquisition time, to allow multiple experiments repetitions.

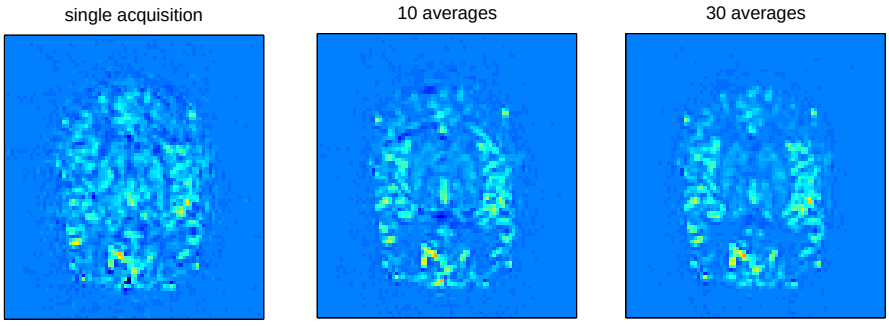

Figure 2.4: SNR improvment following images averaging is clearly shown in figure. To reach an adequate SNR level thus ASL experiment has to be repeated more times, lengthening the total scan duration.

Arterial spin labeling is based on a quite simple idea, but in practice its execution requires to consider several sources of systematic error. Dealing with these technical difficulties is a critical aspects of

ASL methods, because any uncontrolled confounding effect may contribuite to loose the perfusion weightening of the small signal that is aimed to measure.

2.2 Implementing ASL experiment

Pratical implementation of ASL idea has to be able of bracket in a unique pulse sequence the exigence of generate tracer, i.e. magnetically label the arterial blood water molecules, and the capability of detect it effectively despite its intrinsically small amplitude. The whole has to be implemented avoding any contamination of the former request onto the latter and ensuring the right timing between them, because the magnetic label acting as tracer progressively vanishes with time (with a scale time set by longitudinal relaxation time T_1 of bloodT_{1b}, and tissue T_{1t}, respectively $1.6s$ and $1.3s$ at $3T$), but also need a time delay before imaging to reach tissue of interest. Answering to this double claim, straight consequence of ASL idea, in a low SNR signal context, is the reason why ASL is a technique challenging to implement, that demands advanced technical solution to face with a large set of potential degrading factors.

A generic ASL experiment can be thought as composed of three phase (figure 2.5):

1. **labeling**: in which bolus of labeled blood to deliver to tissue is created by inverting magnetization of spins in proton waters

2. **post-labeling**: (optional) in which a sequence of pulses is apllied to improve SNR or to facilitate the subsequent data quantification step

3. **readout**: in which the actual image (control or label) is acquired

The are a variety of techniques both for spin preparation and imaging acquisition. One important feature of the ASL sequence is that the three components are indipendent each from the others. This fact allows them to be combined as desidered in relation to the specific application. In the following sections the labeling part, the imaging part are discussed, with particular attention to methods used to acquired data considered in this study.

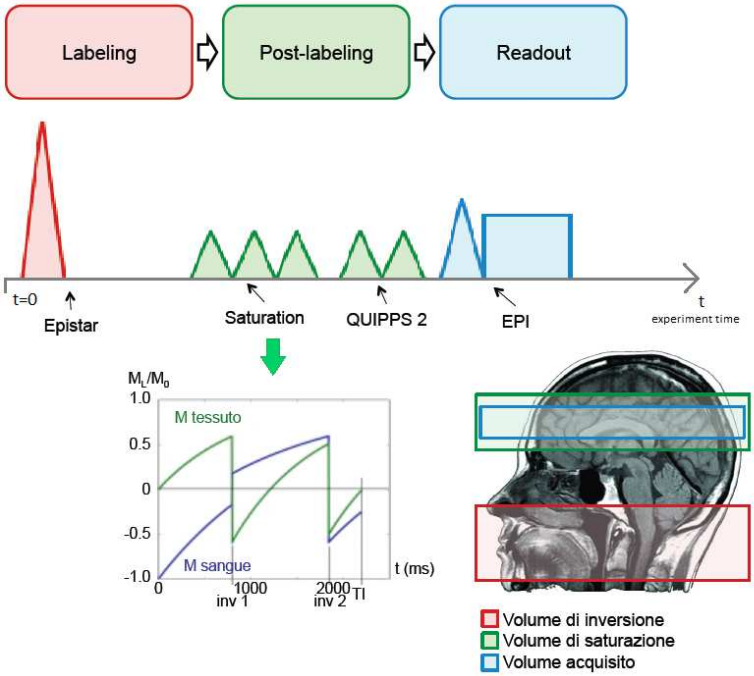

Figure 2.5: a schematic example of an ASL sequence complete of its three phase is reported. The inflowing blood in a thick slab under brain is labeled into different magnetic state during spin preparation (see PASL section 2.2.1), while the actual imaging of the brain occour during image acquisition. In the middle, examples of post-labeling pulses are shown. **Background suppression** (termed as saturation in figure) is a series of inversion pulses carefully designed to reduce the contribution of static spins in acquired image (and consequentely to beat down potential subtraction errorrs deriving from different magnetization of this group of spin in label and control images) [5]. **QUIPPS2** is a protocol that permits to experimental fixing parameters related to duration or timing of labeld blood bolus, otherwise unknown [6].

2.2.1 Labeling of arterial blood

There is a huge variety of methods whereby spins of arterial blood water can be inverted to obtain ASL images. A detailed revision of those methods outsteps the goal of this work, however in the following particular care is given only to methods used in this study.

Conceptually there is two main approaches to label arterial blood water, commonly denoted as pulsed arterial spin labeling (PASL), and continuous arterial spin labeling (CASL). With CASL arterial blood spins are inverted for a certain period as they pass through a plan fixed to a designed location along axial direction, using a long duration ($2-4s$) RF

pulses and availing flow-driven adiabatic inversion principle. Whereas in PASL, instead of a temporal long RF pulse, a spatially confined labeling pulse (of duration $10 - 50ms$) is employed over a large region, as results a large volume of spin is inverted almost simultaneously. Thus in pulsed experiment, the tag is performed in sapace than in time, and this has a straightforward impact on data quantificatiuon, as the duration of the labeld blood bolus delivered to each voxel is absolutely unknown.

In the last years, continuous arterial spin labeling data has been increasingly acquired using a pulsed version of continuous labeling, called pseudo-continuous arterial spin labeling (pCASL) [7]. This technque simulate a CASL protocol by using train of RF pulses and gradient waveform adequately shaped in order to overcome the limitation connected to practical realization of the typical CASL scheme.

In the following sections, pCASL scheme and the specific PASL version used to tag blood in the dataset available are described.

Pulsed arterial spin labeling

Many different approaches have been proposed for PASL, although in the end all implementations create, using a single inversion RF pulse, two images in which arterial blood water has an opposite magnetization state. The differences among these methods are mainly the location of the tagged region and the magnetic state of the tagged spins for the control and label images. The two best-known PASL sequences are:

- flow-sensitive alternating inversion recovery (**FAIR**), which uses slice-selective inversion of the imaging slices as label condition and a non-selective inversion pulse of whole imaging region as control condition

- signal targeting with alternating radiofrequency (**STAR**), which uses a slice selective inversion below the imaging slices as label condition, and no RF pulses for the control image.

Advantages of PASL are the high labeling efficiency (i.e. the fraction of maximum magnetization that is actually inverted by labeling scheme, denoted by the dimensionless number α) and the lower specific absiorption rate (SAR) due to the short RF-pulses. Disadvantages are the potentially lower SNR of the perfusion-weighted images and additional difficulties in quantification, as previously hinted, because labeling is

performed spatially, thereby incorporating a dependency on tagging region arterial tree structure into the duration of bolus parameters, rising in an unknown label duration (τ).

In STAR scheme label image is obtained inverting spins within a thick slab (about $10cm$) proximal to imaging region. The tagging pulse is a spatially selective inversion pulse, the most used is the hyperbolic secant adiabatic one. In control images no tagging is actually performed, but two $180°$ pulses of half power and at the same location respect that one used in label state are applied (figure 2.6, left). The STAR scheme, in principle, provided an asymmetrical pulse application respect to imaging region, so no correction of MT effect that eventually occour in it is accounted for. However, in the scheme just described the RF power of the labeling inversion pulse is counterbalanced by the two consecutive adiabatic pulses of half RF power of the control phase (figure 2.6, right). The associated induced magnetization transfer effects are identical in both cases, which allows multislice acquisition with good MT effect equalization [8]. Anyhow, MT effects are less prominent in PASL techniques, and major care must be paid to reduce the effects of nonideal profile of the tagging pulse on the imaging region, making necessary the introduction of a sufficient spatial gap form labeling to imaging region.

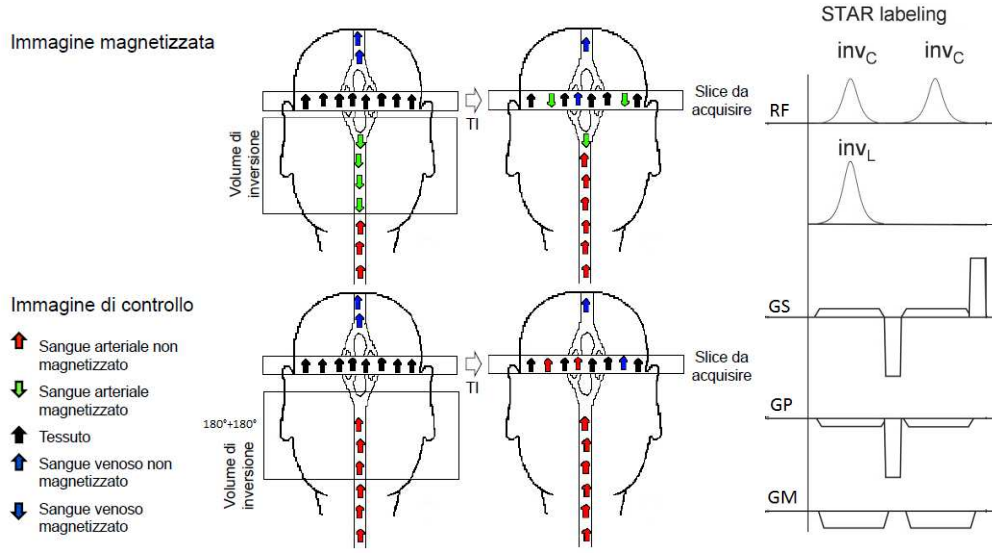

Figure 2.6: conceptual representation of the contributions in imaged slice both for label and control state. From the difference (controlo-label) a positive contribution proprtional to the amount of the inflowing blood can be isolated (left). Example of STAR pulse sequence (right,[8]).

Having a tagged arterial blood that flows into imaging region carrying and inverted magnetization, in STAR experiment the signal from a voxel in labeled image, M_l, is less than control image ones, M_c, (if consistent aamount of blood perfuse it), and thus to have a positive quantity from images subratction as index of labeled blood that has entered into the voxel during inversion time TI , difference signal ΔM has to be defined as:

$$\Delta M = M_c - M_l$$

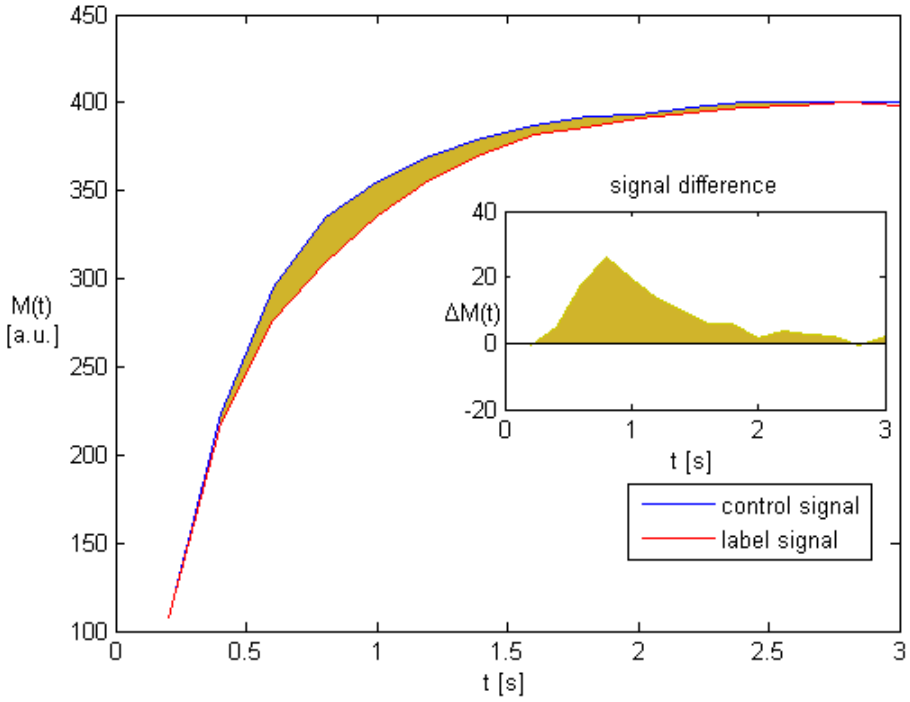

Figure 2.7: example of ASL difference signal Δ in STAR version of pulsed ASL. Signal acquired in label state is perturbated by the inflowing of arterial tagged blood with inverted magnetization. Magnetization in labeled condition does not return to its equilibrium value in the same manner of control condition, originating a signal difference carrying information about CBF. The comparison between the arbirtary scale of the signals (label or control vs. difference) clearly shows the low SNR property of the perfusion weighted ASL measurement.

pseudo continuous arterial spin labeling

Previous studies have demostrated that CASL labeling produces a greater SNR than PASL labeling [7], and also that this theoretical advantage is

reduced by a number of challenges that practical implementation of CASL have to face off. These are inefficiency of labeling, magnetization transfer and limited support for continuous-mode operation on clinical scanners. The last one is surely the most difficult to bypass: the majority of the imagers are optimized for pulsed operation and can not support CASL beacuse of constraints on the RF duty cicle. It means that flow-driven adiabatic inversion, the mechanism producing the labeling, can not be achieved applying constant RF and gradient field. Intuitively, the solution could be found by breaking up the continuous rectangular RF into a train of RF pulses separated by a gap. And actually this is right the basic idea of pCASL.

It has been shown that blood spins can be adiabatically inverted as they pass to a selected plane even using a train of pulsed field excitations, if some conditions on RF pulses sequence and gradients system are met:

1. the train of RF pulses used instead of continuous rectangular RF is prone to cause a number of aliased labeling planes. To limit this effect, appropriated RF pulse shape (Hanning pulse) jointly to a constrain on gradients amplitude has to be considered.

2. the applied gradient should be able to cause the position-dependent phase shift necessary to adiabatic inversion, with an average value between pulses comparable to that used for continuous inversion

3. average RF field between pulses should be comparable to the continuous pulse

If labeling pulses sequence is designed respecting these conditions water blood spins can actually be inverted (*). Control pulses sequence can be achieved by alternating the sign of the RF from pulse to pulse and ensuring that there is zero average gradient between each of them. It permits to have zero average field of RF pulses, but matched magnetization transfer effects between label and control, since the average RF power is the same.

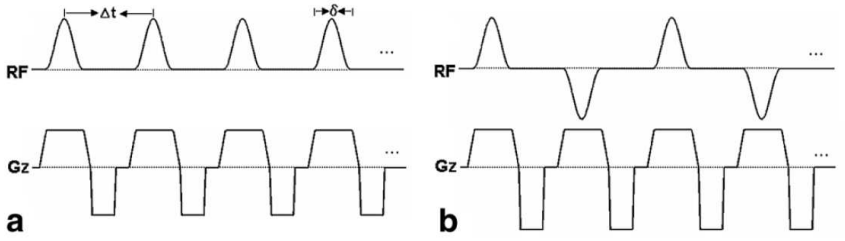

Figure 2.8: pCASL sequence scheme [7]: (a) labeling pulse sequence: Hanning pulse in combination with gradient waveform with maximum strength G_{max} much higher than its average value between two consecutive pulses, G_{ave}, provides great spatial selectivity to aliased planes (condition to met is $\frac{G_{max}}{G_{ave}} \gg \frac{\Delta t}{\delta}$), G_{ave} and B_{1ave} are non null and similar to those used in a hypotetic continuous scheme. (b) control sequence: B_{1ave} and G_{ave} are zero, and magnetization of the blood spin is uninverted, but RF power of the sequence is equal to label sequence one, providing a correction for MT effects.

Pseudo-continuous arterial spin labeling (pCASL) is considered the best method to approach continuous labeling studies because of its appealing properties of provideing high efficiency, multislice capabilities and broad compatibility with existing scanner hardware.

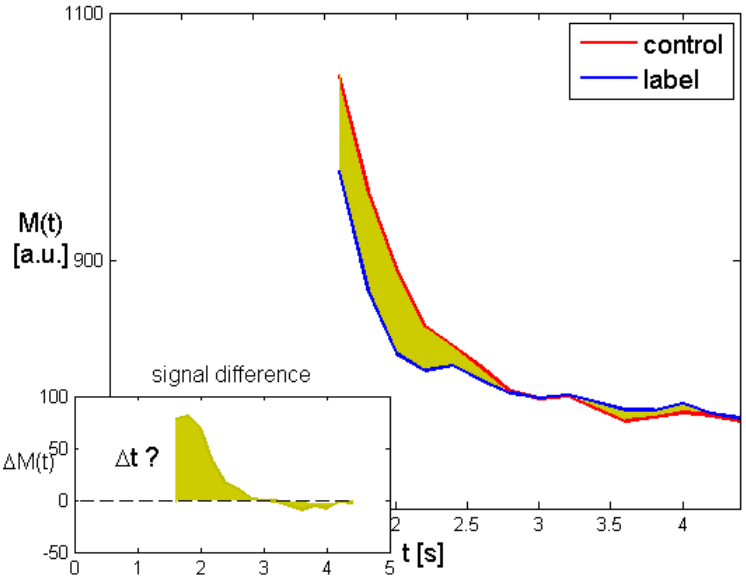

Figure 2.9: pCASL signal derives as PASL form label and control difference (see figure (2.7) for description). Due to long duration of labeling (titpically $1-2s$) no signal is acquired in the early phase of perfusion process, making estimation of the transit delay Δt more difficult because few samples are sensitive to it.

A subtle problem involved in pCASL data is due to the absence of sampling in the early part of the signal, as no imaging pulse can be applied during labeling phase (that in pCASL last longer enough to allow signal rising in tissue). This could entangle qauntification step, especially transit delay Δt estimation, since a portion of model can not fit any data (figure 2.7).

2.2.2 Readout approach for ASL

In principle, any readout sequence can be used for ASL as long as the sequence is predominantly proton density weighted. However,due to the samll amount of the blood signal and to the decayment of labeling before measurement time, delayed on purpose to allow perfusion, an ideal imaging sequence should have high SNR and meantime allow fast acquisition. Single-shot echo planar imaging (EPI) or fast low-angle shot (FLASH) readout sequences are the most commonly used readout protocols when 2D multislice imaging is performed. Recently, 3D acquisition methods (such as GRASE) have gained much attentions since they have inherently higher SNR than multislice sequences and allow blood inflow informations to be acquired exactly at the same moment (no temporal offset is inserted between two consecutive slices acquisition). However, 2D multislice acquisiton is still the most widesprad strategy employed to acquire ASL images.

In a single shot-EPI a rapid series of gradient echoes is generated to cover the k-space in a back and forth scanning pattern, after a single excitation pulse. In figure (2.10) a EPI k-space sampling trajectory and semplified pulse sequence diagram (for a single-shot EPI) are shown.

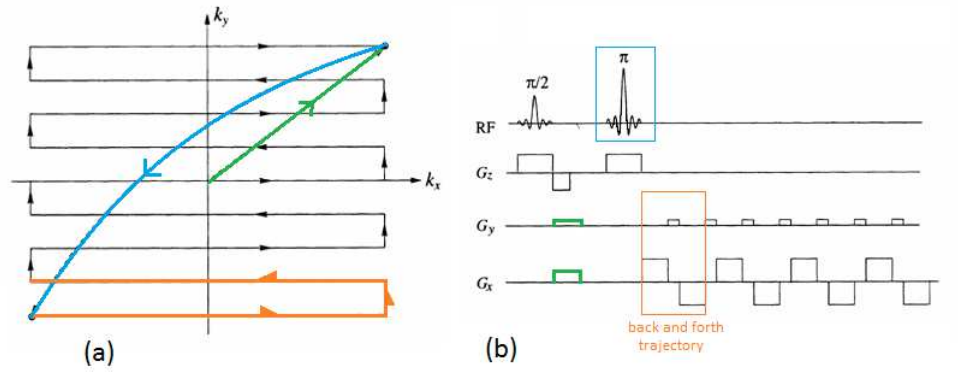

Figure 2.10: single slice EPI pulse sequence (b), and its k-space trajectory (a). Initial positive G_x and G_y gradients and the RF inversion pulse moving the sampling poitn to the bottom-left of the k-space. Then the boxed pulses are repeated $\frac{N}{2}$ times to acquire N lines of k-space in alternate direction. The sign of G_x indicates wheter the trajectory of the straight line along k_x moves from left to right (positive value) or contrarily (negative value). The samll y gradients pulses, called bilps, shift the k-space sampling to a new line in an upper k_y level. The duration of this pulses gives is the rise time of the gradient system.

The intial pulses move the location of k-space sampling to $-k_{max}$ both along x and y axis, and then the repetition of the gradient echo modules produces a back and forth scannig of k-space. Since all of k-space must be filled following a single excitation pulse, the data must be acquired before significant T_2* decay can occour (tipically the acquisition window is limited by those effect to about $100ms$). To confine data acquisition in a tempral window shorter than T_2*, and mantaining at the same time a reasonable spatial resolution (i.e. sampling a large number of line in k-space), strong gradients and rapid switching capabilities are required. The total imaging time infact depends on how quickly the sampling of the k-space grid occour, and its is governed by two properties of the gradients coils used for imaging: the maximum gradient strenght and the slew rate (or in alternative the rise time).

The most common EPI artifacts derive from inhomogeneities in the magnetic fields (static and gradient field both) that results in signal loess and geometrical distortion.

2.3 Modifications of traditional ASL sequence

The inherently low amplitude of ASL signal, due to the relative small amount of blood that reached the tissue in a typical ASL measurement

time, and the aim to measure it in a completely non invasive way make ASL technique implementation very challenging.

In the following two widely used modification of the ASL sequence that aim to optimize data acquisition are presented. The first regards the englobment into the readout block of the Look Locker sampling strategy to allow multi inversion time measurement keeping global experiment duration in a reasonable extent, the second concernes the application of bipolar gradients to suppress signal form nonperfusion blood.

2.3.1 Look Locker readout

Look-Loocker (LL) acquistion scheme is a sequence that was ideated to speed up the longitudinal relaxation time measurement in a typical inversion recovery sequence. The technique consits of applying, after the initial inversion pulse, a series of low flip angle pulses, α_{LL}(typically is $\alpha < 50°$), to sample the longitudinal magnetization during its recovery to equilibrium (see figure 2.11). The signal from each of these pulses is used to create an image using typical readout protocols. Therefore, LL is a signal sampling strategy rather than a real readout protocol, but if used in combination with the last, so forming a LL-like readout, it can produce a very fast T_1 mapping (in about $3s$).

More formally, a series of N_{LL} RF readout pulses, of the same flip angle α_{LL}, are used to sample multiple point with a fixed interexcitation interval TI_2, starting after a delay TI_1 from the initial excitation pulse. The repetitive perturbation accomplished by the readout pulses during recovery drives magnetization to a steady state $M_{0,eff}$, lower than original equilibrium magnetization M_0, through an effective longitudinal relaxation time observed,$T_{1,eff}$, shorter than actual T_1. The real signal evolution, $M_z(t)$, when LL pulses are applied has been derived in [*ref. Look and Locker]. It should show a jagged shape as consequence of consecutive perturbation introduced by low flip angle that progressively beat down by a fraction (α_{LL} dependent) the recovered signal. However approximating M_z time course to be continuous like, it can be described as follows:

$$M_z(t) \approx M_0 - (M_0 + M_{0,eff})\, \mathrm{e}^{-\frac{t}{T_{1,eff}}} \tag{2.1}$$

where the effective steady state magnetization, $M_{0,eff}$, and the effective longitudinal relaxation time, $T_{1,eff}$, defined by LL sequence are given

by:

$$M_{0,eff} = M_{0t}\frac{1-\mathrm{e}^{-\frac{TI_2}{T_1}}}{1-(cos\alpha_{LL})\,\mathrm{e}^{-\frac{TI_2}{T_1}}}$$

$$T_{1,eff} = \frac{1}{\left(\frac{1}{T_1} - \frac{ln(cos\alpha_{LL})}{TI_2}\right)}$$

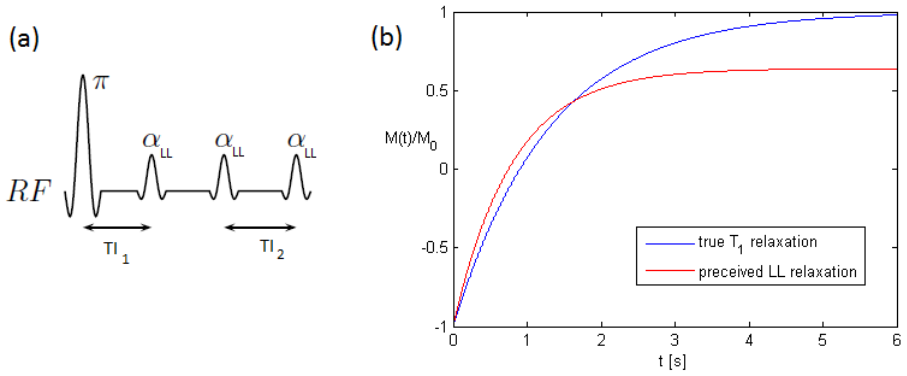

Figure 2.11: schematic Look Locker pulse sequence is drawn in panel (a). After initial $180°$ RF pulse that invert longitudinal magnetization, a series of low flip angle α_{LL} excitation is applied, to sample the recovery of signal multiple times within a unique TR. The effect of the LL scheme on acquired signal is shown in panel (b): a new steady state value is set, and a shorter relaxation time is observed ($\alpha_{LL} = 25°$ and $TI_2 = 0.2s$ are used).

Look Locker sampling strategy has found an important application in ASL experiment. As will be discussed in section 3.5, typical ASL experiment is made up by imaging control and label state at a single time point. But the ability of visualize the whole temporal dynamics of perfusion would be of great advantage, in brief it would help to unmask some confoundifng effects that could angle CBF estimates. Unfortunately sampling the signal evolution after labeling at more point is not feasible with traditional ASL sequences, if the total scan time needs to be kept relatively short. Infact, signal is measured at a one fixed inversion time after magnetic labeling, and beforesequence could be repeated, adopting a new inversion time, a delay of approximatively $3s$ (MTT of water in brain tissue) has to be introduced to allow complete wash out of the labeled blood form the capillary exchange sites, Furthermore, to achieve good SNR several experiment repetitions are necessesary to perform images averaging procedures. As example, let consider 20 averages of an ASL signal sampling just at 3 time points

a with single-shot imaging technique, such EPI. It results in a total measurement time of [9]:

$$\underset{\substack{\downarrow\\ \text{time for}\\ \text{single TI}}}{3s} \times \underset{\substack{\downarrow\\ \text{different}\\ \text{TI point}}}{3} \times \underset{\substack{\downarrow\\ \text{number of}\\ \text{averages}}}{20} \times \underset{\substack{\downarrow\\ \text{control and}\\ \text{label state}}}{2} = 6min$$

Traditional ASL sequences are thus time-consuming and inefficient, since just one single measurement is made within the long TR needers to be used, and any other information is not sampled during this time.

In this context LL sequence provides a great improvement.The combination of LL sampling strategy with any spins preparation scheme allows to sample a series of images after each labeling pulse, making possible the monitoring of the perfusion signal time course with adequate number of temporal samples, within a reasonable total scan time.

2.3.2 Vascular crushing

As it has been shown, ASL techniques produces a series of images which are themselves an undirect measurement of brain perfusion. The main effort in extracting precise measures of perfusion state of the brain from these data is usually performed by mathematical models, which can be formultaed with different degrees of complexity and detail. Several techniques able to improve the perfusion-sensitive nature of the data could be adopted still in the acquisition stage. Improve data quality, i.e. make them more informative, without stressing excessively the modeling step is of crucial importance. However one should keep in mind that ASL suffers of low SNR. Hence the possibility of adopting simpler model (with less parameters) to quantify perfusion, justyfied by a more carefull data acquisition scheme, is a great benefit and helps to achieve a better accuracy in estimates.

Tipically these technical solution are applied between labeling and acquisition scheme. In the following, it will be emphasized the technique of vacular crushing to reduce the so called vascular artifacts.

Vascular artifacts can have substantial effects on quantification of CBF. These are contributions to difference images non perfusion-related, due to tagged blood that at measurament time is still in the vasculature tree. Vascular artifacts are evident particulary in the early acquistions, where blood is supposed to be still in large arteries. Often in the very first acquired images bright spots are clearly visible, which

doubtless attests for tagged blood inflowing in large arteries. These contributions act as confounding effects since they originate from arterial blood that is just flowing into large arteries contained in the voxel, but that is destined to perfuse more distal tissues. A more subtle vascular artifacts are then contributions to signal difference Δ coming from labeled blood situated in small arteries included in the voxel. These tagged blood is actually a perfusion blood for the local tissue (the voxel considered), but at the time of measurement hasn't reached the exchange site yet. Since perfusion are defined as the blood flow rate to capillary bed, this kind of pre-perfusion blood contribution must be considered properly. Vascular artifacts complicate brain perfusion quantification, leading to severe overestimation of CBF. The quantitative determination of perfusion requires correction for those vascular artifacts.

A common way to deal with these artifact is to insert small magnetic field gradients after the spin labeling stage and prior to the readout excitation pulses [10]. The contribution of arterial blood water spins to Δ signal can be reduced if those gradients, called crusher gradients, are used to dephase the signal from spins in arterial blood that is flowing with a velocity greater then a specified vascular crushing velocity: the encoded velocity v_{enc}.

Vascular crushing is tipically performed by applying a bipolar gradient . If bipolar gradient is made up by two lobes of equal duration and magnitude but opposite polarity, it will cause no resultant phase shift of the stationary spins. However, moving spins will acquire a phase shift, as they move along gradient direction axis during its application, since they do not experience both gradients equally. If it is assumed that spins flow into vessels with costant velocty v $[\mathrm{mm/s}]$, the phase shift ϕ $[\mathrm{rad}]$ they acquired during the bipolar gradient phaser is linearly proportional to velocity, in this manner:

$$\phi = \gamma \delta \Delta_G G v \tag{2.2}$$

where $\gamma = 42.58 \frac{\mathrm{rad}}{sT}$ is the gyromagnetic ratio of hydrogen proton nuclei, δ $[ms]$ is the duration of gradient lobe, Δ_G is the time distance between the centres of the gradient lobes, and G $[\mathrm{mT/m}]$ is the gradient strength. Hence, the encoded velocity v_{enc} that characterized crusher gradients can be calculated from (2.2) when $\phi = \pi$:

$$v_{enc} = \frac{\pi}{\gamma \delta \Delta_G G}$$

The encoding velocity is the cut-off velocity, above which the spins will be dephased giving no detectable signal, whereas below this level

the spins will still be visible in the final image. In brief, bipolar gradients can be used to slectively suppress the signal form moving blood-water, because the velocity of blood that is intended to be suppressed is inversely proportional to the strenght of the gradient, which can be manipulated by the user to get the desired performance. In diffusion MRI, gradients are usually characterized by a unique variable b, the b-value (or b-factor), that condensated all the user-dependent parametrs involved in gradient design. For example, assuming a rectangular-shaped gradient pulses, the b-value (in a unit of $^{\mathrm{s}}/_{\mathrm{mm}^2}$), can be expressed as $b = (\gamma\delta G)^2 \left(\Delta_G - \frac{\delta}{3}\right)$, which is uniquely defined once a cut off velocity v_{enc} is chosen. Value greater than $b = 1.7\frac{\mathrm{s}}{\mathrm{mm}^2}$ have been found to remove significant amount of intravascular signal.[11]

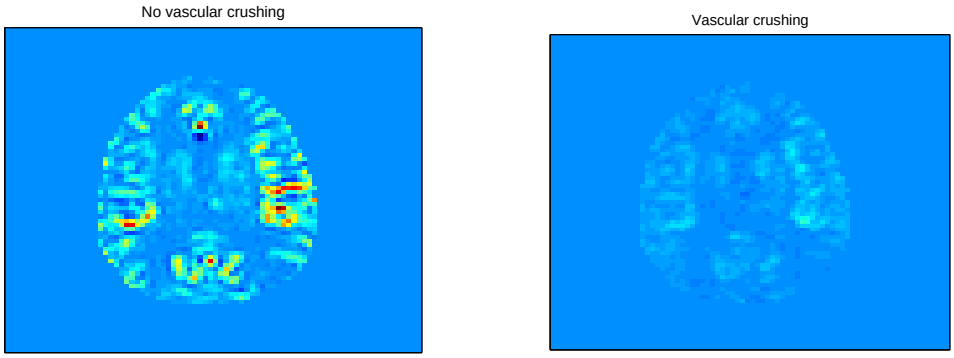

Figure 2.12: example of a brain slice acquired after $PLD = 0.21s$ the end of a pseudo continuous labeling scheme without (on the left) and with (on the right) bipolar gradients for flow suppression **($b = 3\frac{s}{mm^2}$).**

However, the appropriate threshold of flow velocity to remove in a individual case is not easily defined, and so gradient strenght is generally chosen empirically. Moreover, the flow suppression gradient is often applied only in one direction to avoid the reduction in SNR associated with the increased echo time TE required for multiple directions. Insofar, some of the signal for vessels with flow component perpendicular to gradient may remain. It is the case of every feeding arteries parallel to the image plane, if crusher gradients are applied in the slice selection direction. Another possibile problem with crushed experiments is the fact that diffusion gradients, used for eliminating the signal from fast-flowing blood, would add a diffusion weightening to the image. However, when using common bipolar gradients of $v_{enc} = 30\frac{\mathrm{mm}}{\mathrm{s}}$ (equivalent of $b = 1.7\frac{\mathrm{s}}{\mathrm{mm}^2}$), the resulting effect contribuites to a signal drop inferior of 0.14% (in gray matter), which is negligible compared to an

excepted signal change of $1-2\%$ due to perfusion [11].

Vascular crushing technique operate a reduction of ASL signal, making it more perfusion related naturally at the expense of lower SNR. The correction of vascular artifacts using vascular crusher gradients could involve some problems, and sometimes the explicity model of the intravascular signal should be preferred.

Chapter 3

Quantification of ASL data with parametric models

3.1 Introduction

ASL techniques produces a set of tagged and control images, which subtracted ones form the others (accordingly to the labeling scheme used) provide a series of perfusion-weighted images (PWI). Each voxel value in the difference imagesvrepresents the blood flow measured during the acquisition. If Δ is the value of a difference image voxel, we can distinguish two types of contribution in it:

- $\Delta^{(phy)}$: the effect due to the pysiological behaviour of the tracer (labeled blood) that can be detected in the PWI obtained from difference of control and tag.
- $\Delta^{(non-phy)}$: all the other effects that are not related to the physiological functioning of the brain. A typical examples of these unwanted contributions are off resonance effects difference and magnetization transfer effects (MT) difference between control and label images, which are due to imperfections and technical limatations in ASL experiment implementation. They are typically called subtraction errors because they arise from unexcepted discrepances between label and control images.

Thus the ASL signal could be thought as the sum of these two groups of magnetization contributions:

$$\Delta = \Delta^{(phy)} + \Delta^{(non-phy)}$$

However when a (parametric) model for cerebral perfusion quantification from ASL data is used, the quantity $\Delta^{(non-phy)}$ is generally ig-

nored. This is why the purpose of such models is to describe how kinetics and relaxation combining each other to extract a quantitative measurament of perfusion, condensated in some parameters whose physiological meaning is well-defined. The central assumption of quantification methods is that the control and tag subtraction is ideally perfect, and so no subtraction error contribute to the measured signal ($\Delta^{(non-phy)} = 0$). Every potential source of $\Delta^{(non-phy)}$ contributions should be previously accounted by appropriate mathematical modeling of these effects (in a preprocessing step) or using accurate technical solutions which could prevent or reduce them.

The ASL signal is simply proportional to the difference in longitudinal magnetization in the tissue due to blood that entered the voxel and is still present at the measurament time. To make it more clear, it is helpful to think as there were two groups of spin, defined by their location just after the labeling inversion pulse: static untagged tissue spins in the image voxel, and tagged arterial blood spins that travel to the voxel. Then the essential assumption is that the longitudinal magnetization of the first group is identical during the two parts of the experiment. It means that the signal difference Δ only depends on the difference of the longitudinal magnetization of the labeled blood, and gives a direct measure of how much of the original arterial magnetization, created by the inversion pulse, has been delivered to the voxel and survives to the time of measurement. So every model proposed to quantify ASL data assumed that the static tissue is subtracted accurately, and focused on the interpretation of the difference signal as a measure of magnetization delivered by arterial flow [3].

The perfusion-weighted signal, that ASL technique produces, reflects perfusion of the tissue f, but also depends on a number of factors that are not directly related to perfusion itself. They are rather a technique by-product, the results of how ASL detects perfusion. Passage of labeled blood in large vessels not perfusing the tissue through which they pass, distance between labeling region and imaging voxel which vary on voxel location, magnetization relaxation time function of tissue type (and of readout) are some examples. All of these confounding effects must be taken into account along with others calibration factor and parameters which defined the absolute scale of the signal. Inversion efficiency and the equilibrium magnetization of arterial blood have to be measured or supposed to be known, if an absolute quantification of perfusion is required. Vector Δ reflects the principal factor to

be described by ASL models:

$$\Delta = \Delta(t, f, T_{1t}, T_{1b}, \alpha, M_{0b}, \Delta t, \tau, \ldots)$$

In table (3.1) a list of parameters considered in ASL-MRI data quantification, with their definition and unit, is reported. Some of them have just been discussed, the other will be explained afterwards:

parameter	**description**	**unit**
$CBF \quad (f*)$	cerebral blood flow	$\frac{mL}{100g\,min}$
Δt	transit delay	s
τ	bolus duration	s
T_{1t}	tissue longitudianl relaxation time	s
T_{1b}	blood longitudinal relaxation time	s
α	inversion efficiency of labeling pulse	a.u.
M_{0t}	equilibrium magnetization of tissue	a.u.
M_{0b}	equilibrium magnetization of arterial blood	a.u.
λ	brain-blood partition coefficient (*)	$\frac{mL}{g}$
α_{LL}	flip angle of readout scheme employed	rad

Table 3.1: definition of parameters. [*see section 1.1 for concepts on relation existing between CBF and f]

As it will be discussed in the following section, ASL data could be sampled at single or multiple time after blood inversion. In both cases sampling time will be generically denoted as t (global experiment time) with the implicit assumption that its value represents the time from the start of labeling. In the context of pulsed techniques t is often referred to inversion time (TI), i.e. the time from the inversion pulse which is substantially the time from the start of labelling since the labelling pulse used has a limited extent (tipically $20 - 50\,ms$). With continuous labeling, sampling times are sometimes expressed as post-labeling delay (PLD), i.e. time delay after the end of labelling, which need to be added to the labeling duration to get sampling time in terms of global experiment time t.

3.2 Single inversion time vs multi inversion time

Among the parameters reported in table (3.1), great importance is covered by transit delay (Δt). Transit delay (also termed as arterial arrival time AAT, bolus arrival time BAT, or arterial transit time) represents the time tagged blood takes to move form the tagging location (a plane for continuous labeling, a spatial position inside a volume for pulsed labeling) to the imaging voxel. It arises because the tagged blood must cross a gap between tagging and imaging regions. Δt is then dependent from ASL acquisition parameters (those distance between tagging and imaging regions). However, Δt is known to vary markedly across the brain, for example longer transit delay to the occipital lobe are typically observed realtive to the frontal-parital-temporal lobe. This differences in Δt are completely indipendent of acquisition parameters because they reflect the different pathways that labeled bolus follows to reach imaging voxels. Probably the posteriors cerebral arteries travel a longer distance parallel to the imaging plane to reach the occipital lobe, whereas the middle cerebral arteries travel directly upward to the parietal lobes [12]. In general, the network of cerebral arteries and arterioles exhibits a complex geometry, with blood supplyig different parts of the brain following different trajectories at varying velocities, making Δt a variable parameters over the whole brain. Δt is thus somewhat governed by the vasculature, providing useful information about its state: many pathological conditions are known to results in a very slow blood flow and consequently in very long transit times to tissue. Δt measurements also help to understand whether the hypoperfusion, typically found in cerebrovascular disorders cases, is due to actual flow deficit or an artifact due to the delayed arrival of labeled blood. Moreover in healthy individuals, Δt has been shown to decrease during neuronal activity. Transit delay evaluation is thus a useful complement to CBF measurement.

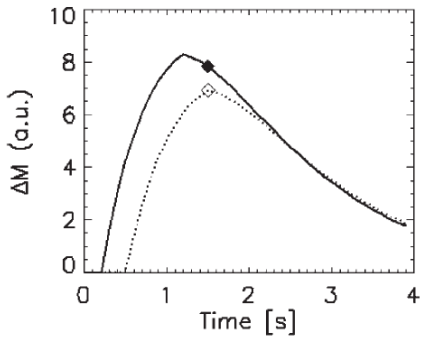

Figure 3.1: example of two voxels having the same CBF but different Δt. Measuring signal at a single inversion time would result in a lower CBF estimates a the voxel with longer Δt as compared with the voxel with shirter Δt [11].

This local nature of Δt makes particulary problematic the attemp to accuraltely quantify CBF with usual ASL acquisition schemes. Tipically, ASL measurements are conducted at a single inversion time (or post labeling delay) between tag generation and image readout, and so no informations about transit time are acquired. The only way to extract quantitative measure of CBF from these poor data is simply neglecting transit time effects. Inappropiate values and uncertains on this parameters can lead to both over and understimation of perfusion, making the accuracy of CBF quantification from single time point acquisition highly dependent on the actual Δt values (figure 3.1). Moreover with single inversion time acquisition, not only the quantification of CBF is weak, but relative perfusion values between regions are not valid either. Modifications to the basic techniques have been introduced to minimize Δt sensivity of the measured signal Δ in a single TI experiment ([13, 6]). The basic idea to account for an unknow Δt is to sufficiently delay the acquisition time point. Nevertheless, the reduced sensivity to Δt might be compromised whenever transit times are unexpectedly long (for istance in many pathological conditions) making this artifice ineffective. In addition, there is another consideration that potentially limits the advantages introduced by these techniques, expecially for PASL data. The TI required to face prolonged Δt could be so long as to degrade the SNR of the magnetization difference images, being higher the signal reduction that occur due to magnetization relaxation. Since SNR is already a critical issue in ASL techniques, the use of very long delay before imaging should be ideally avoided.

The problem can be solved acquiring images at multiple inversion time and therefore measuring a signal difference time course instead

of a single sample.

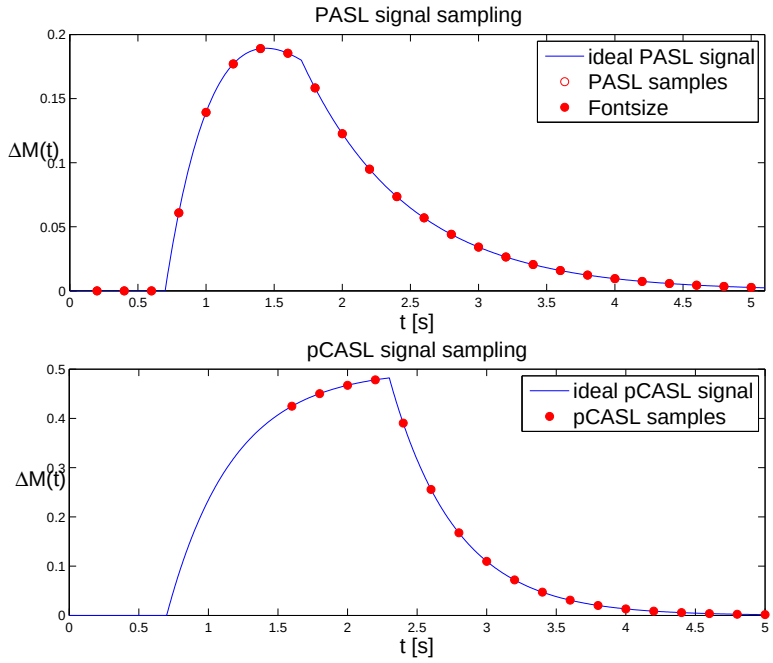

Figure 3.2: typical sampling time points for PASL and pCASL labeling techniques.

The improvment of the infomation available with dynamic perfusion acquisition is associated with a time penalty due to the need of sampling multiple inflow periods. Special readout schemes, such as Look Locker readout, have to be used to overcome this incovenient, since the standard sequences are generally too lengthy to be suitable for clinical examination if more than one sample is needed. The theory of Look-Locker has been reviewed in section 2.3.1, while the implications on the quantification model will be discussed in the follow. Acquisition time can be reduced also if an optimal sampling is designed, since less experiment repetitions have to be performed to get the desired SNR by averaging procedure.

3.3 ASL perfusion quantification

To extract quanitative CBF measurements from ASL dynamic data, a detailed model of the process combining kinetics and relaxation is needed. There are two main approaches to model ASL experiment, they differ on how signal in difference image Δ is interpreted when a model ΔM is built:

- **Compartmental models**: ΔM is thought to be a measure of concetration of labeled spins in difference images. It represents the measured signal of a system of compartments describing the distribution and the exchange of labeled water spins within the voxel. The equations of each compartment, which quantify the rate of change of longitudinal magnetization in each pool, are versions of Bloch equation modified by the inclusion of the exchange terms. That is, labeled blood water molecule is the system tracer, and usual compartimetal modeling is applied to it, giving a set of differential equation each one describing the rate of change of this tracer concentration inside the compartment. Since the measured signal Δ is modeled as the magnetization due to labeled spin concentration within the voxel rather than an actual tracer concentration, a modification to this set of equation has to be introduced to taking into account the magnetic properties of the ASL tracer. The final result is a set of reviewed Bolch equations describing the rate of change of the longitudinal magnetization of the labeled water molecules inside the compartment due both relaxation and exchange processes. Single and multi-compartment (accounting for finite capillary water permeability) have been proposed in literature [14]. In section 3.3.1 single compartment model is explained.

- **Tracer kinetics model**: ΔM is considered to be the fraction of the original concentration of a tracer bolus that is still in the voxel at the time of measurement. The labeling procedures produced a bolus of inverted water spins which is treated like a general bolus of tracer delivered to the tissue by arterial flow, and cleared by venous flow. The experiment is described by a linear system whose input and output functions are respectively the arterial tracer concentration and the measured signal Δ, and whose impulse responses lump all the underlying phenomenon involved in transport and uptake. In section 3.3.2 general tracers kinetics model in the context of ASL experiment are reviewed, and a common version of this model, the so called standard model, are exhaustively exposed in 3.4.

3.3.1 Single compartment theory

The imaging voxel is assumed to be a single well-mixed compartment, genearlly called tissue compartment. Labeled water is treated like a diffusible tracer that freely crosses the blood brain barrier and fills the

extravascular space. It eneters and leaves the voxel with perfusion rate f, relaxes with tissue longitudinal relaxation time T_{1t}, and no difference is made between intra- and extra-vascular water.

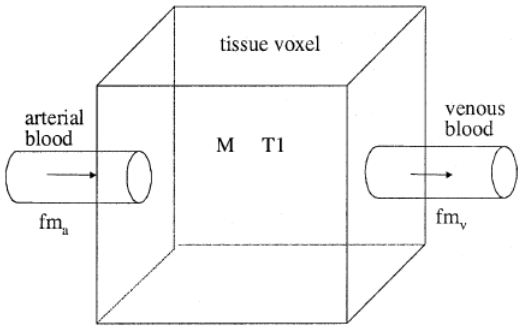

Figure 3.3: schematic diagram of single compartment model.

The Bloch equation is modified to including the incoming of arterial magnetization $m_a(t)$ and the outgoing of venous magnetization $m_v(t)$, giving:

$$\frac{dM(t)}{dt} = \frac{M_{0t} - M(t)}{T_{1t}} + fm_a(t) - fm_v(t)$$

where $M(t)$ is the longitudianal magnetization of the voxel and M_{0t} is the equilibrium magnetization of the tissue. Single well-mixed compartment assumption imply that immediately labeled blood water homogenuosly distribuites within the compartment, so that labeled blood water molecules and extravascular water molecules equilbrate each other and are not discernable. Water in the blood leaving the voxel contains labeled molecules at the same concentration as water in the tissue voxel, weighted by the increased water concentration of blood to tissue.Mathematically it is traduced by stating:

$$m_v(t) = \frac{M(t)}{\lambda}$$

where λ is the brain-blood partition coefficient for water. Considering the magnetization of the difference image, and assuming that the physical quantyties f, T_{1t}, M_{0t} do not change between the two scan, the single compartmental model equation is:

$$\begin{aligned}\frac{d\Delta M(t)}{dt} &= \frac{0 - \Delta M(t)}{T_{1t}} + f\Delta m_a(t) - \frac{f}{\lambda}\Delta M(t) \\ &= -(\frac{1}{T_{1t}} + \frac{f}{\lambda})\Delta M(t) + f\Delta m_a(t)\end{aligned}$$

defining:

$$\frac{1}{T_{1t,app}} = \frac{1}{T_{1t}} + \frac{f}{\lambda}$$

it yields to:

$$\frac{d\Delta M(t)}{dt} + \frac{\Delta M(t)}{T_{1t,app}} = f\Delta m_a(t) \tag{3.1}$$

where $\Delta M(t)$, the quantity described as a single compartiment, can be though as a measure of concentration of labeled molecules in the diffrence image [14]. This equation is a first order differential equation that can be solved once an expression for the input function $\Delta m_a(t)$ is provided. That is not a problem because the form of $\Delta m_a(t)$ can easily derived from knowledge on the type of labeling used. The assumption that the phisiology of the system is in a steady state implies that f and $T_{1,app}$ remain costant over time during the experiment. So, the single compartment model equation (3.1) can be viewed as the state equation of LTI system: $\dot{x}(t) = Fx(t) + Gu(t)$, where $x(t) = \Delta M(t)$ is the state variable. The explicit solution of the differential equation is simply given by the state output function with null initial condition ($\Delta M(0) = 0$) of the LTI system:

$$x(t) = e^{Ft}x(0) + \int_0^t e^{F(t-t')}Gu(t')dt'$$

$$\Downarrow$$

$$\begin{aligned}\Delta M(t) &= \int_0^t e^{-\frac{1}{T_{1,app}}(t-t')} f\Delta m_a(t')dt' \\ &= \int_0^t e^{-\frac{1}{T_{1,app}}(t-t')} f\Delta m_a(t')dt' \\ &= f\Delta m_a(t) * g(t)\end{aligned}$$

Single compartment assumption clearly appears in the exponential form $e^{-\alpha t}$ of impulsive response of the linear system $g(t)$. It is simply $e^{-\frac{f}{\lambda}t}$ when only kinetics of the agent are modelled, or become a more complex expression $e^{-(\frac{f}{\lambda}+\frac{1}{T_{1t}})t}$ when also the magnetization decay is considered. The main restriction of single compartment model is to costrain clearance of labeled blood water and relaxation of its magnetization to follow the same law, making these two different processes simply two aspects of the same more general one: magnetization outflow from the voxel.

3.3.2 General kinetic model

The general kinetic model directly derives from tracer kinetics theory which provide a mathematical description of the dynamic tissue concentration of any tracer that is delivered to the tissue by blood flow.

Dealing with ASL data, some adaptions to the general theory has to be apported. The tracer considered here is labeled blood water, which is measured in term of quantity of magnetization instead of concentration. The measured signal $\Delta(t)$ is thus considered as a quantity of magnetization that is carried into the voxel by arterial blood. The amount of this magnetization at a time t will depend on the history of delivery of magnetization by arterial flow and clearance by venous flow and longitudianl relaxation [15]. These various physical process can be described by defining three functions of time, that we call kinetic model functions:

- delivery function $c(t)$: normalized arterial concentration of magnetization arriving at the voxel at time t
- residue function $r(t, t')$: is the fraction of tagged water molecules that arrived at time t' and is still in the voxel at time t. This function contains most of the details of the distribution and the kinetics of the agent.
- magnetization relaxation function $m(t, t')$: is the fraction of the original longitudinal magnetization tag carried by the water molecules that arrived at time t' that remains at time t. This function justifyies the other way in which the agent can "clear" from the voxel in addition to venous flow.

If the physiological state of the tissue is not changing, then $r(t, t')$ and $m(t, t')$ are functions of just the interval $t - t'$, and could be written as $m(t)$ and $r(t)$, with t having that time difference meaning.

With these definitions the amount of magnetization delivered to a particular voxel between t' and $t' + dt'$ is $2\alpha M_{0b} f c(t')dt'$, where f is the CBF (expressed in units of $^{\mathrm{ml}}/_{\mathrm{ml\,s}}$), M_{0b} is the equilibrium magnetization of a fully arterial blood filled voxel, and α is the labelling efficiency, the fraction of the maximum possible change in longitudinal magnetization, so that $2\alpha M_{0b}$ is the arterial magnetization difference after the labeling phase. The fraction of magnetization that remains at time t is $r(t-t')m(t-t')$. Then $\Delta M(t)$, the amount of magnetization in the voxel at time t, is simply given by adding up all the magnetization contributions

that had arrived in the past weighted with the probability they are still in the voxel:

$$\begin{aligned} \Delta M(t) &= 2\alpha M_{0b} f \int_0^t c(t')r(t-t')m(t-t')dt' \\ &= 2\alpha M_{0b} f \{c(t) * [r(t)m(t)]\} \\ &= fQ(t) \end{aligned} \tag{3.2}$$

The last form of (3.2) emphasizes the central role of the perfusion in determining the ASL signal, making explicit its perfusion-weighted nature. The measured magnetization difference is modeled as the product of f and $Q(t)$, that can be thought as a calibration factor that convert the local cerebral flow into a measured magnetization difference. This factor control the SNR of the experiment: for a larger $Q(t)$ the same local f will produce a larger ASL signal difference $\Delta M(t)$.

Summarizing, the general ASL model need to consider transit delays from the tagging region to the voxel, magnetization decay, exchange of water between blood and tissue, clearance by venous flow and different forms of arterial tagging. All of these process can be taken into account with appropriate forms of the delivery function $c(t)$, the resiude function $r(t)$ and the magnetization deacy function $m(t)$.

3.4 The Standard ASL model

The standar model for ASL data is based on three key assumptions that, in the frame of the kinetic model, correspond to three particular forms for the functions $c(t)$, $r(t)$ and $m(t)$ [3].

1. the arrived of labeled blood at a particular voxel is assumed to be via uniform plug flow. It leads to a picewise definition of the delivery function which allows the labeled blood to eneter the voxel only in a precise temporal window defined by two parametrs: transit delay Δt, and bolus duration τ. The transit delay Δt is the time required to labeled blood to begin to appear in the tissue voxel after the start of labeling, and its role has been previously investigated. The bolus duration τ is the temporal extent of the delivery of labeled blood to voxel. These two parameters define when the perfusion process became detectable by the ASL experiment so they are directly related to the pysiology state of the tissue, but also depend on how the labeling is accomplish. The meaning of

uniform plug flow assumption is that $c(t)$ is nonzero only in the interval $\Delta t < t < \Delta t + \tau$, where for continuous labeling is $c(t) = e^{-\frac{\Delta t}{T_{1b}}}$ while for pulsed labeling is $c(t) = e^{-\frac{t}{T_{1b}}}$.

2. the kinetics of water exchange between tissue and blood are assumed to be described by single compartment kinetics: whatever compartements may exist within the tissue are undergoing such rapid exchange of water that their concentration ratios remain constant even though the total tissue concentration is function of time. This mean that the tissue concentration $\Delta M(t)$ and the venous conetration $\Delta m_v(t)$ are equal once they are corrected for the different water conetent between blood and tissue. It has been shown that this assumption is equivalent to take the exponential form for the reisude function $r(t) = e^{-\frac{f}{\lambda}t}$

3. as soon as the labeled water molecules have reached the tissue voxel, the magnetization is assumed to decrease with the relaxation time of the tissue T_{1t}. This essentially means that water is completely extracted form the vascular space immediately after arrival in the voxel. Thus magnetization relaxation function is given by $m(t) = e^{-\frac{t}{T_{1t}}}$.

The standard model can be summarized, in terms of delivery, kinetics and relaxation function, as:

$$
\begin{aligned}
c(t) &= \begin{cases} 0 & t \leq \Delta t \\ \hline e^{-\frac{t}{T_{1b}}} \quad \text{(pulsed)} & \\ e^{-\frac{\Delta t}{T_{1b}}} \quad \text{(continuous)} & \Delta t < t \leq \Delta t + \tau \\ \hline 0 & \Delta t + \tau \leq t \end{cases} \\
r(t) &= e^{-\frac{f}{\lambda}t} \\
m(t) &= e^{-\frac{t}{T_{1t}}}
\end{aligned}
\tag{3.3}
$$

It can be shown that these setting for the kinetic models function leads to the same model provided by single compartmental theory, in which modify Bloch equations approach is used. For the sake of completeness the demonstration of this equivalence, proved in [16], is reported here. To Defining the arterial magnetization in the difference image as $\Delta m_a(t) = 2\alpha M_{0b} c(t)$, and using the exponential forms [] for residue and relaxation functions, the voxel magnetization difference in the general

kinetic model frame can be rewritten as:

$$\Delta M(t) \;=\; f\int_0^t \Delta m_a(t')r(t-t')m(t-t')dt'$$

due to exponential form, $r(t)$ and $m(t)$ can be scomposed as:

$$r(t-t') = e^{-\frac{f}{\lambda}(t-t')} = e^{-\frac{f}{\lambda}t}e^{-\frac{f}{\lambda}(-t')} = r(t)r(-t')$$
$$m(t-t') = e^{-\frac{1}{T_{1t}}(t-t')} = e^{-\frac{1}{T_{1t}}t}e^{-\frac{1}{T_{1t}}(-t')} = m(t)m(-t')$$

giving:

$$\Delta M(t) = fr(t)m(t)\int_0^t \Delta m_a(t')r(-t')m(-t')dt'$$

differentiating both sides of this equation, remembering derivate of product rule (so that $\frac{d(r(t)m(t))}{dt} = (\frac{f}{\lambda}+\frac{1}{T_{1t}})r(t)m(t)$), fundamental theorem of calculus (so that $\frac{d}{dt}(\int_a^t f(t')dt') = f(t)$, if $F(t) = \int_a^t f(t')dt'$ is contonuous in $[a,t]$ and differentiable in (a,t)) and the exponential form of functions $m(t)$ and $r(t)$ (that imply $r(t)r(-t) = 1$ and $m(t)m(-t)$=1), it gives:

$$\begin{aligned}\frac{d\Delta M(t)}{dt} &= f(\frac{f}{\lambda}+\frac{1}{T_{1t}})r(t)m(t)\int_0^t \Delta m_a(t')r(-t')m(-t')dt' + fr(t)m(t)\Delta m_a(t)r(-t)m(-t)\\ &= (\frac{f}{\lambda}+\frac{1}{T_{1t}})\Delta M(t) + f\Delta m_a(t)\\ &= \frac{1}{T_{1t,app}}\Delta M(t) + f\Delta m_a(t)\end{aligned}$$

which is the same equations describing the single compartment model.

It has been shown that assuming residue function to be $r(t) = e^{-\frac{f}{\lambda}t}$ is equivalent to the single compartment assumption on difference of venous magnetization, $\Delta m_v(t) = \frac{\Delta M(t)}{\lambda}$, which implies that water exchange occouring across capillary walls between blood and tissue within the voxel is such rapid that the ratio of concentration of water in venous blood vs. tissue space is constant over time and equal to λ. Furthermore, assuming magnetization deacy to be governed only by the tissue relaxation ($m(t) = e^{-\frac{t}{T_{1t}}}$), make possible a single compartment modeling for $\Delta M(t)$, the magnetization difference in the voxel.

3.4.1 Standard Model equations

Using formulations 3.3, explicit expression for the magnetization difference model $\Delta M(t)$ can be obtained by inserting them into (3.2) and

analitically resolving the convolution integral. The equivalence between single compartment and kinetic model under standard assumption on the kinetic functions (i.e. steady state conditions), as it has been previously proved, ensure the same expressions result form analitical resolution of first order differential equation (3.1) with $\Delta m_a(t) = 2\alpha M_{0b} c(t)$ as driving function. It has been chosen to show how to derive $\Delta M(t)$ equations by resolving convolution integral instead of differential compartment equation. The extremely flexible nauture of the general kinetic approach allows standard assumptions to be relaxed modifying the expressions of the kinetcs functions without altering the structure of the model. Ideally all physiologic effects of the system can be modelled by appropriate definitions of those three functions, although analitical solution is possible only in some simple cases. Elsewhere they must be handled numerically [17, 3].

The following notations is used:

$$R_{1t} = \frac{1}{T_{1t}} \;\Big|\; R_{1b} = \frac{1}{T_{1b}} \;\Big|\; R_{1,app} = \frac{1}{T_{1t,app}} = R_{1t} + \frac{f}{\lambda} \;\Big|\; \delta R = R_{1b} - R_{1,app} \qquad (3.4)$$

Pulsed arterial spin labeling

Recalling (3.3), kinetic functions expressions for standard model are:

$$c(t) = \begin{cases} 0 & t \le \Delta t \\ e^{-\frac{t}{T_{1b}}} & \Delta t < t \le \Delta t + \tau \\ 0 & \Delta t + \tau < t \end{cases} \qquad r(t) = e^{-\frac{f}{\lambda} t} \qquad m(t) = e^{-\frac{t}{T_{1t}}}$$

coping them into the convolution integral, it yields to

$$\Delta M(t) \quad = \quad \begin{cases} 0 & t \le \Delta t \\ 2\alpha M_{0b} f \int_{\Delta t}^{t} e^{-\frac{1}{T_{1b}} t' - \frac{f}{\lambda}(t-t') - \frac{1}{T_{1t}}(t-t')} dt' & \Delta t < t \le \Delta t + \tau \\ 2\alpha M_{0b} f \int_{\Delta t}^{\Delta t + \tau} e^{-\frac{1}{T_{1b}} t' - \frac{f}{\lambda}(t-t') - \frac{1}{T_{1t}}(t-t')} dt' & \Delta t + \tau \le t \end{cases}$$

the general solution for second and third segment is given by (using (3.4)):

$$\begin{aligned}
\Delta M(t) &= 2\alpha M_{0b} f \int_{n_1}^{n_2} e^{-R_{1b}t' - \frac{f}{\lambda}(t-t') - R_{1t}(t-t')} dt' \\
&= 2\alpha M_{0b} f \int_{n_1}^{n_2} e^{-R_{1b}t' - R_{1,app}t + R_{1,app}t'} dt' \\
&= 2\alpha M_{0b} f \int_{n_1}^{n_2} e^{-\delta R t' - R_{1,app}t} dt' \\
&= 2\alpha M_{0b} f e^{-R_{1,app}t} \left(\frac{1}{-\delta R}\right) \left(e^{-\delta R n_2} - e^{-\delta R n_1}\right) \\
&= -\frac{2\alpha M_{0b}}{\delta R} f e^{-R_{1,app}t} \left(e^{-\delta R n_2} - e^{-\delta R n_1}\right)
\end{aligned}$$

For $n_1 = \Delta t$ and $n_2 = t$ (second segment), it becomes :

$$\begin{aligned}
\Delta M(t) &= -\frac{2\alpha M_{0b}}{\delta R} f e^{-R_{1,app}t} \left(e^{-\delta R t} - e^{-\delta R \Delta t}\right) \\
&= -\frac{2\alpha M_{0b}}{\delta R} f e^{(\delta R - R_{1b})t} \left(e^{-\delta R t} - e^{-\delta R \Delta t}\right) \\
&= -\frac{2\alpha M_{0b}}{\delta R} f e^{-R_{1b}t} \left(1 - e^{-\delta R (t - \Delta t)}\right)
\end{aligned}$$

and for $n_1 = \Delta t$ and $n_2 = \Delta t + \tau$ (third segment):

$$\begin{aligned}
\Delta M(t) &= -\frac{2\alpha M_{0b}}{\delta R} f e^{-R_{1,app}t} \left(e^{-\delta R(\Delta t + \tau)} - e^{-\delta R \Delta t}\right) \\
&= -\frac{2\alpha M_{0b}}{\delta R} f e^{(\delta R - R_{1b})t} e^{-\delta R \Delta t} \left(e^{-\delta R \tau} - 1\right) \\
&= -\frac{2\alpha M_{0b}}{\delta R} f e^{-R_{1b}t} e^{\delta R (t - \Delta t)} \left(e^{-\delta R \tau} - 1\right)
\end{aligned}$$

Standard model for pulsed ASL data is thus:

$$\Delta M(t) = \begin{cases} 0 & t \leq \Delta t \\ -\frac{2\alpha M_{0b}}{\delta R} f e^{-R_{1b}t} \left(1 - e^{-\delta R (t - \Delta t)}\right) & \Delta t < t \leq \Delta t + \tau \\ -\frac{2\alpha M_{0b}}{\delta R} f e^{-R_{1b}t} e^{\delta R (t - \Delta t)} \left(e^{-\delta R \tau} - 1\right) & \Delta t + \tau \leq t \end{cases} \quad (3.5)$$

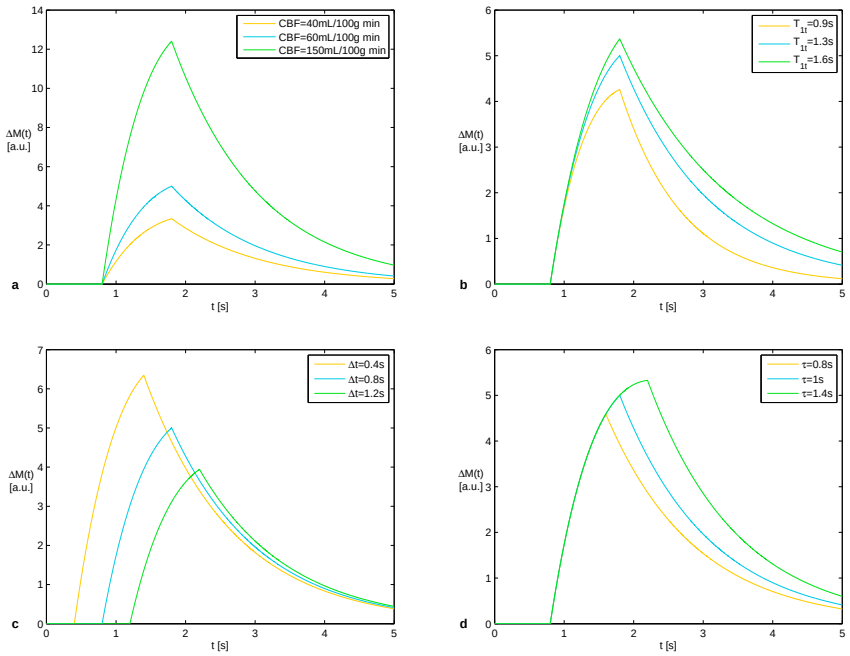

Figure 3.4: PASL standard model with the following parameters settings: $CBF = 60\frac{mL}{100g\,min}$, $T_{1t} = 1.3s$, $\Delta t = 0.8s$, $\tau = 1s$. In each boxe, a parameters is allowed to vary on a grid of values defined in the relative legend.

Continuous or pseudo-continuous arterial spin labeling

To achieve standard model expression with continuous or pseudo continuous labeling scheme can be used the same strategy. The biggest conceptual difference stays in the different description of the delivery function $c(t)$. Using the kinect model functions (3.3) with version (c) for delivery of arterial magnetization $c(t)$:

$$c(t) = \begin{cases} 0 & t \leq \Delta t \\ e^{-\frac{\Delta t}{T_{1b}}} & \Delta t < t \leq \Delta t + \tau \\ 0 & \Delta t + \tau < t \end{cases} \qquad r(t) = e^{-\frac{f}{\lambda}t} \qquad m(t) = e^{-\frac{t}{T_{1t}}}$$

the general model $\Delta M(t)$ becomes:

$$\Delta M(t) \quad = \quad \begin{cases} 0 & t \leq \Delta t \\ 2\alpha M_{0b} f \int_{\Delta t}^{t} e^{-\frac{\Delta t}{T_{1b}} - \frac{f}{\lambda}(t-t') - \frac{1}{T_{1t}}(t-t')} dt' & \Delta t < t \leq \Delta t + \tau \\ 2\alpha M_{0b} f \int_{\Delta t}^{\Delta t + \tau} e^{-\frac{\Delta t}{T_{1b}} - \frac{f}{\lambda}(t-t') - \frac{1}{T_{1t}}(t-t')} dt' & \Delta t + \tau \leq t \end{cases}$$

The general solution for second and third segment is given by (using (3.4) again):

$$\begin{aligned}
\Delta M(t) &= 2\alpha M_{0b} f \int_{n_1}^{n_2} e^{-R_{1b}\Delta t - \frac{f}{\lambda}(t-t') - R_{1t}(t-t')} dt' \\
&= 2\alpha M_{0b} f e^{-R_{1b}\Delta t} \int_{n_1}^{n_2} e^{-R_{1,app}t + R_{1,app}t'} dt' \\
&= 2\alpha M_{0b} f e^{-R_{1b}\Delta t} e^{-R_{1,app}t} \int_{n_1}^{n_2} e^{R_{1,app}t'} dt' \\
&= 2\alpha M_{0b} f e^{-R_{1b}\Delta t} e^{-R_{1,app}t} \left(\frac{1}{R_{1,app}}\right) \left(e^{R_{1,app}n_2} - e^{R_{1,app}n_1}\right) \\
&= \frac{2\alpha M_{0b}}{R_{1,app}} f e^{-R_{1b}\Delta t} e^{-R_{1,app}t} \left(e^{R_{1,app}n_2} - e^{R_{1,app}n_1}\right)
\end{aligned}$$

For $n_1 = \Delta t$ and $n_2 = t$ (second segment), it becomes:

$$\begin{aligned}
\Delta M(t) &= \frac{2\alpha M_{0b}}{R_{1,app}} f e^{-R_{1b}\Delta t} e^{-R_{1,app}t} \left(e^{R_{1,app}t} - e^{R_{1,app}\Delta t}\right) \\
&= \frac{2\alpha M_{0b}}{R_{1,app}} f e^{-R_{1b}\Delta t} \left(1 - e^{-R_{1,app}(t-\Delta t)}\right)
\end{aligned}$$

and for $n_1 = \Delta t$ and $n_2 = \Delta t + \tau$ (third segment):

$$\begin{aligned}
\Delta M(t) &= \frac{2\alpha M_{0b}}{R_{1,app}} f e^{-R_{1b}\Delta t} e^{-R_{1,app}t} \left(e^{R_{1,app}(\Delta t+\tau)} - e^{R_{1,app}\Delta t}\right) \\
&= \frac{2\alpha M_{0b}}{R_{1,app}} f e^{-R_{1b}\Delta t} e^{-R_{1,app}(t-\Delta t)} \left(e^{R_{1,app}\tau} - 1\right)
\end{aligned}$$

The Standard model for continuous or pseudo-continuous labeling is thus:

$$\Delta M(t) = \begin{cases} 0 & t \leq \Delta t \\ \frac{2\alpha M_{0b}}{R_{1,app}} f e^{-R_{1b}\Delta t} \left(1 - e^{-R_{1,app}(t-\Delta t)}\right) & \Delta t < t \leq \Delta t + \tau \\ \frac{2\alpha M_{0b}}{R_{1,app}} f e^{-R_{1b}\Delta t} e^{-R_{1,app}(t-\Delta t)} \left(e^{R_{1,app}\tau} - 1\right) & \Delta t + \tau \leq t \end{cases} \quad (3.6)$$

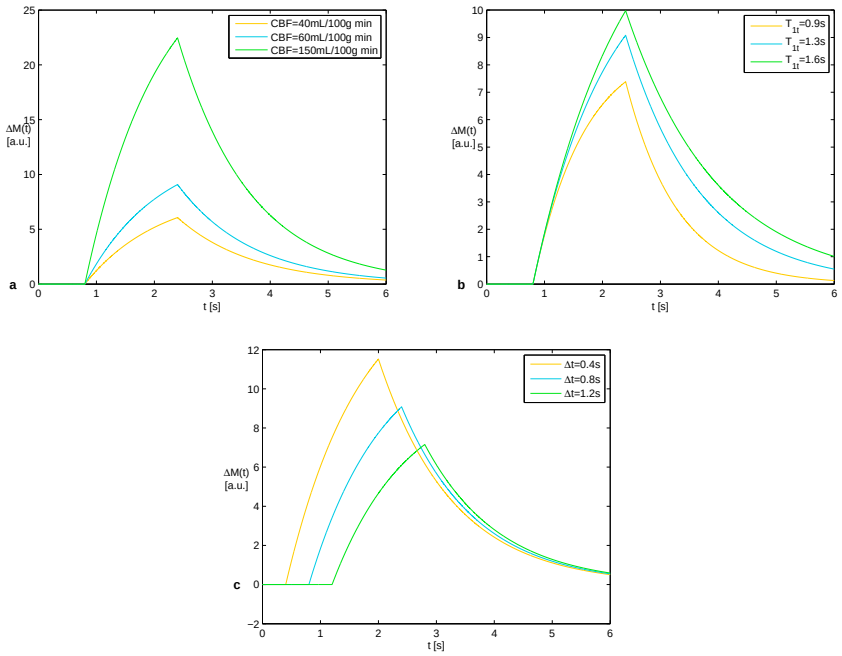

Figure 3.5: pCASL standard model with the following parameters settings: $CBF = 60\frac{mL}{100g\,min}$, $T_{1t} = 1.3s$ and $\Delta t = 0.8s$. In each boxe, a parameters is allowed to vary on a grid of values defined in the relative legend.

3.5 Standard model and Look Locker readout

In section 3.2, the importance of monitoring the inflow of labeled blood at many sampling times has been discussed. In brief, local parameters in addition of CBF can be estimated form data, addressing in a more reliable way the quantification of some confounding effects that influence CBF estimation. This ideal great improvment involves, on the other hand, some potential complications: (a) the need of sampling labeled blood signal at several time points (more than 5 as it's typically performed in ASL dynamic data) to assure the additionl parameters to be estimated with good accuracy despite low SNR of ASL signal, (b) the need of doing that in a limited temporal extension (compatible with clinical experiment), (c) the further model complexity introduced due to either new parameters that have to be estimated and the need of modeling how the acquisition strategy interfers with the process the model aims to describe.

The Look-Locker sampling strategy has been shown to fit very well the first two drawbacks just highlighted (as reported in parte sul readout LL capitolo precedente). It allows a whole dataset to be acquired

within 5 minutes with a temporal resolution between samples of about 100 ms [9]. In the follow, the modifications brought on the perfusion standard model to taking into account multiple RF-pulses in the Look-Locker readout are described.

The Look Locker read out applied to ASL experiment samples a series of images, equally spaced in time, after each spin tagging preparation, employing low flip angle excitations during the relaxation of the longitudinal magnetization to equilibrium, and it is applicable to all the common labeling techiques used. The repetetive perturbation by the LL readout pulses during recovery costantly disturbed the free relaxation, and drives the magnetization to a steady state described by an effective longitudianal relaxation time $T_{1,eff}$ (shorter than usual T_1) and an equilibrium magnetization $M_{0,eff}$ (lower than the undisturbed M_0) in which a dependance from LL readout parameters appear.

The perturbation by the readout pulses can be taken into account, in the frame of standard model, in the computation of magnetization relaxation function $m(t, t')$. When more than one readout pulse is applied, the longitudinal magnetization decays no more with relaxaton time of the tissue T_1, but and addictional flip angle dependent factor must be added, so that:

$$m(t, t') = e^{-\frac{(t-t')}{T_{1t}}} \left[\cos \alpha_{LL}\right]^n$$

where the readout dependent parameters are α_{LL}, the flip angle of each excitation pulses, and n, the number of readout pulses experienced by the labeld blood bolus since its entrance in the voxel. Parameter n is thus function of time, and is given by:

$$n = floor\left(\frac{t}{TI_2}\right) - floor\left(\frac{t'}{TI_2}\right)$$

where TI_2 denoted the equally spaces time between LL readout pulses. The floor function returns the largest integer smaller than its argument, and it is intrinsically a discontinue function. This discontinue nature of the parameter n, entailed in $m(t, t')$ definition, make the convolution integral (3.2) not analytically resovable. To preserve one of the most appealing properties of the standar model, the analytical form of its solution as showed in section (soluzioni analitiche standard model), the magnetization relaxation function must be approximated by a continuous function in which floor function is ommitted. The parameter n is thus given by $n = \frac{t-t'}{TI_2}$, and the magnetization function $m(t, t')$ be-

comes:

$$\begin{aligned} m(t,t') &= e^{-\frac{(t-t')}{T_{1t}}}\left[\cos\alpha_{LL}\right]^n \\ &= e^{-\frac{(t-t')}{T_{1t}}} e^{n\ln[\cos\alpha_{LL}]} \\ &= e^{-\frac{t-t'}{T_{1t}}+\frac{t-t'}{TI_2}\ln[\cos\alpha_{LL}]} \\ &= e^{-\left(\frac{1}{T_{1t}}-\frac{\ln[\cos\alpha_{LL}]}{TI_2}\right)(t-t')} \end{aligned}$$

The magnetizaion relaxation function now depends on the time difference $t-t'$, as was naturally assumed in the standard model by recalling the steady state of the physiologic system modelled. Moreover, $m(t-t')$ is again a exponential-shape function, where the longitudinal relaxation rate is now $R_{1,eff} = \frac{1}{T_{1,eff}} = \frac{1}{T_{1t}} - \frac{\ln[\cos\alpha_{LL}]}{TI_2}$, the effective LL relaxation rate, instead of the orignal tissue relaxation rate $R_{1t} = \frac{1}{T_{1t}}$. Defining:

$$\begin{aligned} R_{1,eff,app} = \frac{1}{T_{1,eff,app}} &= \frac{1}{T_{1t}} + \frac{f}{\lambda} - \frac{\ln\left[\cos\alpha_{LL}\right]}{TI_2} \\ \delta R = \frac{1}{T_{1b}} - \frac{1}{T_{1,eff.app}} &= R_{1b} - R_{1,eff,app} \end{aligned}$$

the expression of the standard model is directly obtained, using this new definition of δR for pulsed experiments, or substituing $R_{1,app}$ with $R_{1,app,eff}$ for continuous experiments. In both cases the special form of the Look-Locker readout scheme is apparent only in the modified apparent relaxation time $T_{1,eff,app}$ (which appear explicitely in countinuous model while is included in δR in pulsed model), due to the presence of a readout dependent factor $\frac{\ln[\cos\alpha_{LL}]}{TI_2}$, missing in standard acquisition methods.

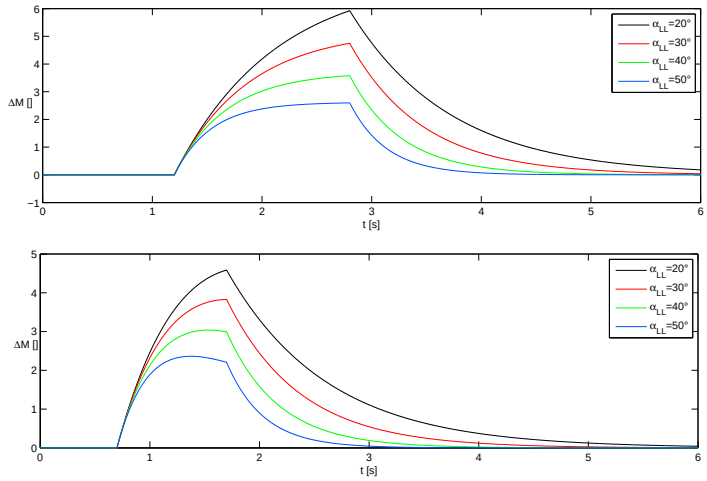

Figure 3.6: effect of flip angle, α_{LL}, in pCASL (top) and PASL (bottom) model. Model parameters are the same used in figures (3.4,3.5).

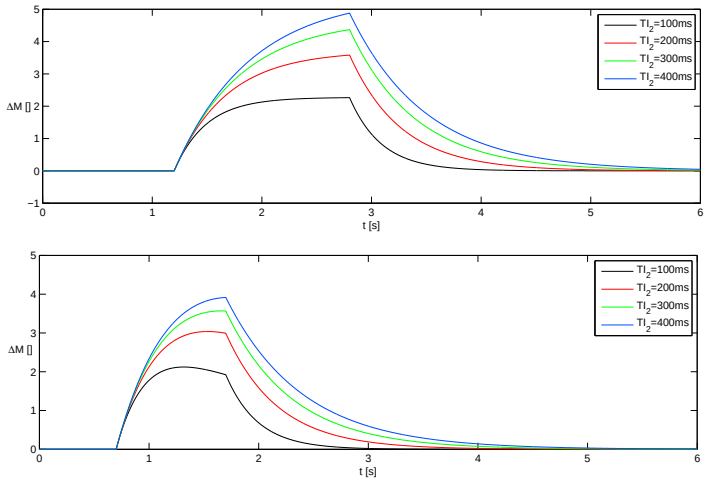

Figure 3.7: effect of sampling time, TI_2, in pCASL (top) and PASL (bottom) model.

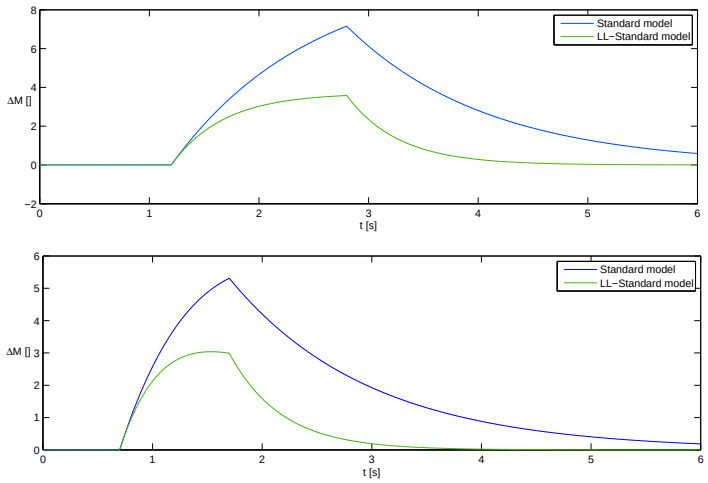

Figure 3.8: comparison between standard model and standard model with LL readout both for pCASL (top) and PASL (bottom). Parameters for standard models are those used in figures (3.4,3.5), $\alpha_{LL} = 40°$ and $TI_2 = 0.2s$.

The LL readout introduces in the standard model several measurement parameters that highly impact the predicted signal. These are the flip angle α_{LL}, and the time between successive data acquisition TI_2 (which contribuite to define the total measurement time togheter with N_{LL}. Optimization procedures are usually employed to find an appropriate set of these measurement parameters that minimizes a particular cost function (for exemple, a function that relate the variance of CBF to the adjustable LL parameters, or express SNR of the acquired signal in terms of the LL parameters[]). However, when parametric models are fitted to ASL data, these LL-dependent parameters are fixed to their experimental (eventually optimal) nominal values, and the main issue is to ensure they don't differ. Form this point of view, while TI_2 is usually well-definie, α_{LL} is a very fairy parameters because is likely to vary largerly within the acquisition volume, actually limiting the reliability of Look-Locker measurements. Due to this reason, LL measurement require either a good field homogeneity or an additional measurement of the flip angle spatial distribution to limit or account for its deviation [9].

3.6 Proposed models restrictions

Standard ASL model is the result of a series of assumptions condensated in the kinetic functions definition (3.3). They provide an oversemplified description of blood exchanges within brain tissue, by a severe

hypothesis on tissue voxel considered as a single well mixed compartment. More realistic description of perfusion process should take into account the limited permeability to water of capillary blood (implying that water is not completely extracted during capillary transit), or the fact that tissue\blood exchange of water is not istantaneous but require to begin at least a time lag after entering the voxel, to allow blood to travel down the vascular tree of the voxel till capillary bed. Although this improvements, in principle, can be implemented in the frame of general kinetic model by adequate reshaping of kinetics function $r(t)$ and $m(t)$, they has been mostly indagated through the adoption of pluri compartmental models [*ref].

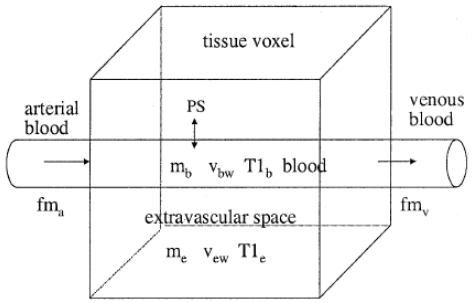

Figure 3.9: schematic diagram of two compartmentals model proposed by [*ref]. Water exchanges between blood and extravascular space are described in terms of PS, the permeability (P) surface area (S) product of brain capillaries to water, per volume of tissue. PS published values in whole brain vary from $0.9 - 1.7min^{-1}$. In single compartmental (i.e. standard ASL model) capillary wall permeability to water is else assumed to be infinite [14].

Assumption regarding the shape of input function $c(t)$, however, can be relaxed without modify the basic single compartment structure underlying standard ASL model, and furthermore without lose the possibility of deal with analytical expression. In the standard model described above, sudden and simultaneous arrival of tagged blood into the imaged region is assumed (the uniform plug flow assumption). This makes leading and trailing wavefront of tagged blood bolus to form sharp-edge step functions, noticeable in the 'rect' like shape of delivery function $c(t)$. A more realistic approach aims to replace $c(t)$ with a smoother input function that accounts for the statistical nature of the arrival time. Infact, tagged blood water molecules proceed to the imaging slice along pathways of varying lengths and at different speeds. This randomness has a consequence of smoothing the edges of the

$c(t)$. Remembering the definition of standard delivery fucntion for PASL and pCASL:

$$c(t) = \mathrm{e}^{-\frac{\Delta t}{T_{1b}}} w(t) \qquad \text{pCASL}$$
$$c(t) = \mathrm{e}^{-\frac{t}{T_{1b}}} w(t) \qquad \text{PASL}$$

with $w(t)$ defining tyical boxcar shape (function is non null only for times $\Delta t \leq t \leq \Delta t + \tau$), dispersion effects can be explicitated by taking the convolution of $w(t)$ with the a dispersion kernel $k(t)$, describing how dissipation occour:

$$c(t) = \mathrm{e}^{-\frac{\Delta t}{T_{1b}}} \left[w(t) \otimes k(t)\right] \qquad \text{pCASL}$$
$$c(t) = \mathrm{e}^{-\frac{t}{T_{1b}}} \left[w(t) \otimes k(t)\right] \qquad \text{PASL}$$

Analytical solutions were obtained with uniform dissipation kernel and gaussian dissipation kernel (see figure (3.10)).

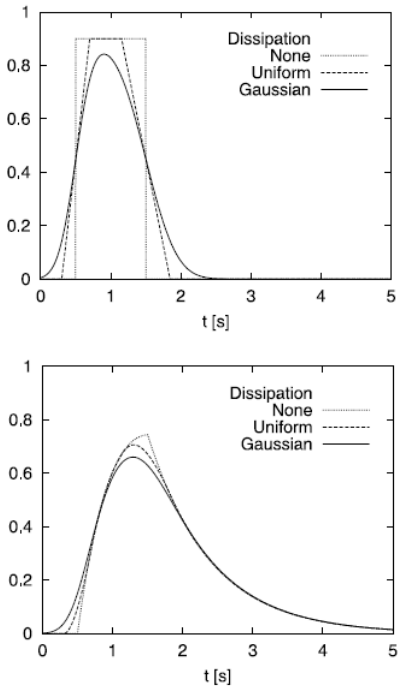

Figure 3.10: effects of input dispersion (top panel) inclusion into PASL model (bottom panel). Smoothing of the input function is shown to affect not only the intial slope but also the maximum obtainable perfusion signal [17].

Recently, a gamma kernel shape has been proposed and suggested as the more realistic solutions to model dispersion in ASL data quantification [18]. Analytical solution for convolution with gamma kernel

is given:

$$w(t)\otimes k(t) = \begin{cases} 0 & t \leq \Delta t \\ Q\left(s(t-\Delta t), 1+sp\right) & \Delta t \leq t \leq \Delta t + \tau \\ Q\left(s(t-\Delta t), 1+sp\right) - Q\left(s(t-\Delta t-\tau), 1+sp\right) & t \geq \Delta t + \tau \end{cases}$$

where $Q(x,y)$ is the incomplete gamma integral defined as $Q(x,y) = \frac{1}{\Gamma(y)}\int_0^x \mathrm{e}^{-u}u^{y-1}du$, and s and p are the parameters of gamma dispersion kernel.

Another limitation regards the introduction of the LL readout effects in standard model (see section 3.5). In the model proposed blood spins are assumed only to experience perturbations when they are visible in the experiments, that is before Δt, when bolus has not reached the tissue yet, magnetization tag is supposed to be insentive to RF pulses of LL readout. Actually longitudinal magnetizaion of water molecules is already diminuished by the readout excitations, albeit they reside in arterial blood instead of tissue. By modifying the function $c(t)$, the additional RF-excitations in LL acquisition can be modeled:

$$c(t) = \begin{cases} 0 & t \leq \Delta t \\ \hline e^{-\frac{t}{T_{1b}}}\left[cos\alpha_{LL}\right]^{n_c} \quad [\text{pCASL}] & \Delta t < t \leq \Delta t + \tau \\ e^{-\frac{\Delta t}{T_{1b}}}\left[cos\alpha_{LL}\right]^{n_c} \quad [\text{PASL}] & \\ \hline 0 & \Delta t + \tau \leq t \end{cases}$$

with $n_c = floor\left(\frac{\Delta t - \delta t_{min}}{TI_2}\right)$ providing the number of excitations of LL pulsing scheme experienced by blood before reaching the voxel, being δt_{min} the time at which tagged blood entered the imaging region. The addictional cosine factor, $\left[cos\alpha_{LL}\right]^{n_c}$, can be separted from the convolution model (3.2), and acts only as a scaling factor for the perfusion. However this factor is difficult to calculate because n_c is not precisely known, and can vary in dependance of which artery is feeding the voxel.

Chapter 4

Materials and Methods

In this chapter datasets available is briefly described. Methods used in this work to quantify these data is then accurately exposed, giving also their theoretical background.

4.1 Materials

MR images were acquired with a Philips ACHIEVA 3T MRI-scanner using a 32-channel neurovascular head coil. Six healthy human subjects (27.5 ± 1.68 years of age, 2 males and 4 females) were scanned using the same protocol. All subject gave informed consent after the nature of the procedure examinations were explained. The acquisition session was constituited of:

- high resolution T_1-weighted MR images, acquired using a magnetization prepared rapid gradient echo (MPRAGE) sequence ($256 \times 256 \times 160$ matrix dimension, $1 \times 1 \times 1 mm^3$ voxel dimension), providing anatomical informations.

- perfusion-weighted ASL images. They were acquired using a multislice gradient-EPI readout in combination with Look-Locker sampling strategy. EPI readout was designed to accomplish the acquisition of six axial slices (64×64 matrix, with $3.5 \times 3.5 mm^2$ in plane resolution, slice thickness of $6mm$), in a temporal windown of $T_{slice} = 33ms$ per slice. For LL sequence, parameter set was given by $TI_2 = 200ms$ sampling period, $N_{LL} = 15$ number of TI, and$\alpha_{flip} = 40°$ flip angle of multiple excitation pulses. With these settings, 15 images at TI ranging from $10ms$ to $3010ms$ after the end of labeling scheme, equally spaced in time by amount $\Delta TI = TI_2$, were acquired in order to adequately sample the kinetic curve of inflow-

ing blood and allow model fitting. Tag\control pairs acquisition was repeated $N = 30$ times for subsequent signal averaging. Two kind of labeling scheme was performed: (a) signal targeting with alternate radiofrequency (STAR) version of pulsed ASL (TR=$5s$), (b) pseudo-continuous ASL, with a labeling duration $\tau = 1.6s$. In both schemes gap between labeling plane (or inversion slab center for pulsed label) and lowest imaged slice was $7,5cm$. LL-EPISTAR adn LL-pCASL experiments were repeated with and without bipolar gradients to compare differenece in perfusion-weighted images due to signal from intra-arterial blood. The diffusion-sensitizing bipolar gradients (diffusion b-value =$3\frac{s}{mm^2}$) were applied in all spatial directions directly after readout preparation to dephase flowing spins, with $TE = 16ms$ long enough to accomodate theeir presence. All acquisitions used a sense acceleration factor of 2.5.

- M_0 sensitive images, a series of calibration images in which no spin tagging was performed (same readout dimension of pCASL and PASL, $TE = 16$ ms, $TR = 20s$ long enough to approach a magnetization equilibrium state).

4.2 Methods

In the work presented here, CBF and other pefusion realated parameters were estimated by fitting appropriate models to ASL data. Model fitting procedure is usually preceded by a preprocessing step, in which correction for motion\acquisitions artifacts, outliers analysis and spatial filtering, are generally performed. In this work, all acquired data were involved in quantification step, and preprocessing reduced to a simple masking of slice images to exclude from the analysis background voxels.

Two aspects of ASL data quantification was mainly discussed in this work:

1. the definition and the validation of a general scheme of settings to perform ASL standard model quantifiation [3] with a variegated set of data. In this study PASL (STAR) and pCASL data with and without vascular crushing was considered.

2. the study of an improved version of Standard model. The aim was to correct one of its typical limit that severly restricts its use, especially when data are acquired without vascular flow suppression

as single well mixed compartment assumption is far to be satisfied in that case.

4.2.1 Voxel wise standard model

ASL dynamic data is describe at voxel level using the following voxel wise model of observations:

$$\Delta(t_k) = \Delta M(t_k, \underline{p}) + v(t_k) \qquad k = 1, \ldots, N_{LL} \tag{4.1}$$

where $\Delta(t_k)$ is the measured signal difference at istant t_k, $\Delta M(t_k, \underline{p})$ is the magnetization difference (which takes form (3.5) for PASL, and form (3.6) for pCASL data, see chapter 3 for theoretical description) for a given time point t_k. $\underline{p}$ is the parameters vector $\underline{p}$, and $v(t_k)$ is the additive noise corrupting measures at time t_k.

Defining $\underline{t} = [t_1, t_2, \ldots, t_{N_{LL}}]$ as the vector of temporal grid at which ASL images are sampled, the time dependence in (4.1) can be including in ASL model using a vector notation, in which vector element at position k refers to sampling time t_k. Thus, voxelwise ASL model is thus:

$$\begin{gathered} \underline{\Delta} = \underline{\Delta M}(\underline{p}) + \underline{v} \\ \begin{bmatrix} \Delta_1 \\ \Delta_2 \\ \vdots \\ \Delta_{N_{LL}} \end{bmatrix} = \begin{bmatrix} \Delta M(t_1, \underline{p}) \\ \Delta M(t_2, \underline{p}) \\ \vdots \\ \Delta M(t_{N_{LL}}, \underline{p}) \end{bmatrix} + \begin{bmatrix} v_1 \\ v_2 \\ \vdots \\ v_{N_{LL}} \end{bmatrix} \end{gathered} \tag{4.2}$$

where $\underline{\Delta}$ is the set of observation, $\underline{\Delta M}$ is the vector of model predictions, and $\underline{v}$ is the vector of random noise samples. Each vector has a dimension of $[N_{LL} \times 1]$, where N_{LL} is the total number of RF pulses in the LL readout. Parameters vector $\underline{p}$ contains parameters that have to be estimated from data to obtain the optimal fit. The exact content of vector $\underline{p}$ depends also on how model inference is performed (LS approach or bayesian approach), beside labeling technique used. In table [4.1] a resumptive scheme of parameters vector is shown.

	LS approach	MAP approach
PASL scheme	$\underline{p} = [f,\, T_{1t},\, \Delta t,\, \tau]^T$	$\underline{p} = [f,\, T_{1t},\, \Delta t,\, \tau,\, M_{0b}]^T$
pCASL scheme	$\underline{p} = [f,\, T_{1t},\, \Delta t,]^T$	$\underline{p} = [f,\, T_{1t},\, \Delta t,\, M_{0b}]^T$

Table 4.1: unknown parameters in each of inference settings. Standard PASL model requires τ to be estimated from data respect to pCASL data model. Bayesian approach allow M_{0b} to be estimated using a-priori information, instead of fixing it to a data-driven value as with LS approach.

All the other parameters included in standard model definition, accurately described in section 3.5, has to be considered known from literature or experimental setup when model (4.2) is fitted to data. Table (4.2) reports the setting of these auxiliary parametrs used with ASL standard model.

	PASL	pCASL
α	0.95 literature	0.8 literarure
λ	$0.9\frac{g}{mL}$ literature	$0.9\frac{g}{mL}$ literature
T_{1b}	$1.68s$ literature	$1.68s$ literature
α_{flip}	$40°$ experimental setup	$40°$ experimental setup
TI_2	$0.2s$ experimental setup	$0.2s$ experimental setup
τ	unknown	$1.6s$ experimental setup
M_{0b}*	extracted from data*	extracted from data*

Table 4.2: λ and T_{1b} are global parameters independent from labeling scheme with well defined values derivable from literature [3, 19][3, 19]. α is dependent from the type of labeling, whose value can be extracted from data. However in this thesis it was set to values obtain from published studies [7]. α_{flip} and TI_2 are parameters of readout sequence. τ has different meaning dipending on labeling approach used: with pCASL it indicates labeling duration and is fixed by experimental setup, with PASL it becomes bolus duration at voxel level and has to be estimated. [*] M_{0b} is generally calucalated from data using correction factor deriving form literature studies, but when model inference is performed in a Bayesian framework it becomes part of vector $\underline{p}$ and treated as unkown parameter, to better account for its fundamental role as main CBF scaling factor (for details see section 4.2.3).

4.2.2 Weighted nonlinear least squares estimation

The first attemp to fit model for magnetizion difference $\Delta M(t, \underline{p})$ to ASL $\Delta(t)$ was performed using least squares (LS) approach. Briefly, the optimal set of parameter values when LS approach is used, $\underline{p}^{LS}$, is the one who minimizes a cost function given by the residual sum of squares (RSS), where residuals,$r(t_k)$ with $k = 1, \ldots, N_{LL}$, are defined as the differences between data and model predictions. In the context of ASL model, it can be formalize as follows:

$$\underline{p}^{LS} = \underset{\underline{p}}{argmin} \left[\| \underline{r}(\underline{p}) \|^2 \right] = \underset{\underline{p}}{argmin} \left[\| \underline{\Delta} - \underline{\Delta M}(\underline{p}) \|^2 \right] \tag{4.3}$$

where vector $\underline{p}$ of unknown is defined in table (4.1). The nonlinear nature of ASL standard model $\Delta M(t, \underline{p})$ precludes the existence of a close-form solution for minimization problem explicitated by (4.3). In practice, to find $\underline{p}^{LS}$ non linear version of LS estimator has to be used. A lot of algorithm can be used for nonlinear optimization, however all of them consist of an iterative scheme in which substantially a linear solution approximation is maden at each step. In this work nonlinear least square (NLLS) optimal parameters were calculated using MatLab rountine lsqnonlin() in which trust region reflective optimization algorithm is set as default [20].

A refined version of LS estimation could be obtain associating a weight to each data point Δ_k, so that when computing the RSS each of them will contribuite to the total amount in proprotion to the amplitude of its weight. One can refernce this approach as weighted NLLS (WNLLS). The meaning of data weights is to decrete how reliable is each sample to better address parameters identification. A natural choiche for weight is to use inverse of measurement noise standard deviation, when it is known. Elsewhere they must be evaluate somehow, for example using data or knowledge about experiment [21].

In ASL, data weights to include in NLLS estimator can be derived directly form data, taking advantage form the multiple experiment repetitons performed to face with low SNR of the perfusion signal. Each ASL signal sample, Δ_k, is the result of an average procedure along N experiment repetition, from which a measure of variance of the sample can be derived. There is two way to evaluate standard deviation of measures, depending on how signal difference is considered: (a) difference between average of labeled and control images, (b) average of labeled and control difference images. Details on weights calculation, in both manner, are given in A. In WNLLS estimation, weights derived using (b), the

so called mean of differences model for weights, was choosen. Summarizing, from multiple ASL experiment repetitions a vector of data weights $[w_1, w_2, \ldots, w_{N_{LL}}]$ were extracted for each voxel, and introduced in LS estimator. Adopting a matrix notation, LS solution of parameters identification is given by:

$$\begin{aligned} \underline{p}^{LS} &= \underset{\underline{p}}{argmin} \left[\sum_{k=1}^{N_{LL}} \left(w_k r_k(\underline{p}) \right)^2 \right] \\ &= \underset{\underline{p}}{argmin} \left[\left(\underline{\Delta} - \underline{\Delta M}(\underline{p}) \right)^T W \left(\underline{\Delta} - \underline{\Delta M}(\underline{p}) \right) \right] \end{aligned} \tag{4.4}$$

where W is the diagonal $[N_{LL} \times N_{LL}]$ matrix, whose elements are simply data weights w_k. Parameter values obtained from equation (4.2.2) are referred to weighted non-linear least square (WNLLS) estimations of ASL standard model parameters. The intial values of parameters, required by nonlinear estimation algorithm to initialize iterative resolution scheme, were set to accepted physiological values.

4.2.3 Bayesian inference with ASL data

As it will be shown in section (risultati), the traditional model fitting approach that makes use of WNLLS estimate experiences some problems when it is applyied to ASL data. Model nonlinearity coupled with low SNR data points could easily lead to local optimum solutions, or to the lack of convergence of non linear estimator. This unwanted behaviour, at a fixed SNR level, is the more likely the more is the number of parameters to be estimated. This implies that with WNLLS estimation, particular care must be paid to the number of unknown parameters included in the model, an usually with dynamic data no more than two parameters (f and Δt) are estimated. The aim of extracting useful information form data is thus limited by these numerical issues, and as consequence local parameters, such as T_{1t} (and τ for PASL data), are fixed to a whole brain unique value. When there is no valid reason to fix them (for expample with Q2-TIPS, τ can be sperimentally determined with good roboustness), it inevitabily introduces bias in f (and Δt) estimates. In the context of ASL data fitting, a more powerful approach to model inference, such as bayesian approach, can lead to a strong improvments as concern the capability to obtain more reliable estimates and add an important informtion on the precision of each estimate (an example can be found in [22]).

In the basic bayesian inference problem there is a series of measurements $\underline{y}$ that are to be used to determine the parameters $\underline{p}$ of chosen

model $\mathcal{M}$. The gain beside least squares estimation is that information on parameters (or some of them), ideally independent on experimental measurements, are available somehow, and can be exploited to improve parameters estimation. The method is based on Bayes theorem:

$$P(\underline{p} \mid \underline{y}, \mathcal{M}) = \frac{P(\underline{y}, \underline{p} \mid \mathcal{M})}{P(\underline{y} \mid \mathcal{M})} = \frac{P(\underline{y} \mid \underline{p}, \mathcal{M})P(\underline{p} \mid \mathcal{M})}{P(\underline{y} \mid \mathcal{M})}$$

which gives the posterior probability of the parameters given data and model, $P(\underline{p} \mid \underline{y}, \mathcal{M})$, in terms of: the likelihood of the data given the model and its parameters $\underline{p}$, $P(\underline{y} \mid \underline{p}, \mathcal{M})$, the prior probability of the parameters for the model, $P(\underline{p} \mid \mathcal{M})$, and the evidence for the measurements given the chose model, $P(\underline{y} \mid \mathcal{M})$. A more familiar expression for Bayes theorem, already referred to ASL data, is given by:

$$P(\underline{p} \mid \underline{\Delta}) = \frac{P(\underline{\Delta} \mid \underline{p})P(\underline{p})}{P(\underline{\Delta})} \tag{4.5}$$

where measured data $\underline{y}$ are formed by signal difference $\underline{\Delta}$, and where the dependance upon the model used is implicity assumed.

As previously noted, the key advantage of the bayesian approach is that a priori information about the parameters based on physiologic or physics knowledge can be incorporated in estimation procedure.

Parameters estimation in a bayesian framework can be obtain also without the need of evaluate the entire posterior porbability distribution which is a high computationally demanding step. Numerical methods as variational Bayes and Markov Chain Monte Carlo, have to be employed since analitycal forms for posterior are admitted only in few simple cases. In fact, bayesian inference can be accomplish simply extracting from $P(\underline{p} \mid \underline{\Delta})$ puntual estimates and their (approximated) variance. When this kind of approach is performed, the terms that do not depend on the parameters in (4.5) can be discarded, that is the normalization factor provided by the evidence term $P(\underline{\Delta})$ is ignored, leaving:

$$P(\underline{p} \mid \underline{\Delta}) \propto P(\underline{\Delta} \mid \underline{p})P(\underline{p}) \tag{4.6}$$

$P(\underline{\Delta} \mid \underline{p})$ is calculated form the model, in particular it depends on the statistical description of noise vector $\underline{v}$, and $P(\underline{p})$ incorportaes prior knowledge of the parameter values and their variability.

A number of puntual estimator can be obtained from (4.6), such as minimum variance (MV) estimator, and maximum a posteriori (MAP) estimator. In this work maximum a posteriori (MAP) criterion is used to obtain parameters estimation within a bayes framework. Adopting MAP

criterion, the primary interest is on the location of the maximum of the posterior probability, i.e. parameters estimated values are those which maximize the posterior probability distribution $P(\underline{p} \mid \underline{\Delta})$. Maximum a posteriori criterion is mathematically expressed by:

$$\underline{p}^{MAP} = \underset{\underline{p}}{argmax} \left[P(\underline{p} \mid \underline{\Delta})\right] = \underset{\underline{p}}{argmax} \left[P(\underline{\Delta} \mid \underline{p})P(\underline{p})\right] \tag{4.7}$$

A straightforward interpretation of expression (4.7) is to view $\underline{p}^{MAP}$ rendered by MAP criterion as maximum likelihood estimates balanced by the a priori information, condensated in the prior probabilty term $P(\underline{p})$.

In this study an informative prior is associated to T_{1t}. This parameter well fits with the requirements of bayesian schemes. Infact it is a local tissue parameter, having a certain degree of variability, but it is also widely charctarized in MRI studies and so strong prior knowledge is available for it. Generally, equilibrium magnetization of blood (M_{0b}) is considered a fixed parameters in ASL data quantification. However, it is always obtained undirectly form tissues other than brain, and with procedures that introduce variability and uncertains on it. All these aspects can be accounted for defining an appropriate prior distribution for this parameter. Physiological parameters such as f, Δt, and τ (only for PASL data) are considered not subject to a-priori information, and thus their estimation relies only on data (uninformative priors are used for them).

As LS approach, MAP bayesian approach involves the resolution of a nonlinear optimization problem. The details of problem formulation and resolution will be exposed in 4.2.4, while the procedures used to define prior distributions on parameters T_{1t} and M_{0b} are explained below.

Longitudinal magnetization relaxation time: T_{1t}

Tissue longitudinal relaxation time T_{1t} is usually considered a fix parameters in ASL model inference. Although it is a well known parameters and accurate measures are available for it, conceptually T_{1t} represents a potentially local parameter variable in relation to type and state of local tissue. Other sources of variability in T_{1t} could be introduced by the LL used for imaging in this study. Flip angle is treated as a fixed parameters, set to its nominal value. Discrepancies, that field inhomogeneities introduce, between the nominal flip angle value and the flip angle that is actually expericenced by local tissue, could be somehow accounted by admitting local variability on T_{1t} values. Physiological and

experimental knowledge therefore suggest that a more refined ASL data quantification approach should include T_{1t} in the vector of unkown parameters, allowing it to be estimated from data.

To regularize T_{1t} estimation in face of all this confounding factors, a prior distribution was introduced for this parameter: a lognormal prior shape was chosen. Lognormal distribution is a probability distribution of a random variable whose logarithm is normally distribuited. Then, if T_{1t} is lognormally distribuited, the former definitions gives:

$$T_{1t} \sim LN(\cdot\,,\cdot) \Longleftrightarrow \exists X \sim N(\mu_{T_{1t}}, \sigma^2_{T_{1t}}) \mid T_{1t} = \mathsf{e}^X \tag{4.8}$$

where it is shown as T_{1t} prior distribution can be completely defined by mean and variance of the associated normal distribution, $\mu_{T_{1t}}$and $\sigma^2_{T_{1t}}$. T_{1t} a-priori probability density function is thus given by:

$$P(T_{1t}, \mu_{T_{1t}}, \sigma_{T_{1t}}) = \frac{1}{T_{1t}\sqrt{2\pi}\,\sigma_{T_{1t}}} \mathsf{e}^{-\frac{1}{2}\left(\frac{ln(T_{1t})-\mu_{T_{1t}}}{\sigma_{T_{1t}}}\right)^2} \tag{4.9}$$

Lognormal shape for T_{1t} prior was chosen to accomodate the pronounced right tail showed by the distribution of T_{1t} estimates with WNLLS. Moreover, lognormal prior has the appealing property, stated by (4.8), of ensure the non negativity of the estimated T_{1t} values. The prior was designed so that its most probable value (the mode), given by $\mathsf{e}^{\mu-\sigma^2}$ in a lognormal distribution, would be $1.3s$, the commonly accepted value at 3T for longitudinal magnetization relaxation time in GM [22], while the variance was set empirically form a grid of plausible $\sigma^2_{T_{1t}}$ (variance of normal associated sitribution). In detail, starting from a grid of ascending $\sigma_{T_{1t}}$ value, $[0.1,\ 0.3,\ 0.5,\ 0.7]$, a set of four prior was built with a mean $\mu_{T_{1t}}$ that satisfaced the constrain on distibution mode:

$$max(P(T_{1t})) = 1.3 = \mathsf{e}^{\mu-\sigma^2} \Longrightarrow \mu_{T_{1t}} = ln\,(1.3) + \sigma^2_{T_{1t}}$$

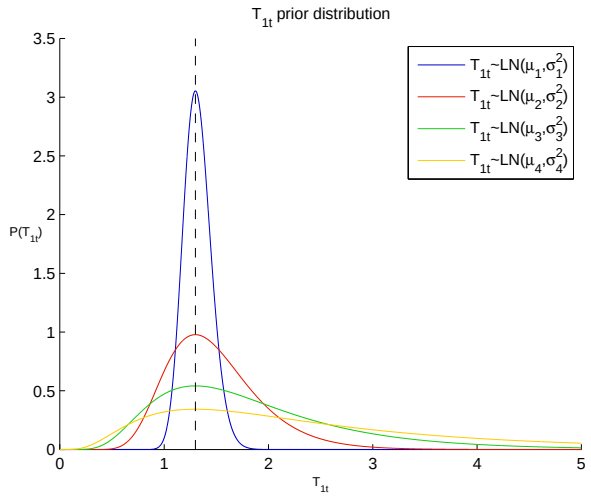

Figure 4.1: set of priors used for T_{1t} bayesian approach estimation in standard ASL model. Lognormal priors are difined in term of μ_k and σ_k^2, mean and variance of associated normal distributions. The standard deviation, σ_k, take values in grid $[0.1,\ 0.3,\ 0.5,\ 0.7]$, that progressively flattering prior distribution. As consequence the weight of prior information in MAP estimation is reduced. The mean μ_k is constrained to produce a mode in lognormal distribution equal to $1.3s$, (GM T_{1t} value at 3T), so taking values $[0.272,\ 0.352,\ 0.512,\ 0.7524]$.

Parameters vector $\underline{p}$ was evaluated for each of the prior designed. The the choice of the proper prior was done afterwards, comparing standard deviation of every T_{1t} prior distribution with the standard deviation showed by a T_{1t} estimated values distriubtion (on a meaningful group of voxel) deriving from the use of that prior. This was done essentially to guarantee an adequate balance among prior strenght (governed by its variance) and adherence to data. The group of voxels where T_{1t} estimates distributions were evaluated is said to be meaningfull because those voxel were selected using a method (see appendix mappe di score) that approximatively sample them form GM areas, where the prior is intended to be effective.

Arterial blood equilibrium magnetization: M_{0b}

ASL method rely on correct measurement of the arterial blood equilibrium magnetization M_{0b}, that convert relative perfusion estimates in absolute perfusion unit measurements. M_{0b} has been previuosly defined as the equilibrium magnetization of a voxel fully filled by arterial blood and, it is the most important scaling factor in any ASL experiments for quantitative measure of CBF: any error in M_{0b} will propagate

directly to the uncertainity in the perfusion estimate.

However, in practice it is difficult to measure accurately such parameter. The typical spatial resolution whereby ASL images are acquired (about $3 - 4mm^3$) is too coarse to find vessels voxels that are totally filled with arterial blood, and so partial volume effects with sorrounding tissue play an influential role on this kind of measurament. A lot of methods can be adopted to circumvents these problems entailed in M_{0b} determination. The basic idsea underlies the major part of these methods is to measure equilibrium magnetization in a different type of tissue, and then correct it with proper scaling coefficient dependent on blood properties [*ref]. In this study arterial blood equilibrium magnetization M_{0b} was derived via estimation of more easily measured cerebrospinal fluid equilibrium magnetization, M_{0csf}.

M_{0csf} was obtained extracting, from a manual selected ROI, the magnitude of the fully relaxed CSF signal in the proton density image (M_0 images). The ROI was drawn so that it accurately bordered ventricule areas where fully CSF voxels are likely to be found. All image slices were considered in ROI determination, but it were effectively drawn only in those slices where ventricules appeared clearly visible. M_{0csf} value has to be corrected for the different proton density and transverse relaxation time of the blood compared to the values of CSF. It was done using:

$$M_{0b} = RM_{0csf}\mathrm{e}^{\Delta R_2^* TE} \tag{4.10}$$

where R is the proton density ratio of CSF to blood, defined as $R = \frac{\rho_b}{\rho_{csf}}$ and equal to $0.87\frac{mL}{mL}$ [*ref], and ΔR_2^* is the difference in transverse relaxation rate (the inverse of tranverse relaxation time T_2^*) bewtween CSF and blood, given by $\Delta R_2^* = \frac{1}{T_{2csf}^*} - \frac{1}{T_{2b}^*}$, in which T_{2csf}^* was set to $74.9ms$, whereas $T_{2b}^* = 43.6ms$ was used for blood [19]. The transverse relaxation time of blood is difficult to measure in vivo, indeed its value is obtain from an analytical expression in which $T_{2b}^*$is function of blood oxygentaion level, fixed in this case to 75% that corresponds approximately to the oxigention level in the capillaries. It should be noted that expression (4.10) is applicable, with properly correction factor, also when $M_{0b}$is derived form other tissue than CSF, as could be global WM, local tissue or venous blood from sagittal sinous [*ref].

Usually a unique value for M_{0b} is obtain from an average value of M_{0csf} inside the selected ROI (and this was effectively done with WNLLS estimator). In particular CSF signal does lend itself to this procedure, being a very stable signal with limited intra and inter subject variability. Thus, deriving equilibrium arterial blood magnetization form CSF

measures is an approach that well agrees with the exposed theory of standard model, which asserts that M_{0b} is a single global scaling factor for all voxels, being a blood properties. However, CSF equilibrium magnetization might show a certain degree of variability which reflects onto M_{0b} estimates, despite its attractive stability. This variability associated to CSF equilibrium signal M_{0csf} is due to different aspects: (a) voxels selected as candidates of fully CSF unit of volume could show different degree of partial volume effects whenever ROI selection is performed manually from proton density images, without any help from anatomical images (b) the sensivity of the imaging coil could be subject to spatial variation (expecially at high field), causing differeces in measured signal among CSF filled voxels (ideally this aspect should be corrected by the acquisiton and subsequent normalization of coil sensitivity images) [19].

In this study corrections for variability in CSF singal was not performed. CSF signal variability was just taken into account by adopting a conceptually simple strategy: M_{0b} was considered as an unknown parameter subjects to a prior information extracted from CSF user dependent ROI. That is bayesian inference was apllied also in M_{0b}, so that the primary role played by this parameter could be addressed in a more reliable way, allowing limited oscillations of its value to occour. The prior distribution for M_{0b} was completely data driven. In particular, M_{0csf} ROI voxel values were converted into M_{0b} values using (4.10). manual ROI was then progressively depured using a thresholding procedure based on a CSF-score map, that quantify quality of each voxel in the ROI as CSF sample (see appendix CSF score). The selectivity of the thresholding was increased untill the distribution of blood magnetization voxel values resemble a normal distribution, condition that was validated through a statistic test of gaussianity. Lilliefors test with significance level α set to 5% was used (for a complete descriprion of the procedure used to validate M_{0b} prior see figure 5.5). Mean and standard deviation of distibutions obtianed from the validated subset of the initial ROI was used as mean $\mu_{M_{0b}}$ and standard deviation $\sigma_{M_{0b}}$of the prior normal distribution associated to parameters M_{0b}. A-priori information on equilibrium magnetization of arterial blood was described by:

$$M_{0b} \sim N(\mu_{M_{0b}}, \sigma^2_{M_{0b}}) \tag{4.11}$$

CSF score map.

4.2.4 Implementing bayesian inference

Let consider the voxelwise model described by (4.1), using a vector notation:

$$\underline{\Delta} = \underline{\Delta M}(\underline{p}) + \underline{v}$$

The meaning of vectors $\underline{\Delta}$ and $\underline{\Delta M}(\underline{p})$ has been previously defined. When a bayesian approach is performed, also a stitistical description of random error vector is required. In this study the common assumption on vector $\underline{v}$ were taken: random error vector $\underline{v}$ were considered to be a relization of an additive withe gaussian noise (AWGN) process, with zero mean and covariance $[N_{LL} \times N_{LL}]$ matrix given by:

$$\Sigma_v = \begin{bmatrix} \sigma_1^2 & & \\ & \ddots & \\ & & \sigma_{N_{LL}}^2 \end{bmatrix}$$

Note that the variance of random the process describing $\underline{v}$ is not constant over time. Statistical description given to random error vector can be condensated in:

$$\underline{v} \sim N(\underline{0}, \Sigma_v).$$

In bayesian framework, vector $\underline{p}$ contained the parameters to be estimated with MAP criterion, that were:

$$\begin{aligned} \underline{p} &= [f,\, T_{1t},\, \Delta t,\, \tau,\, M_{0b}]^T \qquad \text{[PASL]} \\ \underline{p} &= [f,\, T_{1t},\, \Delta t,\, M_{0b}]^T \qquad \text{[pCASL]} \end{aligned} \tag{4.12}$$

for PASL and pCASL data respectively. These were essentially the same vectors defined for WNLLS estimation, updated by the appending of M_{0b}, considered now unkown. As largely explained above, a priori distributions were considered informative only for parameters T_{1t} and M_{0b}, while for the other parameters. This can be formally handled by associating to these parameters generic prior distributions (e.g.. normal) with infinite variance. Pratically it means to use a flat prior that allows parameter to take any values with the same probability:

$$\begin{aligned} T_{1t} &\sim LN(\mu_{T_{1t}},\, \sigma_{T_{1t}}) \\ M_{0b} &\sim N(\mu_{M_{0b}},\, \sigma_{M_{0b}}) \\ f,\, \Delta t,\, \tau &\sim N(\cdot,\, \infty) \quad \text{uninformative priors} \end{aligned} \tag{4.13}$$

A general statistical description of a-priori information on paramenters vector $\underline{p}$ can be given in terms of mean vector $[M \times 1]$, and covariance

matrix $[M \times M]$:

$$\underline{\mu_p} = \begin{bmatrix} \cdot \\ \mu_{T_{1t}} \\ \cdot \\ \cdot \\ \mu_{M_{0b}} \end{bmatrix} \qquad \Sigma_p = \begin{bmatrix} \infty & & & & \\ & \sigma^2_{T_{1t}} & & & \\ & & \infty & & \\ & & & \infty & \\ & & & & \sigma^2_{M_{0b}} \end{bmatrix} \tag{4.14}$$

where the mean vector and covariance matrix are written respecting the same order used in parameters vector definition (4.12) (note that the sizes of (4.14) are referred to PASL data, i.e. $M = 5$). Σ_p definition implictly assumes statistical independence of parameters, denoted by null off-diagonal elements, while the absence of useful prior knowledges for some parameters is highlighted by the infinity variance elements.

The set of optimal parameters defined by MAP criterion are those that maximize the posterior probability of parameters given the data (the objective function in MAP estimations). Remembering considerations that lead to [4.6], $\underline{p}^{MAP}$is given by:

$$\begin{aligned} \underline{p}^{(MAP)} &= \underset{\underline{p}}{argmax} \left(P(\underline{p} \mid \underline{\Delta}) \right) \\ &= \underset{\underline{p}}{argmax} \left(P(\underline{\Delta} \mid \underline{p}) P(\underline{p}) \right) \end{aligned} \tag{4.15}$$

where the likelihood function $P(\underline{\Delta} \mid \underline{p})$, under assumption of indepenedce between vector parameters $\underline{p}$ and noise vector $\underline{v}$ and acccording to random error vector $\underline{v}$ statistical description is a multivariate normal distribution:

$$\begin{aligned} P(\underline{\Delta} \mid \underline{p}) &= N(\underline{\Delta M}(\underline{p}), \Sigma_v) \\ &= \frac{1}{\sqrt{(2\pi)^{N_{LL}} det\left[\Sigma_v\right]}} \mathsf{e}^{-\frac{1}{2}(\underline{\Delta} - \underline{\Delta M}(\underline{p}))^T \Sigma_v^{-1} (\underline{\Delta} - \underline{\Delta M}(\underline{p}))} \end{aligned} \tag{4.16}$$

and the prior probability $P(\underline{p})$ can be expressed as the product of single parameter probability distribution (see equations (4.13)), as consequence of having assumed parameter a-priori distributions to be statistically indipendent:

$$\begin{aligned} P(\underline{p}) &= \prod_{m=1}^{M} P(p_m) = P(T_{1t}) P(M_{0b}) P(\underline{p}^{ni}) \\ &= \frac{1}{T_{1t}\sqrt{2\pi}\,\sigma_{T_{1t}}} \mathsf{e}^{-\frac{1}{2}\left(\frac{ln(T_{1t}) - \mu_{T_{1t}}}{\sigma_{T_{1t}}}\right)^2} \frac{1}{\sqrt{2\pi}\,\sigma_{M_{0b}}} \mathsf{e}^{-\frac{1}{2}\left(\frac{M_{0b} - \mu_{M_{0b}}}{\sigma_{M_{0b}}}\right)^2} P(\underline{p}^{ni}) \end{aligned} \tag{4.17}$$

In above eqaution, $\underline{p}^{ni}$ indicates the subset of parameters for which no a-priori knowledge is assumed ($\underline{p}^{ni} = [f, \Delta t, \tau]$ for PASL data or $\underline{p}^{ni} = [f, \Delta t]$ for pCASL data). It automatically means that $P(\underline{p}^{ni})$ takes a costant value whatever value the parameters subset $\underline{p}^{ni}$ assumes ($P(\underline{p}^{ni}) = K, \forall \underline{p}^{ni} \in \mathbb{R}^{3(2)\times 1}$). Taking together (4.16), (4.17) and combining them into (4.15), optimal MAP parameter values are given by:

$$\begin{aligned}
\underline{p}^{MAP} &= \underset{\underline{p}}{argmax} \left[P(\underline{\Delta} \mid \underline{p})P(\underline{p})\right] \\
&= \underset{\underline{p}}{argmax} \left[\frac{\mathrm{e}^{-\frac{1}{2}(\underline{\Delta}-\underline{\Delta M}(\underline{p}))^T \Sigma_v^{-1}(\underline{\Delta}-\underline{\Delta M}(\underline{p}))}}{\sqrt{(2\pi)^{N_{LL}} det\left[\Sigma_v\right]}} \frac{\mathrm{e}^{-\frac{1}{2}\left(\frac{ln(T_{1t})-\mu_{T_{1t}}}{\sigma_{T_{1t}}}\right)^2}}{T_{1t}\sqrt{2\pi}\,\sigma_{T_{1t}}} \frac{\mathrm{e}^{-\frac{1}{2}\left(\frac{M_{0b}-\mu_{M_{0b}}}{\sigma_{M_{0b}}}\right)^2}}{\sqrt{2\pi}\,\sigma_{M_{0b}}} P(\underline{p}^{ni})\right] \\
&= \underset{\underline{p}}{argmax} \left[\frac{\mathrm{e}^{-\frac{1}{2}(\underline{\Delta}-\underline{\Delta M}(\underline{p}))^T \Sigma_v^{-1}(\underline{\Delta}-\underline{\Delta M}(\underline{p}))} \mathrm{e}^{-\frac{1}{2}\left(\frac{ln(T_{1t})-\mu_{T_{1t}}}{\sigma_{T_{1t}}}\right)^2} \mathrm{e}^{-\frac{1}{2}\left(\frac{M_{0b}-\mu_{M_{0b}}}{\sigma_{M_{0b}}}\right)^2}}{T_{1t}\sqrt{(2\pi)^{N_{LL}+2} det\left[\Sigma_v\right]}\,\sigma_{M_{0b}}\sigma_{T_{1t}}}\right]
\end{aligned} \tag{4.18}$$

where the costant value assumed by factor $P(\underline{p}^{ni})$ (independent form parameters as consequence of flat priors adopted) permits to discars it from the optimization function. The objective function is given by the product of non-negative monotonic functions (probability distribution), so taking the natural logarithm of (4.18) will not change the global optimum. This reduces objective function into a form more suitable for numerical methods used to resolve optimization problem, and permits to depure the expression from terms that not include parameters, yielding:

$$\begin{aligned}
\underline{p}^{MAP} &= \underset{\underline{p}}{argmax} \left[ln\left(P(\underline{\Delta} \mid \underline{p})P(\underline{p})\right)\right] \\
&= \underset{\underline{p}}{argmax} \left[-\frac{1}{2} \parallel \underline{\Delta} - \underline{\Delta M}(\underline{p}) \parallel^2_{\Sigma_v^{-1}} -\frac{1}{2}\left(\frac{M_{0b}-\mu_{M_{0b}}}{\sigma_{M_{0b}}}\right)^2 - \frac{1}{2}\left(\frac{ln(T_{1t})-\mu_{T_{1t}}}{\sigma_{T_{1t}}}\right)^2 - ln(T_{1t}\right.
\end{aligned} \tag{4.19}$$

$$\underline{p}^{MAP} = \underset{\underline{p}}{argmin} \left[\underbrace{\frac{1}{2} \parallel \underline{\Delta} - \underline{\Delta M}(\underline{p}) \parallel^2_{\Sigma_v^{-1}}}_{\text{fidelity to data}} + \underbrace{\frac{1}{2}\left(\frac{M_{0b}-\mu_{M_{0b}}}{\sigma_{M_{0b}}}\right)^2}_{\text{normal prior}} + \underbrace{\frac{1}{2}\left(\frac{ln(T_{1t})-\mu_{T_{1t}}}{\sigma_{T_{1t}}}\right)^2 + ln(T_{1t})}_{\text{lognormal prior}}\right] \tag{4.20}$$

It represents the final form of the cost function when MAP criterion is applied to obtain optimal model parameters value in a bayesian framework. It emerges from the general assumptions that has been made:

(a) unknown parameters $\underline{p}$ were independent form noise statisical description, and (b) statistical independence between parameters to be estimated. The meaning of the different terms that contribuite to general cost function can be clearly recognized: the first represents cost function to be minimized when simple WNLLS approach is used for parameters estimation, second terms represents the penalty due to normal prior on M_{0b} and the third contributions (third and fourth terms) is the penalty due to lognormal prior on T_{1t}. Note that as long as assumption (a) and (b) are valid, prior knowledge on other parameters can be inserted in the computation simply by adding an appropriate (normal or lognormal) terms inside the cost function (4.20).

Equation (4.20) shows that $\underline{p}^{MAP}$ evaluation requires the knowledge of Σ_v. Noise covariance matrix were modeled as follow:

$$\Sigma_v = \sigma^2 B$$

where matrix B is kwnown, set to the inverse of weights matrix W used in WNLLS, $B = W^{-1}$, while σ^2 is an unknown scaling factor that had to be estimate a-posteriori. Unbiased estimator of σ^2 is given by $\frac{WRSS}{N-M}$, where $WRSS$ (weighted residuals sum of square) is $\| \underline{\Delta} - \underline{\Delta M}(\underline{p}) \|^2_{B^{-1}}$ evaluated at its minimum. In the bayesian framework adopted in this study, σ^2 a-posteriori estimation required an iterative schemes since every modification of σ^2 altered cost function optimum due to the presence of priors terms in addition to residuals sum of squares, and new value of $\underline{p}^{MAP}$ should be updated. σ^2 can be though as correction on realtive weight of data respect to a-priori information in MAP cost function (4.20). The following scheme was used to determine σ^2 and the final estimations for parameters:

$$\Sigma_v^{(0)} = B \quad \text{(initialization)}$$

$$\Downarrow$$

$$\underline{p}^{MAP(0)} \Rightarrow \sigma^{2(0)} = \frac{WRSS}{N-M} \Rightarrow \Sigma_v^{(1)} = \sigma^{2(0)}\Sigma_v^{(0)} \Rightarrow \text{condition on } \sigma^{2(0)}? \quad \text{(iteration 1)}$$

$$\Downarrow$$

$$\underline{p}^{MAP(1)} \Rightarrow \sigma^{2(1)} = \frac{WRSS}{N-M} \Rightarrow \Sigma_v^{(2)} = \sigma^{2(1)}\Sigma_v^{(1)} \Rightarrow \text{condition on } \sigma^{2(1)}? \quad \text{(iteration 2)}$$

$$\Downarrow$$

$$\dots$$

At every step, covariance matrix were updated by a new a-posteriori $\sigma^{2(k)}$ correction. The termination condition were met when the last cor-

rection factor was considered uneffective, that is $0.95 \leq \sigma^{2(k)} \leq 1.05$. The final parameters vector estimation was given by $\underline{p}^{MAP(k)}$ and the a-posteriori σ^2 estimation was given by:

$$\sigma^2 = \prod_{i=0}^{k-1} \sigma^{2(i)}$$

where k was the iteration number where output condition was met. A further exit condition was introduced, to limit the maximum number of iteration to $k = 5$.

The knowledge of noise covariance matrix Σ_v make possible also the measure of the uncertainty of estimates. Cramer-Rao inequality [23] estabilishes a lower bound for covariance matrix of estimates, $\Sigma_{p^{MAP}}$, and expresses it in terms of Fisher matrix information, $F(\underline{p})$, evaluated at optimal parameters vector value $\underline{p}^{MAP}$:

$$\Sigma_{p^{MAP}} \geq \left[F(\underline{p}^{MAP})\right]^{-1} = (S^T \Sigma_v^{-1} S + \Sigma_p)^{-1} \tag{4.21}$$

where S is sensitivity matrix of dimensions $[N_{LL} \times M]$, whose generic element at position$[i, j]$ is given by $\left[\frac{\partial \Delta M(t_i, \underline{p})}{\partial p_j}\right]$. The equivalence at second member of (4.21) holds if random vectors $\underline{p}$ and $\underline{v}$ are gaussian. This condition were not satistfy because T_{1t}, belonging to parameters vector, were supposed to be lognormally distribuited. However, equation (4.21) was considered likewise, because lognormal distributions with mean far from zero can be well approximated by normal distributions. Variance of estimated parameters were approximated to the second to member of (4.21), thus ignoring inequalities and giving an understimation of actual estimates uncertainity. This can be viewed as a Laplace approximation on the posterior distribution, which is forced to be a multivariate normal distribution with covariance matrix $\Sigma_{p^{MAP}}$ in the corrsipondence of its maximum [4]. Beyond all these considerations, the effect of a-priori knowledge inclusion on prameters model identification is clearly visible: the final estimate of $\underline{p}^{MAP}$ shows smaller variance than when no prior information is used (that ideally yields $\Sigma_p^{-1} = \underline{0}$).

Implementing MAP in MatLab

MAP estimation of model parameters was performed by minimization of cost function (4.20), which is essentially the cost function of WNLLS data fitting approach complicated by the presence of prior terms. The estimation availed of MatLab function lsqnonlin(), a powerful tool

to solve nonlinear leat squares problems when no close-form solutions are admitted. In detail, lsqnonlin() computes the minumum with respect to parameters of a function made up by a sum of squares. This sum of squares is essentially the euclidean norm of a vector coming form the evaluation of an input function $f(t, \underline{p})$ at series of time point $t_1, t_2, \ldots, t_{N_{LL}}$, nothimg but the acquisition time points of the experimet. To meake it clear, in data fitting problems $f(t, \underline{p})$ is simply the residuals, i.e. discrepances between observed data and model predictions (eventually normalized by proper weights). Hence, lsqnonlin() formalizes minimization problem as:

$$\begin{aligned} \underline{p}^{LSQ} &= \underset{\underline{p}}{argmin} \left[\| \, f(\underline{t}, \underline{p}) \, \|^2 \right] \\ &= \underset{\underline{p}}{argmin} \left[f(t_1, \underline{p})^2 + \ldots + f(t_{N_{LL}}, \underline{p})^2 \right] \end{aligned}$$

where $f(t_k, \underline{p})$ can be interpreted as the element k of the vector:

$$\underline{f}(\underline{p}) = \begin{bmatrix} f_1(\underline{p}) \\ f_2(\underline{p}) \\ \vdots \\ f_{N_{LL}}(\underline{p}) \end{bmatrix}$$

If MAP estimation has to be solved using lsqnonlin, its cost function needs to be expressed as a sum of squares so that the appropriate vector $f(\underline{p})$ to pass to lsqnlin() can be easily extracted. This requirement ideally could be satisfacted in a straightforward manner by taking the square roots of each terms in (4.20) to form vector $\underline{f}$. Unfortunately, the lognormal prior, in particular the term $ln(T_{1t})$, hindered a non trivial complications. The natural choiche would lead to treat $ln(T_{1t})$ as the square of an hypothetical element vector $\sqrt{ln(T_{1t})}$. This solution was not accomplishable becasue likely to provoke the arrest of the computation, since negative values for $ln(T_{1t})$ (forbidden with $\sqrt{\cdot}$ operator) could be reached during optimization (at each iterations lsqnonlin evaluates vector $\underline{f}(\underline{p})$). It happened whenever T_{1t} assumed values inferior to $1s$, which was a very common situation since T_{1t} excepted values for WM and GM fall right on this critical value: at 3T T_{1t} is known to be about $0.9s$ and $1.3s$ for WM and GM respectively. For these reasons the term associated to lognormal prior has to be riarranged so that it could be expressed as a sqared term.

Let K be the set of lognormal terms in [4.20], it can be elaborated as follow:

$$
\begin{aligned}
K &= ln(T_{1t}) + \frac{1}{2}\left(\frac{ln(T_{1t}) - \mu_{T_{1t}}}{\sigma_{T_{1t}}}\right)^2 \\
&= ln(T_{1t}) + \frac{1}{2\sigma^2_{T_{1t}}}\left(ln^2(T_{1t}) - 2ln(T_{1t})\mu_{T_{1t}} + \mu^2_{T_{1t}}\right) \\
&= \frac{1}{2\sigma^2_{T_{1t}}}\left(2\sigma^2_{T_{1t}} ln(T_{1t}) + ln^2(T_{1t}) - 2ln(T_{1t})\mu_{T_{1t}} + \mu^2_{T_{1t}}\right) \\
&= \frac{1}{2\sigma^2_{T_{1t}}}\left(ln^2(T_{1t}) + 2ln(T_{1t})(\sigma^2_{T_{1t}} - \mu_{T_{1t}}) + \mu^2_{T_{1t}}\right) \qquad (4.22)
\end{aligned}
$$

The overall goal is to reduce K to a squared form like $Cg(\underline{p})^2$, with C scalar coefficient and $g(\underline{p})$ a scalar function of model parameters vector. Then the element of vector $\underline{f}$ (input vector of lsqnonlin()) associated to lognormal prior would be clearly defined, simply it would be $\sqrt{K} = \sqrt{C}g(\underline{p})$. The expression in bracket in (4.22) resembles the square of a binomial, but to be exactly a square of binomial it needs an adjustment. Adding and subtracting the quantity $\sigma^4_{T_{1t}} - 2\mu_{T_{1t}}\sigma^2_{T_{1t}}$ to the third term in brackets, it results:

$$
\begin{aligned}
K &= \frac{1}{2\sigma^2_{T_{1t}}}\left[ln^2(T_{1t}) + 2ln(T_{1t})(\sigma^2_{T_{1t}} - \mu_{T_{1t}}) + \mu^2_{T_{1t}} + \sigma^4_{T_{1t}} - 2\mu_{T_{1t}}\sigma^2_{T_{1t}} - \sigma^4_{T_{1t}} + 2\mu_{T_{1t}}\sigma^2_{T_{1t}}\right] \\
&= \frac{1}{2\sigma^2_{T_{1t}}}\left[\left(ln^2(T_{1t}) + 2ln(T_{1t})(\sigma^2_{T_{1t}} - \mu_{T_{1t}}) + \sigma^4_{T_{1t}} - 2\mu_{T_{1t}}\sigma^2_{T_{1t}} + \mu^2_{T_{1t}}\right) - \sigma^4_{T_{1t}} + 2\mu_{T_{1t}}\sigma^2_{T_{1t}}\right]\right] \\
&= \frac{1}{2\sigma^2_{T_{1t}}}\left[\left(ln^2(T_{1t}) + 2ln(T_{1t})(\sigma^2_{T_{1t}} - \mu_{T_{1t}}) + (\sigma^2_{T_{1t}} - \mu_{T_{1t}})^2\right) - \sigma^4_{T_{!t}} + 2\mu_{T_{1t}}\sigma^2_{T_{1t}}\right] \\
&= \frac{1}{2\sigma^2_{T_{1t}}}\left[\left(ln(T_{1t}) + (\sigma^2_{T_{1t}} - \mu_{T_{1t}})\right)^2 - \sigma^4_{T_{1t}} + 2\mu_{T_{1t}}\sigma^2_{T_{1t}}\right] \\
&= \frac{1}{2\sigma^2_{T_{1t}}}\left(ln(T_{1t}) + (\sigma^2_{T_{1t}} - \mu_{T_{1t}})\right)^2 + \frac{1}{2\sigma^2_{T_{1t}}}\left(-\sigma^4_{T_{1t}} + 2\mu_{T_{1t}}\sigma^2_{T_{1t}}\right)
\end{aligned}
$$

Combining this new expression for lognormal term into (4.20), and discarding the second part independent from parameter T_{1t} value, MAP cost function becomes a sum of squares and can now be implemented

into lsqnonlin():

$$\underline{p}^{MAP} = \underset{\underline{p}}{argmin} \left[\frac{1}{2} \parallel \underline{\Delta} - \underline{\Delta M}(\underline{p}) \parallel^2_{\Sigma_v^{-1}} + \frac{1}{2} \left(\frac{M_{0b} - \mu_{M_{0b}}}{\sigma_{M_{0b}}} \right)^2 + K \right]$$

$$= \underset{\underline{p}}{argmin} \left[\frac{1}{2} \parallel \underline{\Delta} - \underline{\Delta M}(\underline{p}) \parallel^2_{\Sigma_v^{-1}} + \frac{1}{2} \left(\frac{M_{0b} - \mu_{M_{0b}}}{\sigma_{M_{0b}}} \right)^2 + \frac{1}{2} \left(\frac{ln(T_{1t}) + (\sigma^2_{T_{1t}} - \mu_{T_{1t}})}{\sigma_{T_{1t}}} \right)^2 + \dots \right]$$

$$\left[\dots + \frac{-\sigma^4_{T_{1t}} + 2\mu_{T_{1t}}\sigma^2_{T_{1t}}}{2\sigma^2_{T_{1t}}} \right] \tag{4.23}$$

$$= \underset{\underline{p}}{argmin} \left[\underbrace{\parallel \underline{\Delta} - \underline{\Delta M}(\underline{p}) \parallel^2_{\Sigma_v^{-1}}}_{\text{fidelity to data}} + \underbrace{\left(\frac{M_{0b} - \mu_{M_{0b}}}{\sigma_{M_{0b}}} \right)^2}_{\text{normal prior}} + \underbrace{\left(\frac{ln(T_{1t}) + (\sigma^2_{T_{1t}} - \mu_{T_{1t}})}{\sigma_{T_{1t}}} \right)^2}_{\text{lognormal prior}} \right] \tag{4.24}$$

From (4.24), input vector of lsqnonlin() is directly obtain by taking the square root of each term:

$$\underline{f}(\underline{p}) = \begin{bmatrix} \frac{\Delta(t_1) - \Delta M(t_1, \underline{p})}{\sigma_1} \\ \frac{\Delta(t_2) - \Delta M(t_2, \underline{p})}{\sigma_2} \\ \vdots \\ \frac{\Delta(t_{N_{LL}}) - \Delta M(t_{N_{LL}}, \underline{p})}{\sigma_{N_{LL}}} \\ \frac{M_{0b} - \mu_{M_{0b}}}{\sigma_{M_{0b}}} \\ \frac{ln(T_{1t}) + (\sigma^2_{T_{1t}} - \mu_{T_{1t}})}{\sigma_{T_{1t}}} \end{bmatrix}$$

It shows that MAP estimation criterion can be formulated in terms of LS approach, when normal and lognormal prior distribution for model parameters is chosen. As consequence MAP optimal parameter values were achieved using MatLab function lsqnonlin(), adopting (4.24) as final cost function to be minimized.

4.2.5 Correction of vascular aritfacts: two component model

In the following section an improvment of standard model is presented. In addition to magnetization difference described by standard model equations, henceforward termed as ΔM_t as accounting for tagged blood carried into tissue, another component, ΔM_a, is added to give reason of signal from tagged blood contained into arteries that pass through the voxel. This model is called two-component ASL model. Theoretic basis of such model, definition of its equations, and application on datasets available are discussed below.

Two component ASL voxelwise model

The ASL standard model, as previously discussed, provides an oversemplified description of the system involved in the perfusion process. Principally, structural complexity of brain tissue inside the voxel and the fact that blood water can not be considered as a freely diffusible tracer are ignored, stating that voxel acts as a single well mixed compartmenent respect to blood diffusion into tissue. Thus, predictions of standard model can be totally wrong when the assumption of single well mixed compartment is far to be realized. As result, parameters estimates (first of all CBF), that derive form the fit of standard model to data, are heavly contaminated by this unsuited assumption and can not be used to extract any physiological meaningful information.

The most denotive case in which standard model fails is when ASL signal is contamined by the presence of tagged blood in arterial vessels that is destined to perfuse more distal regions. This intravascular component is particulary significant near major arteries, such as the middle cerebral artery (MCA).

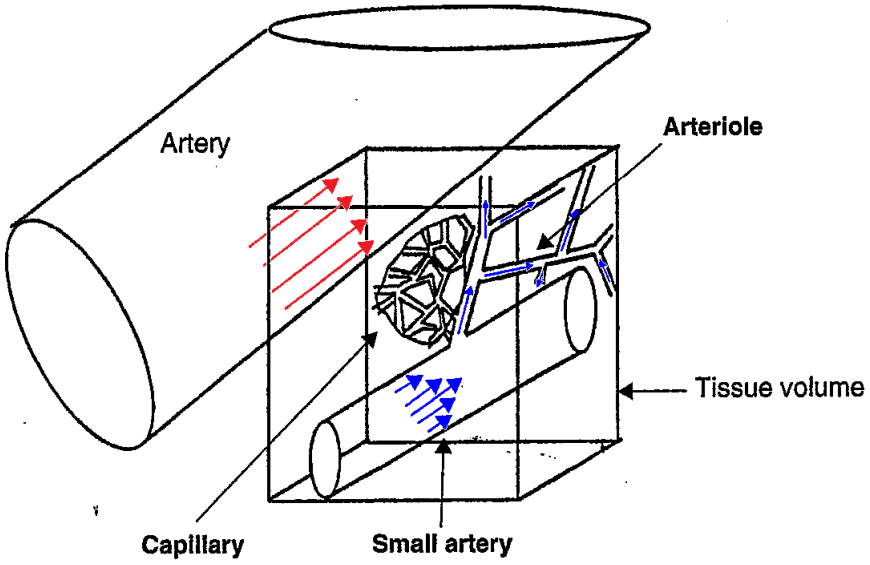

Figure 4.2: a schematic architecture of voxel is shown in figure. Contributions to ASL signal form actual perfusion blood are plotted in blue. Contributions to ASL signal form tagged blood that just passes through the voxel are shown in red. Standard model describes with a single compartment approach only the former contribution, and completely neglects the potential presence of the latter which are considered as perfusion blood to.

Here an alternative approach to correct those vascular artifacts

without compromitting the SNR of the acquired signal is proposed. It aims to explicitely model the intravascular signal and then to include it in a two component model to account for the effects of arterial spins in multi-TI ASL data. The general expression of two component model is:

$$\Delta M(t, \underline{p}, \underline{p_a}) = (1 - aBV)\Delta M_t(t, \underline{p}) + aBV\Delta M_a(t, \underline{p_a}) \tag{4.25}$$

where ΔM_t is the tissue component whose expression is given by standard ASL model and $\underline{p}$ is its vector of unknown parameter, ΔM_a is the new arterial component with vector of parameters $\underline{p_a}$, and aBV is the arterial blood volume fraction, a dimensionless number (milliliter of arterial blood per milliliters of tissue) usually expressed as a percentage of entire voxel volume.

Arterial component model equations

In the following section model equation for arterial component, $\Delta M_a(t)$ is derived, with respect to pulsed and pseudo-countinuous labeling techniques.

In general, arterial component has to represent simply the transit of the labeled blood bolus through a large artery. To model this phenomenon, an application of the general kinetic model (see section parte modelli) is not appropriate. Infact, any residue function $r(t)$ can be defined as the arterial vessels walls are impermeable (large artery do not exchange blood with tissue voxel), and the arterial blood is assumed to pass istantaneously through the voxel.

Arterial component model $\Delta M_a(t)$ is thus essentially the kinetic curve of a bolus of tagged blood that is expected in large arteries. A detailed model can be derived, incorportaing into temporal profile $w(t)$ of the labeled bolus that transit through an artery in ideal conditions, defined by the typical box-car shape:

$$w(t) = \begin{cases} 0 & t < \Delta t_a \\ 1 & \Delta t_a \leq t < \Delta t_a + \tau_a \\ 0 & \Delta t_a + \tau_a \leq t \end{cases}$$

where Δt_a is the arterial transit delay, and τ_a is arterial bolus duration, all the effects that it is expected to experience in an ASL experiment. They are decay of the label with time due to magnetization relaxation, signal attenuation operated by excitation RF pulses as the blood passes through the imaged region, and phyisiological disperison of bolus profile as it travels along vasculature, which can be properly accounted

for by definition of three functions of time,$M(t)$, $R(t)$ and $K(t)$ respectively. Availing of these functions, a general model for arterial component $\Delta M_a(t)$ is derived, adopting the convolution integral formulation given in [*ref Okell]:

$$\begin{aligned}\Delta M_a(t) &= 2\alpha M_{0b} \int_{-\infty}^{\infty} w(t-t_d)K(t_d)M(t,t_d)R(t,t_d)dt_d \\ &= 2\alpha M_{0b} \int_{t-\Delta t_a-\tau_a}^{t-\Delta t_a} K(t_d)M(t,t_d)R(t,t_d)dt_d \end{aligned} \tag{4.26}$$

The dispersion function $K(t_d)$ is a convolution kernel describing the fraction bolus of blood that arrives at the voxel level delayed by time t_d. Previous studies on dispersion occouring in ASL suggest to choiche a gamma shape kernel to model dispersion in large arteries (*ref Chappel), so $K(t)$ is given by:

$$K(t) = \frac{s^{1+sp}}{\Gamma(1+sp)} \mathrm{e}^{-st} t^{sp} \tag{4.27}$$

where s (measured in s^{-1}) characterizes the sharpness of the kernel, and p (measured in s^{-1}) indicates the time-to-peak.

$M(t,t_d)$ describes the T_1 decay experienced by the blood after labeling during its transit from the point it has been labeled to the voxel artery considered. Its definition depends, of course, on the type of labelling performed (pulsed or continuous) and also includes the additional T_1 decay during delay t_d resulting from bolus dipersion effects, so:

$$\begin{aligned} M(t,t_d) &= \mathrm{e}^{-(\frac{t+t_d}{T_{1b}})} && \text{PASL} \\ M(t,t_d) &= \mathrm{e}^{-(\frac{\Delta t_a+t_d}{T_{1b}})} && \text{pCASL} \end{aligned} \tag{4.28}$$

$R(t,t_d)$ accounts for the effects on signal amplitude form the imaging pulses used in the Look-Locker readout. Each pulse collected by blood before transit through the considered voxel reduces the longitudinal magnertization by a factor of $cos\alpha_{LL}$, where α_{LL} is the flip angle used by the LL readout. Thus, function $R(t,t_d)$ is given by:

$$R(t,t_d) = (cos\alpha_{LL})^{N(t,t_d)}$$

where $N(t,t_d)$ gives the actual number of RF pulses experienced by the blood at time t since its entrance in imaging region. For sake of semplicity, in the follow $N(\cdot,\cdot)$ dependance on t_d is ignored, which is equivalent

to considering uneffective the delays effect introduced by dispersion in the computation of the number of RF pulses experienced by blood. Even $N(t)$ expression depends on the type of labeling. In pCASL, since a the same coil is used both for labeling and imaging, during the labeling time pulses no RF excitations pulses are apllied to imaged region. So, starting from t_0, the sampling time in which the first pulses is played out, the number of previous pulses that at time t blood has been affected by is:

$$N(t) = floor\left(\frac{t - t_0}{TI_2}\right) \approx \frac{t - t_0}{TI_2} \tag{4.29}$$

where the contiunuous approximation for $N(t)$ is made, in the same manner in which LL readout pulses are incorporating into standar model (*ref. part e look locker teoria). Expression (4.29) implictly assumes that the imaging region encompasses everything distal to the labeling plane, but often there is a gap between the labeling plane and imaging region within which blood does not experience any imaging pulses. Named δt_{min} time that blood from feeding arteries takes to cross the border of imaging region, the maximum amount of time spent in the imaging region before reaching the voxel of interest is $\Delta t_a - \delta t_{min}$. This time limits the number of RF pulses experienced by the blood, so expression for $N(t)$ becomes:

$$N(t) \approx min\left\{\frac{t - t_0}{TI_2}, \frac{\Delta t_a - \delta t_{min}}{TI_2}\right\} \tag{4.30}$$

where the approximated nature of $N(t)$ must be kept in mind, furthermore remembering that effect due to dipsersion are not accounting in its evaluation.

In PASL, assigning a reliable expression to $N(t)$ is a simpler task. The inflow of labeled blood into the imaging region is entirely sampled due to the short duration of labeling phase (substantially impulsive), so all blood forming labeled bolus experiences the same number of RF pulses during the transit from the lower edge of imaging region to considered voxel. Thus, for PASL $N(t)$ is given by:

$$N(t) \approx \frac{\Delta t_a - \delta t_{min}}{TI_2} \tag{4.31}$$

Using former definitions, arterial component model $\Delta M_a(t)$ expression can be obtain just placing them (taking the right form with respect to the type of labeling) into convolution integral (4.26) and resolving it.

Solution for pCASL and PASL techniques are given by:

$$\Delta M_a(t) = 2\alpha M_{0b} \int_{t-\Delta t_a-\tau_a}^{t-\Delta t_a} K(t_d) M(t,t_d) R(t,t_d) dt_d$$
$$= 2\alpha M_{0b} \left(cos\alpha_{LL}\right)^{\frac{\Delta t_a - \delta t_{min}}{TI_2}} \mathrm{e}^{-\frac{t}{T_{1b}}} \int_{t-\Delta t_a-\tau_a}^{t-\Delta t_a} K(t_d) \mathrm{e}^{-\frac{t_d}{T_{1b}}} dt_d$$

PASL

$$\Delta M_a(t) = 2\alpha M_{0b} \int_{t-\Delta t_a-\tau_a}^{t-\Delta t_a} K(t_d) M(t,t_d) R(t,t_d) dt_d$$
$$= 2\alpha M_{0b} \left(cos\alpha_{LL}\right)^{min\left\{\frac{t-t_0}{TI_2}, \frac{\Delta t_a - \delta t_{min}}{TI_2}\right\}} \mathrm{e}^{-\frac{\Delta t_a}{T_{1b}}} \int_{t-\Delta t_a-\tau_a}^{t-\Delta t_a} K(t_d) \mathrm{e}^{-\frac{t_d}{T_{1b}}} dt_d$$

pCASL

(4.32)

where integral explicitated can be resolved analytically by manipulating solution () given in (*parte dispersione modelli) to define gamma dispersion on the delivery function of standard model $c(t)$.

Toward validation of two component ASL model

The two component model is introduced to adequately account for artifacts coming from large arteries spins signal by means of a mathematical modeling approach. Previuous studies supposed that modeling approach for those vascular artifacts could performace better than technical approach, as vascular crushing, in reduction of CBF bias introduced by macrovascular signal. However, the additional parameters the arterial component carries may be used to fit spurious data not related to arterial flow signal. To avoid overfitting, adverse for parameters estiamtes, two component model should be fitted only in those voxel where data supported it, therefore in each voxel model selection methodologies must be adopted to single out which model provides a better description of acquired signal.

These complete analysis was not performed in this study. But, exploiting the great deal of data available (crushed and uncrushed data, both for PASL and pCASL) steps toward validation of the two component model proposed were accomplished.

It was tried to show that the adoption of arterial component equation (4.32) into the two component model (4.25) is viable solution to

reasonably describe data with marked intra vascular artifact, restoring CBF estimates map into a phsyiological range of values, at least comparable with those calucalted using vascular crushed data.

The arterial model $\Delta M_a(t)$ validation was perforemd fitting the partial component $aBV\Delta M_a(t)$ to a signal given by the difference among data in which no vascular suppressions were applied (NVC data) and those acquired with vascular crushing techniques (VC data). This difference signal (NVC-VC) gives the actual portion of ASL signal crushed by the application of bipolar gradients for flow suppression, and thus can be considered as a good surrogate of the real arterial component associated to the voxel. The fitting of the single arterial model $\Delta M_a(t)$ on this "dedicated" dataset were conducted considering as unknown the following vectors of parameters (for PASL and pCASL):

$$\underline{p_a} = [aBV,\ \Delta t_a,\ \tau_a,\ p,\ s] \quad \text{PASL}$$
$$\underline{p_a} = [aBV,\ \Delta t_a,\ p,\ s] \quad \text{pCASL}$$

A set of a-priori knowledge (informative only on some of them) was considered, by adopting normal prior distributions to be used in a bayesian estimation framework (MAP). Prior distribution parameters was set to values already used in literature (*ref Chappel1, Chappell2, Okkell1), condenstaed in the following table:

	PASL	pCASL
aBV [%]	uninformative prior	uninformative prior
Δt_a [s]	$\sim N(0.3, 0.3)$	$\sim N(0.5, 0.1)$
τ_a [s]	uninformative prior	fixed to labeling duration
p [s]	$\sim N(0.05, 0.1)$	$\sim N(0.05, 0.1)$
s [s^{-1}]	$\sim N(5, 1)$	$\sim N(5, 0.5)$

Table 4.3: specifications of priors (mean and standard deviation of normal distributions) used for arterial component model fitting.

Parameter $\delta t^{(min)}$ could not be measured in this study, and it was fixed to a reasonable values. The implications of this unavoidable practice are explained in discussion chapter.

Arterial model component ΔM_a evaluated in this ideal condition, $\Delta M_a(\underline{p_a^{MAP}})$, was then traeated as a fixed contribution, Y_a, in the two compoent model:

$$\begin{aligned}\Delta M(t, \underline{p}, \underline{p_a}) &= (1 - aBV)\Delta M_t(t, \underline{p}) + \underbrace{aBV\Delta M_a(t, \underline{p_a})}_{\text{NVC}-\text{VC estimate}} \\ &= (1 - aBV)\Delta M_t(t, \underline{p}) + Y_a(\underline{p_a}^{MAP}) \end{aligned} \tag{4.33}$$

to probe the power of this modeling approach in helping standard ASL model to handle with vascular artifacts associated to typical multi-TI ASL data. The tissue contribution, $(1 - aBV)\Delta M_t(t, \underline{p})$ of the two component model, was then fitted to the NVC data, using the same estimation settings defined when standard model parameters estimation was described (see section 4.2.3). The aBV coefficient was constrained to staisfy a relation involving fixed arterial contribution amplitude A_{Y_a} and M_{0b} estimate, expressed by:

$$aBV = \frac{A_{Y_a}}{M_{0b}}$$

to assure coerent scaling between the two component estimated with separte consecutive stages.

Chapter 5

Results

In this chapter results relative to practical implementations of methods described in chapter 4.2 for ASL data quantification are presented. First of all, priors extracted using procedures previously outlined are shown. Then results of estimation procedure defined for standard model are given, with particular attention to the comparison between different labeling types and different approach to vascular signal suppression. Finally, outcomes of the two component model proposed are shown, especially highlighting the correction it introduces on CBF, whose values is addressed by the new component towards a more physiological range.

5.1 Priors definition

5.1.1 Prior on longitudinal relaxation time

The procedure used to define T_{1t} prior distribution required to perform whole model identification varying in a grid of possible lognormal priors (with different standard deviation), to select the one that best account for variability insight data. The grid of prober prior distributions has been defined in section 4.2.3. In brief, distributions mode were fixed to $1.3s$ while standard deviation was allowed to vary from $0.1s$ to $0.7s$ with increasing step of 0.2s.

In figure (5.1), T_{1t} parametric maps and their distributions (over a specific group of voxels) for each prior designed are shown (a representative subject is considered):

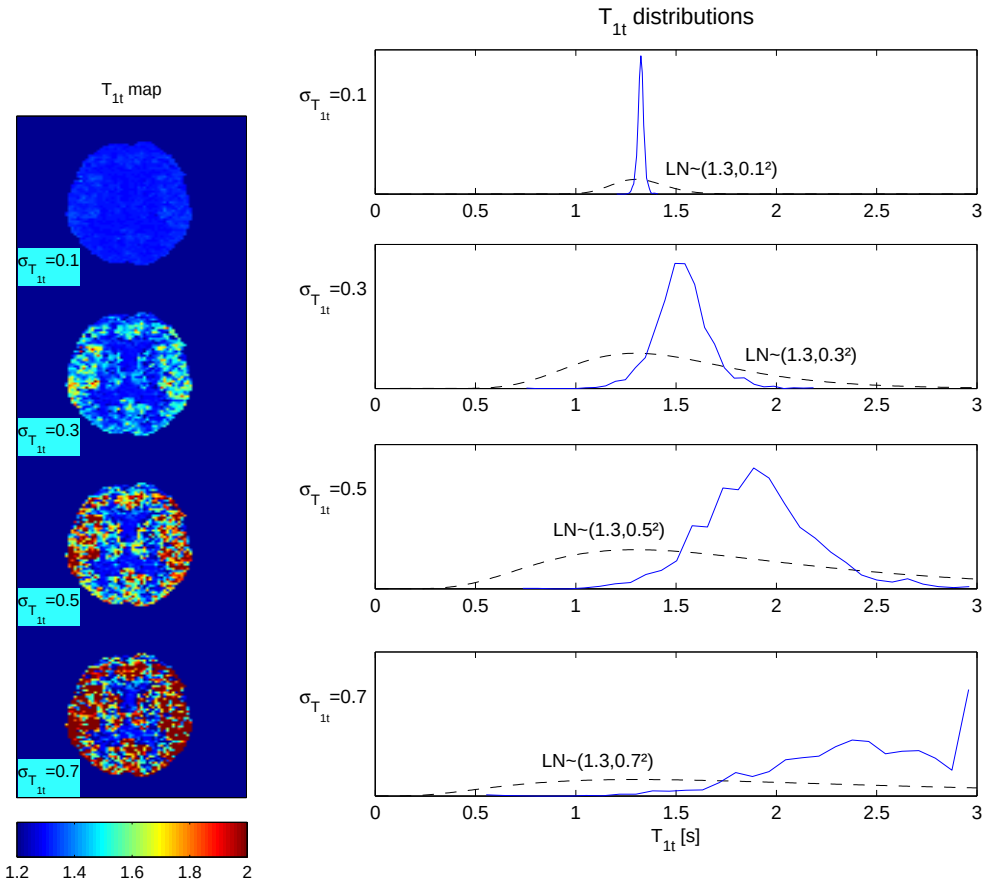

Figure 5.1: (left) T_{1t} estimate maps resulting from the adoption of a progressively increasing prior standard deviation (single slice of an examined subject, pCASL data with vascular crushing was used.). Distributions of T_{1t} values, defined on a selected group of voxel, for each prior attemps (right). Distribution were normalizaed by a scaling factor (to make their area under curve equal to 1) to allow a direct comparison with prior distribution that they follow.

Voxels on which distribution of T_{1t} values has been calculated were extracted by thresholding, at a proper level, a map showing the "goodness of fit" (described in B). This was done essentially to ensure that distributions could be considered an authentic representation, not contamined by voxel in which spurious fit was occoured. It is quite important not include such voxels, since the choice of the appropriate prior for T_{1t} was done by direct inspection of those distributions. Fit score map (see figure 5.2) was thresholded at 20-th percentile, so the 20% "best-fit" voxels entered in the distribution.

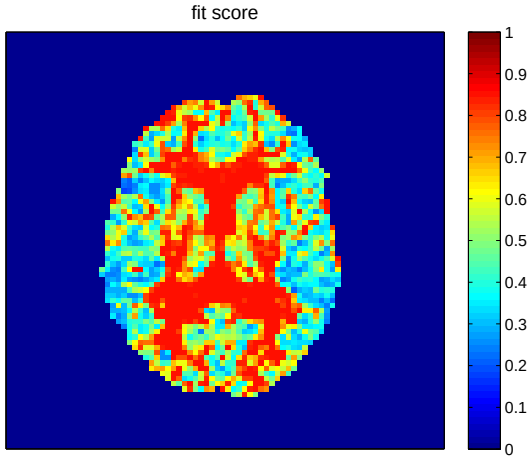

Figure 5.2: example of fit score map in a single slice. After thresholding only voxel with score values lower than threshold estabilished was manteined. Roughly, they come from GM areas where the fitting of ASL model is largely known to work well.

From visual inspection of T_{1t} distributions, like those reported in figure (5.1), lognormal standard deviation prior was set to $0.3s$. This value provides a good agreement between observed distribution variability and prior standard deviation that generate it. At sd=0.1 distribution values were densely located across prior mode, suggesting their estimation was subsatntially driven only by prior term. Over sd=$0.3s$ level, distribution of T_{1t} estimates smeared towards right reaching higher values, whose exceeded any physiological plausible range, till hit, for some voxels, the upper-bound imposed by nonlinear alghorithm used for estimation (set to $3s$).

The improvment carried by bayesian approach in T_{1t} estimates is clearly shown in figure (5.3), where a comparison with performance on T_{1t} estimates of WNLLS approach is reported.

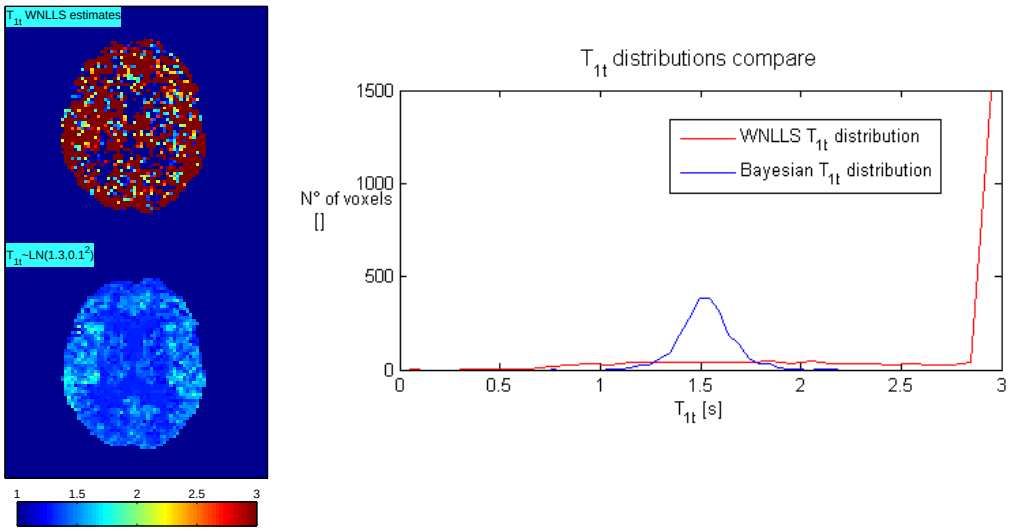

Figure 5.3: T_{1t}estimate maps using WNLLS estimator (on top, left) and bayesian MAP estimator (on bottom, left). Distributions arisings the same group of voxels are shown (right). If T_{1t} was freely estimated from data, it was likely to escape from a desired physiological range, making the settings of the nonlinear algorithm used for estimation inappropriate. The pronounced peak visible at $3s$ is the result of these unwanted constrain on T_{1t} values, that showed the tendecy of overshoot it.

When the standard LS approach were adopted for parameters estimation, T_{1t} estimates was hardly outside the expected range, and most of them touched the upper bound before convergence of the iterative algorithm was reached. The upper bound for T_{1t} parameter needed to be increased till $6s$ to avoid to see a heavy effect of this constrain onto final estimtes (data not shown).

In figure (5.4) an example of T_{1t} map resulting from MAP estimator is give, both for no vascular crushing and vacular crushing data. The effects of using a prior on this parameter instead of fixing it to a unique value is clearly visible in the figure. T_{1t} were allowed to vary locally to better fit the data, and maintaining meantime a reasonable value according the hypothesis made by the model on it. Estimated values in data with vascular crushing were more influenced by prior distribution than estimated values in data where no vascular suppersion were accomplished.

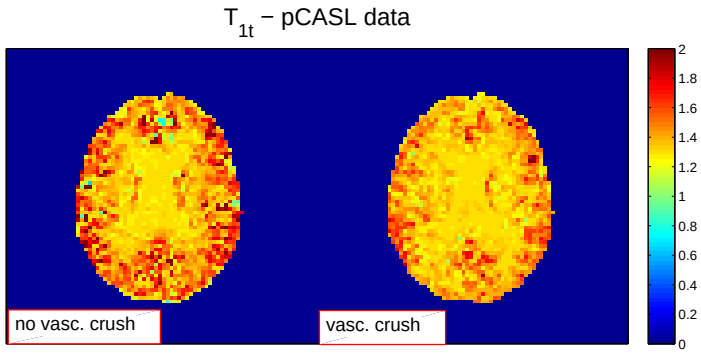

Figure 5.4: T_{1t} parametric map resulting form MAP estimator, for data acquired with (right) and without (left) application of vascular crusher gradients (slice 4 of subject 1 is shown).

5.1.2 Prior on equlibrium arterial blood magnetization

The procedure described in section 4.2.3 to define a prior distribution on M_{0b} has shown to be effective in all subjects. It means that the condition of gaussianity, probed by means of Lilliefors test, was met in all subject, at different levels of thresholding in the map of CSF score used for refined manual CSF ROI. In table (5.1) a resume of the M_{0b} prior distributions extracted form data are reported.

	manual ROI	**final ROI**	**segmented CSF (95%)**
subject 1	1083 (85.3)	1089.7 (74.7)	981.3 (152.9)
subject 2	1163 (130)	1172.5 (137.1)	901.6 (120)
subject 3	960.7(126.1)	965.5 (124.1)	921.9 (253)
subject 4	1062.5 (136.2)	1119.4 (169.3)	1145.7 (189.9)
subject 5	1197.2 (169.6)	1233.6 (180.2)	1386.3 (138.7)
subject 6	1092 (142.2)	1092 (142.2)	1067.2 (185.5)

Table 5.1: first column: mean and standard deviation of M_{0b} values from voxels contained in manually drawn CSF ROI. Second column: mean and standard deviation of M_{0b} values of voxels contained in CSF ROI after iterative thresholding procedure. They represents mean, $\mu_{M_{0b}}$, and standard deviation, $\sigma_{M_{0b}}$, used to describe the normal prior distribution associated to M_{0b}. In third column mean and standard deviation of a CSF probability map, after thresholding at 95% of probability, are reported to allow a comparison.

During the iterative procedure built to extract mean and standard deviation of the M_{0b} normal prior, manually drawn ventricular CSF ROI

could be progressively eaten away with different degree, apiece the quality of the initial manual ROI (that was user-dependent) and the ability of CSF score map to be more or less selective on distinguish CSF voxels from other types of voxels. Also this step might impact differently on the number of iterations necessaries to get a gaussian like distribution, since CSF score map used to correct manual ROI was built using empirical index calculated from the acquired data (see B). Lilliefors non parametric test (which test in a statistic frame if the ditribution of given values come from a gaussian family with unknown mean and variance) was used as automatic tool to decrete at wich level stop the redrawing of CSF manual ROI accomplished by the iterative procedure based on CSF score map evaluation. In the follow, intermediate results of the procedure are shown (just for one subject), whereas in table (5.2) a general report for the whole dataset is given.

	N maual	**N final**	**threshold**	**p value**
subject 1	238	148	5%	0.0849
subject 2	300	58	5%	0.1024
subject 3	385	296	42.5%	0.0513
subject 4	395	77	10%	0.0679
subject 5	362	226	32.5%	0.0575
subject 6	192	192	100%	0.4382

Table 5.2: different levels of thresholding were generally asked by each subject to get a p value greater then 0.05.

From table (5.2), it can be seen that a consistent number of voxel contribuited to the prior definition for all subject. The iterative procedure, fully describe above, although accountable of slight modfications on mean and standard deviation of initial manual CSF ROI, was able to filter initial ROI so that the assumption of a normal prior on M_{0b} could be checked in the data.

The prior information associated to M_{0b} was charcaterized by a thin distribution variance, as results MAP estimation of this parameter allowed just light displacements form the initial value given (data not shown).

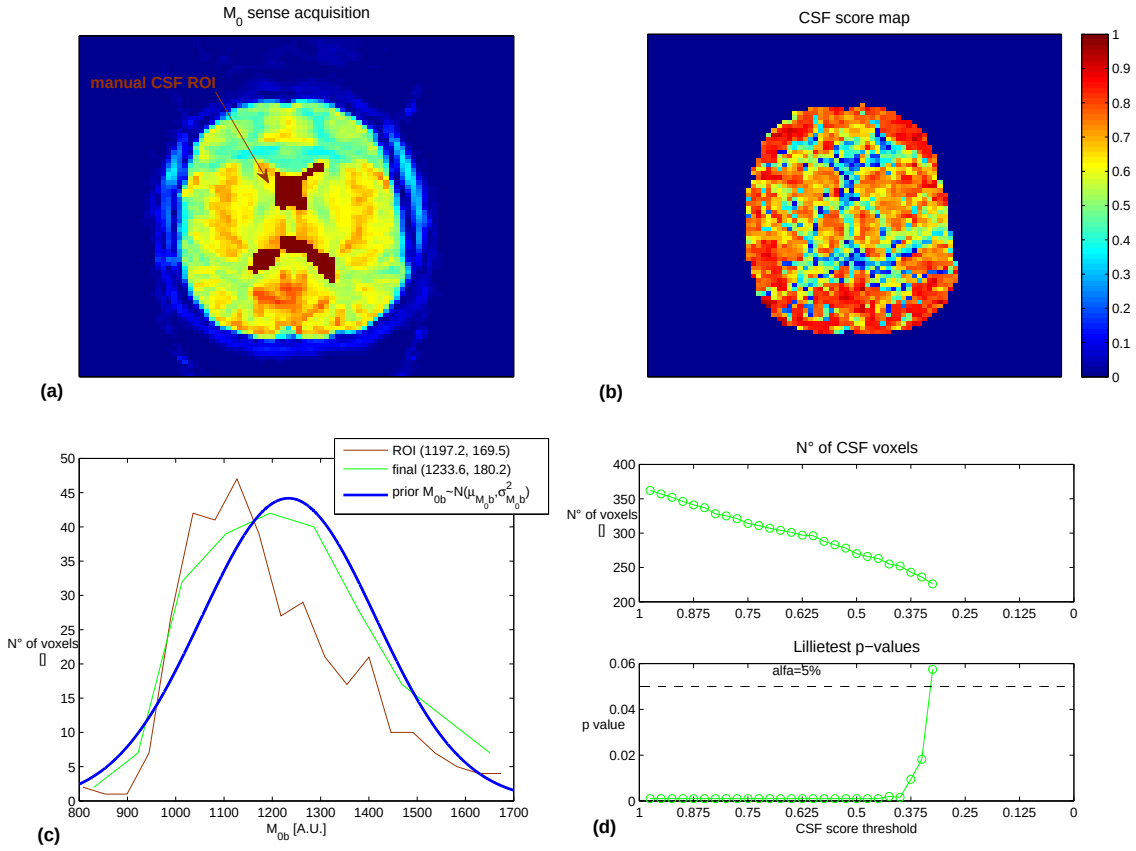

Figure 5.5: (at right) (at left). panel(a): example of a CSF manually selected ROI form a M_0 sensitive image slice. A CSF-ROI can be safty drawn in the lateral ventricles. These are brain structures containing CSF, that can be easily recognized in M_0 acquisitions. Panel (b): CSF score map of the slice shown in panel (a), the less is the score value the more the voxel is considered as a CSF sample. Untill the condition of gaussianity (verifyed by means of statistical test) was not met, CSF ROI starting from the manual drawn one was depurated of those voxel excluded by the thresholding procedure of CSF score map. At each iteration the threshold was made more selective: a total of 40 step, spanning equally a range of all the possible values for CSF score, was provided. The threshold was defined as percentile of the distribution of CSF score value, and decreased by 2.5% at each iteration. Panel (c): final output of the iterative CSF ROI reduction are plotted. In green it is shown the first CSF ROI that satisfy gaussianity test. Mean and standard deviation of this ROI was used as prior for M_{0b} in Standard model, drawn in blue. Panel (d): p-value pattern of Lillietest along iterations is shown (bottom). Untill it did not reach the value $p = 0.05$, the null hypothesis (the distribution is normal) was rejected, and the thresholding procedure continued to erode voxel form CSF ROI. (top) Course of the number of voxel accounted in distribution to be tested at each iteration.

5.2 Standard model

In this section the results of standard ASL model identification with the new estimator setting developped are shown.

5.2.1 Comparing CBF estimates

In figure (5.6) resumptive results of CBF estimation in the 4 dataset acquired for each subject consiedred , are reported.

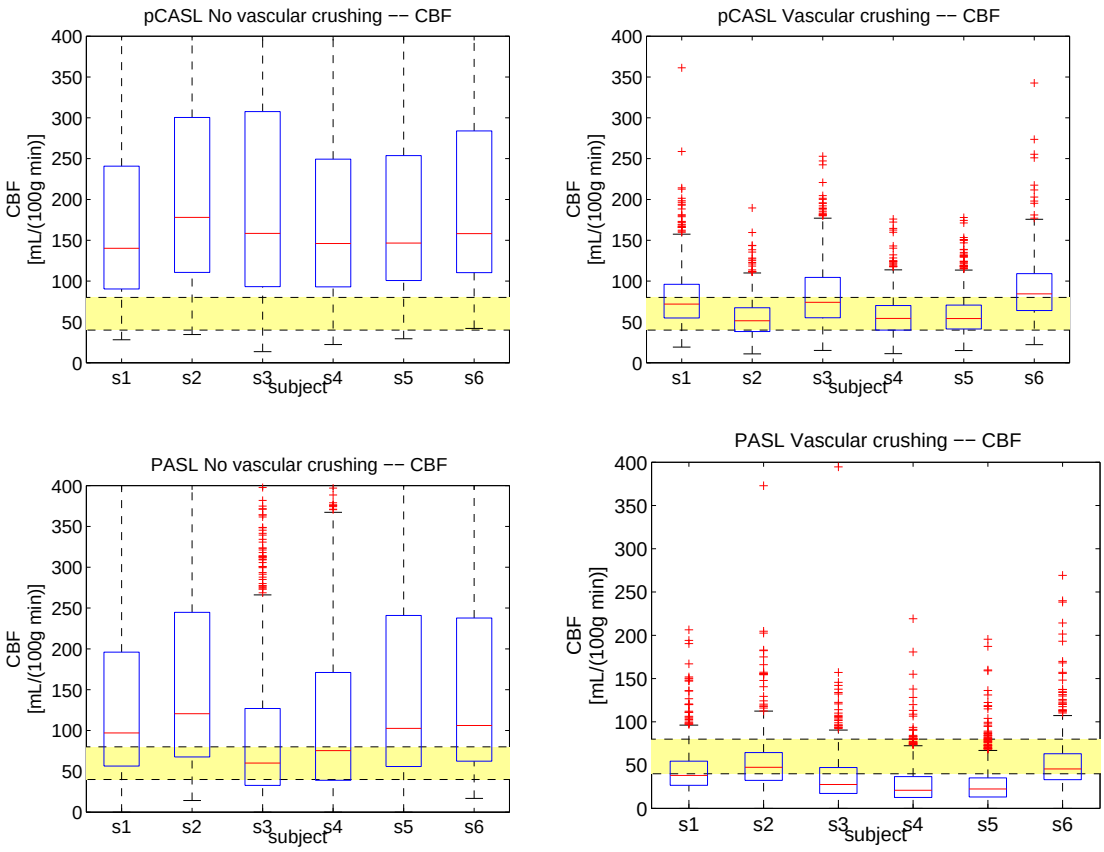

Figure 5.6: boxplots refer to distribution of voxels extracted using a GM mask (calculated using a dedicated software for probabilistic segmentation of tissue) corrected by a fit score map to avoid the contribution of undesired voxels in CBF results comparison. Highlighted yellow band represents the range of CBF values assumed as physiological in literature (in GM tissues).

Standard model clearly showed to overstimate CBF when data were acquired without vascular crushing, both with pCASL and PASL labeling techniques. However, in PASL this behave was less accentuated, and an apppreciable portion of CBF distribution fell inside the accepted

range of values. Thus, standard model seems to be appropriate for CBF estimations when data were acquired in combination with vascular crushing. CBF values, both in PASL and pCASL data, were grately reduced compared with no vascular crushing data. In tables (5.3), a global report on CBF estimate is given.

A comparison between PASL and pCASL CBF estimates were performed on datasets acquired with vascular crushing, i.e. over the kind of datasets in which standard model seems to perform better. In figures (5.7) and (5.8) some examples of CBF maps and correlation anlysis of CBF voxels estimates are shown respectively.

pCASL	**CBF-NVC** $[^{mL}/_{100g\ min}]$	**CBF-VC** $[^{mL}/_{100g\ min}]$
subject 1	188.8 (138)	80.1 (31)
subject 2	207.4 (150)	51.5 (20)
subject 3	213.0 (161)	79.1 (34)
subject 4	175.7 (126)	55.6 (22)
subject 5	189.8 (132)	54.3.6 (21)
subject 6	206.2 (135)	87.4 (32)

PASL	**CBF NVC** $[^{mL}/_{100g\ min}]$	**CBF VC** $[^{mL}/_{100g\ min}]$
subject 1	153.6 (148)	46.9 (54)
subject 2	154.2 (139)	49.0 (46)
subject 3	110.38 (133)	41.1 (76)
subject 4	114.6 (134)	49.85 (117)
subject 5	150.27 (152)	44.1 (101)
subject 6	163.7 (146)	49.4 (44)

Table 5.3: mean and standard deviation of CBF estimate distributions plotted in figure (5.6).

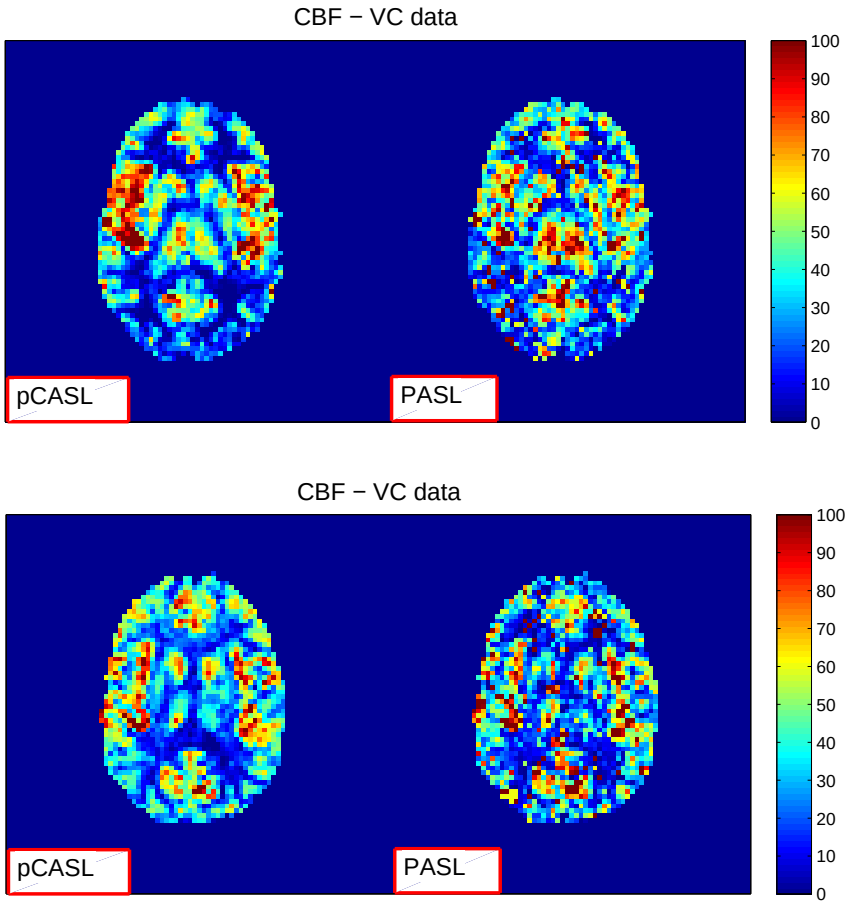

Figure 5.7: maps of CBF estimate in two slice of the same subject (subject 2). As excepted, CBF maps shows a good congruence in both slice. The overall quality of PASL maps is firmly lower than pCASL, reflecting the lower SNR that characterized PASL data, especially when vascular crusher gradients are applied.

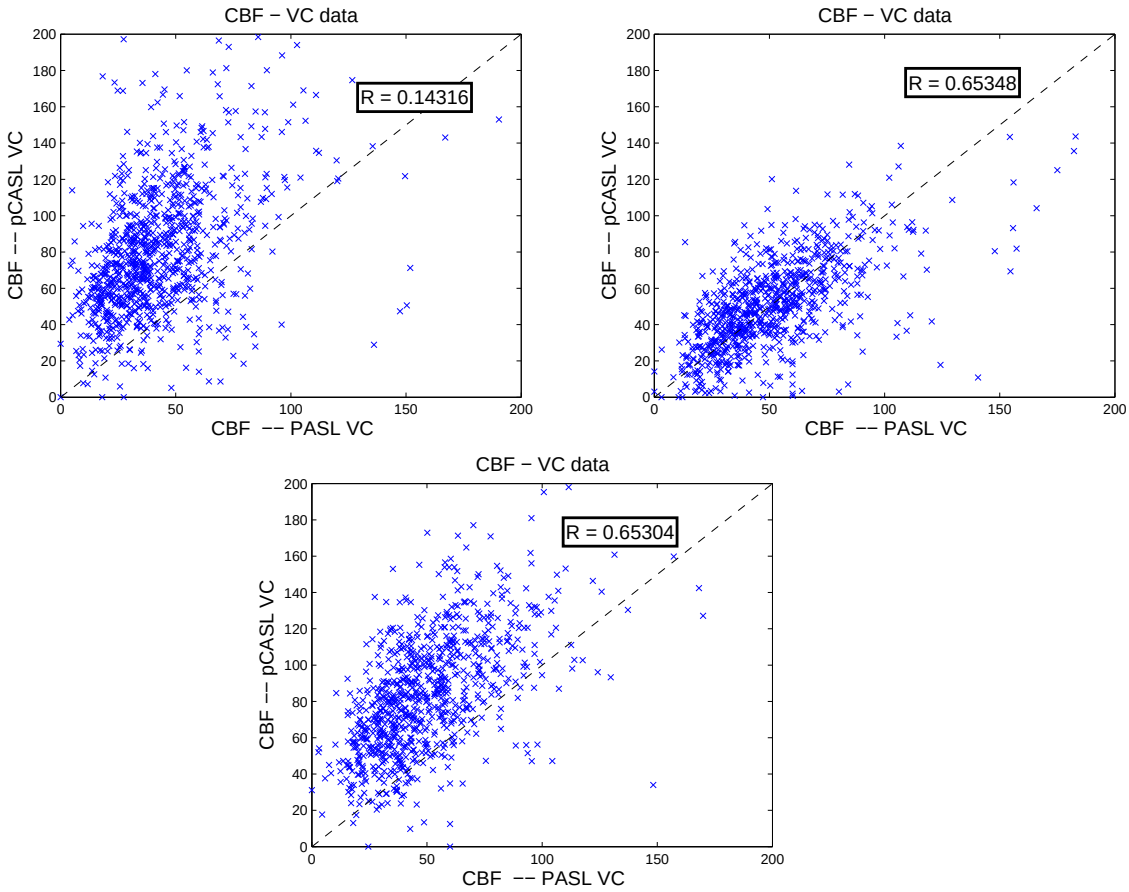

Figure 5.8: correlation of CBF estimates between PASL and pCASL data, with vascular crushing (subject 1, 2 and 6 are shown respectively).

5.2.2 Effects of vascular crushing

The effect of vascular crushing onto acquired signals is evident in figures (5.9) and (5.10) where two samples of voxel difference signals and consequent data fittings are shown (for pCASL and PASL data respectively) .

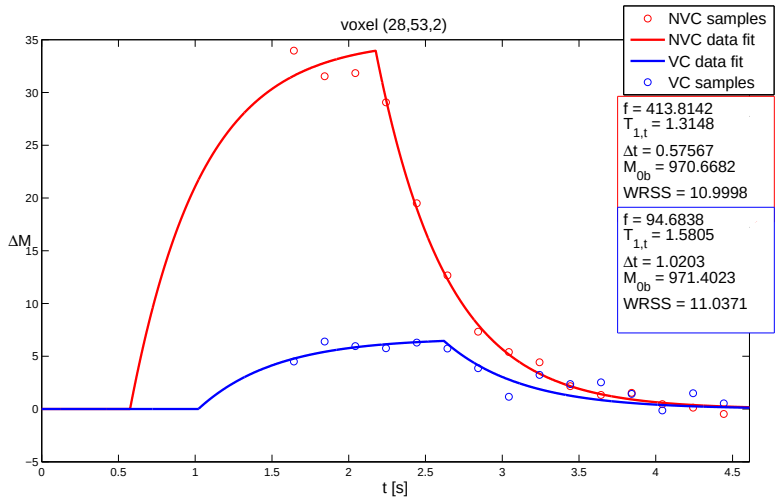

Figure 5.9: measured singal and relative model fit to pCASL without vascular crushing acquisition is drawn in red, measured signal and model fit to pCASL with vascular crushing is plotted in blue. In the associated boxes, results of parameters identification with MAP estimator are shown (units are those reported in table (4.1)).

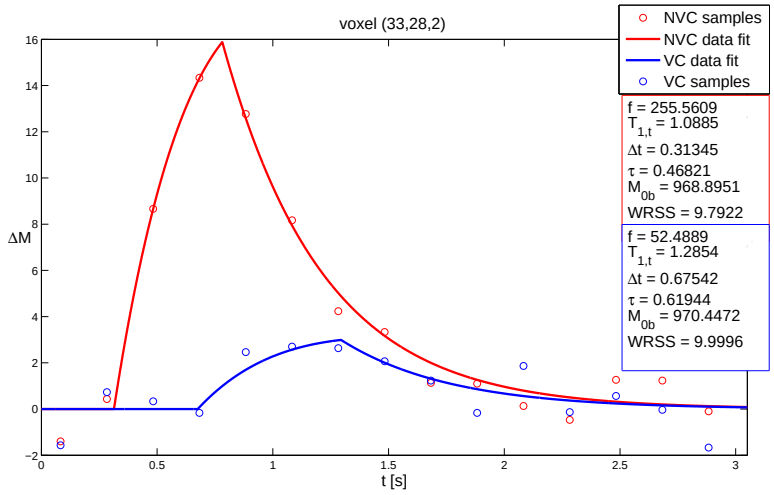

Figure 5.10: measured singal and relative model fit to PASL without vascular crushing application is drawn in red, measured signal and model fit to PASL with vascular crushing is plotted in blue. In the associated boxes, results of parameters identification with MAP estimator are shown (units are those reported in table (4.1)).

Vascular crushing acts in the same manner with PASL and pCASL, essentially modifying the intial part of signal time course when in-

travascular tagged spins give their contribution to the signal. About the end, signal time courses sholud in priciple realign each other since no more fast flowing spin are in the voxel yet.

The modification introduced by vascular crushing in parameter estimates, that locally can already be seen in fit plotted above, are shown in figure (5.11) and (5.12). In these figures, it has been reported CBF and Δt paraemtric maps when vascular crushing is (or is not) used. These two parameters are typically used in ASL to characterized perfusion process, since they provide complemetary informations about the underlying physiology.

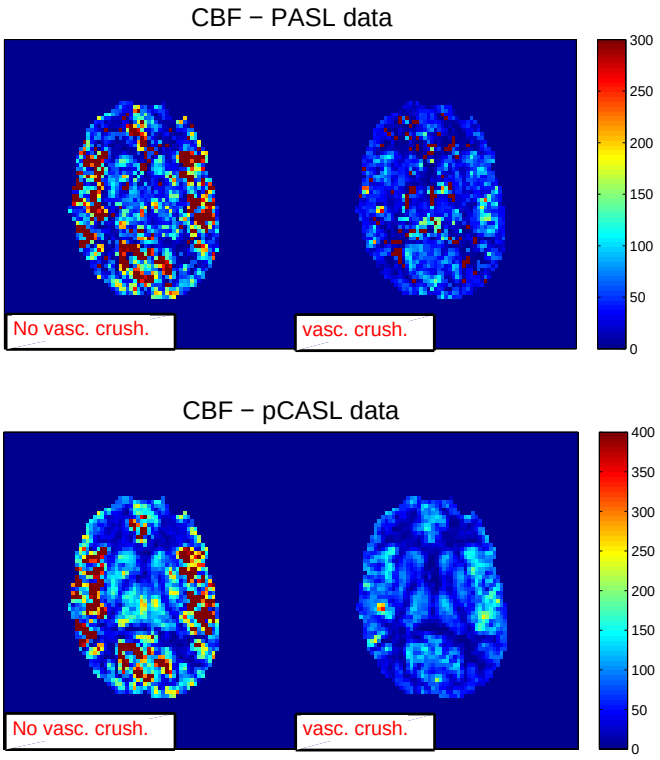

Figure 5.11: CBf maps for PASL (top) and pCASL (bottom) data. As shown above, flow suppression gradients resulted in more physiological CBF values when standard model is used for quantification. Observing CBF maps, more detailed information can be learnt form those relative to pCASL data, reflecting the higher SNR characterizing this technque. This fact must be kept in mind when PASL map, especially with vascular crushing, are analyzed. Slice 2 of subject 6 is shown.

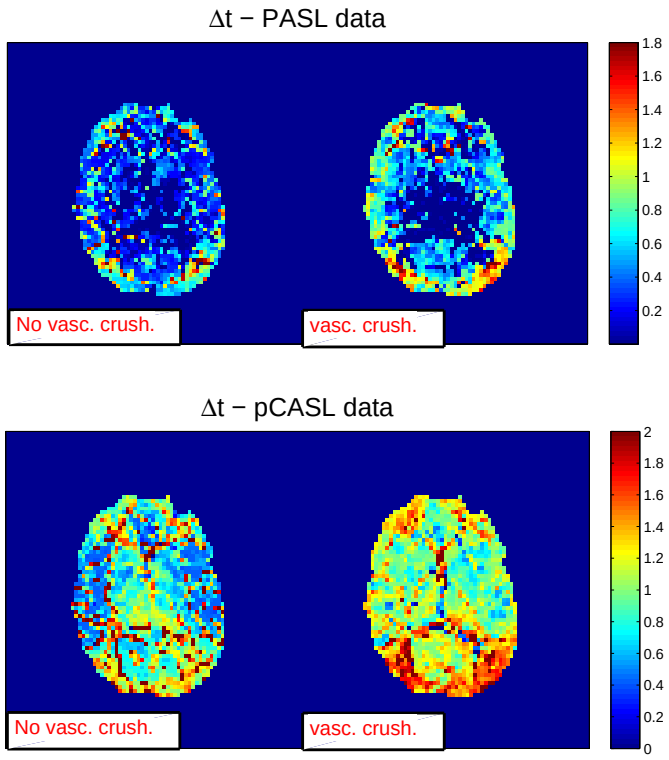

Figure 5.12: Δt maps for PASL (top) and pCASL (bottom) data. An overall Δt increasing is visible form no vascular suppression to vascular suppression data. In particular, pCASL map shows a good agreement with the expected behavior of transit delay pattern accross different brain areas (the longer transit delay of occipital lobe appears in both version of pCASL data).

The bright spot visible in the maps reported in figure (5.11), i.e. groups of voxels with high CBF values, were likely due to the contamination of large arteries in the volume enclosed by the voxel. This suggestion found a good confirmation in Δt maps, where the lowest values were associated right to those voxels supposed to partially including large vessels.

A global representation of the effects due to vascular crushing onto Δt estimation is given in figure (5.13)

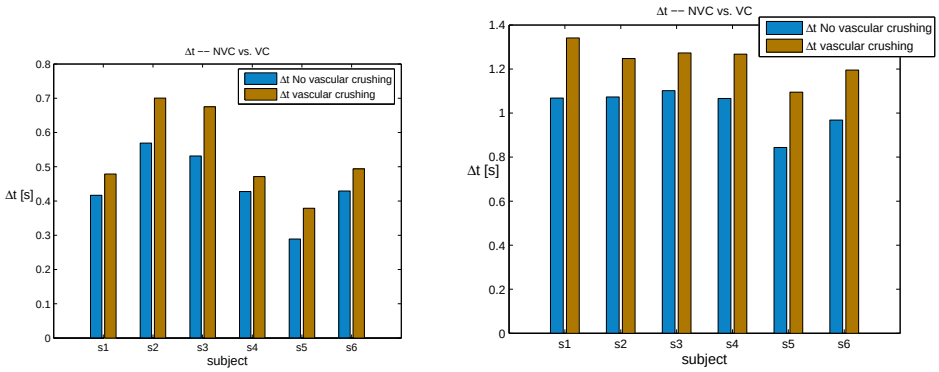

Figure 5.13: global representation of Δt estimated values increasing, that follows the application of flow suppression gradients for PASL dataset (left) and pCASL dataset (right). Columns height are the mean value of Δt estimates of voxels slected by a GM mask (the same used for display CBF estimates in figure 5.6)

5.3 Two component model

In this section a series of preliminary results obtained by the fit of the two component model developped in section 4.2.5 is given. The study of this new model was split up in two subsequent steps in which the ability of the new component to describe arterial contribution and to correct CBF overestimation with no vascular suppression were tested, separately.

5.3.1 Arterial component fitting

The model of arterial component, $\Delta M_a(t)$, were tested in the datset given by the difference between data without vascular crushing and data with vascular crushing, both for PASL model and pCASL model. This difference signal gives the fraction of the measured signal that derives form form tagged blood flowing faster than the cut-off velocity defined by cruher gradients. Thus it can be considered as a good representation of the signal arising form arterial compoent.

In figure (5.14, 5.15) examples of arterial component fit are reported.

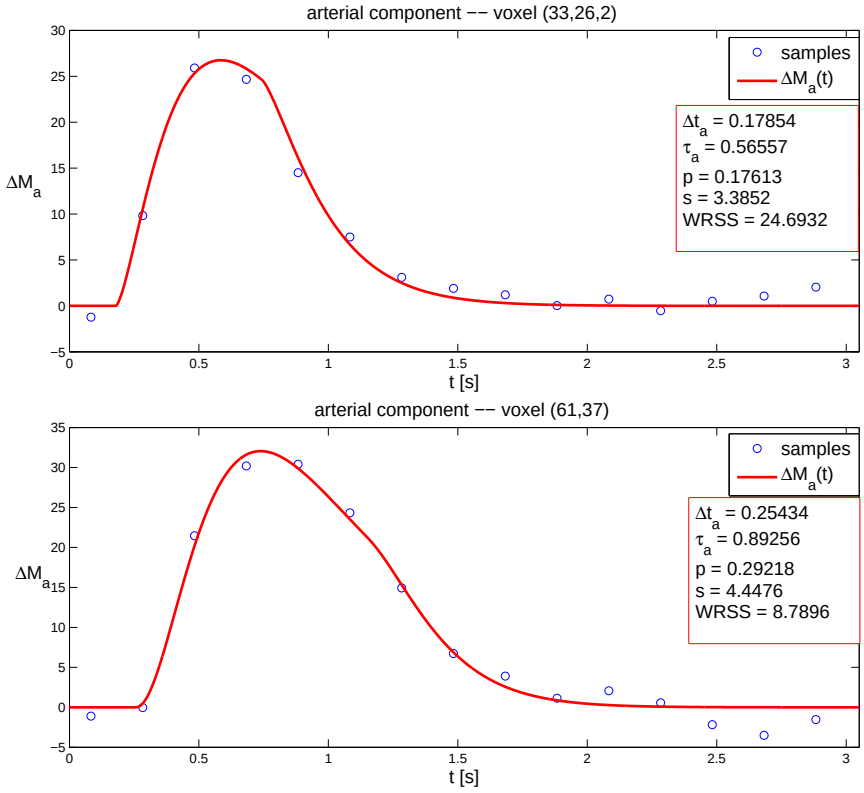

Figure 5.14: example of arterial component model $\Delta M_a(t)$ fit to data difference (uncrushed data minus crushed data) in PASL dataset. Parametrs estimate are reported in the box (units are dined in table 4.3). Data from subject 6.

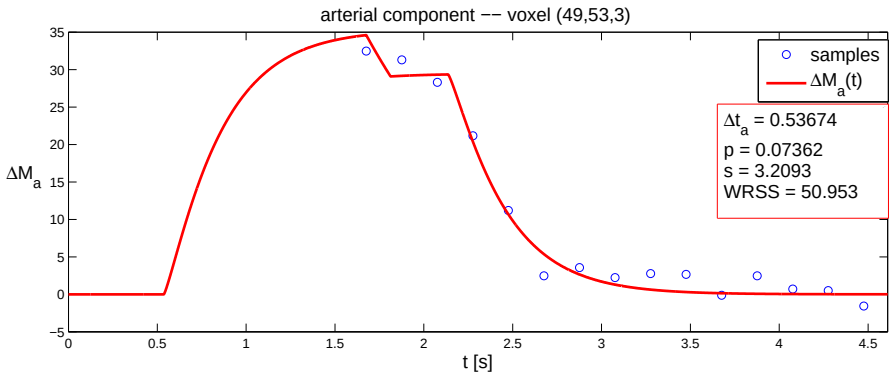

Figure 5.15: example of fitting of arterial component model $\Delta M_a(t)$ to data difference (uncrushed data minus crushed data) in pCASL dataset. Parametr model estimates are reported in the box (units are dined in table 4.3). Data form subject 1.

Parameters contained in arterial model were estimated using a bayesian

approach (MAP estimator). The set of prior knowldge used has been reported in table (4.3). These settings for prior distribution parameters were based on values provided by previuos studies ([4, 18]), with slight modifications according to inital fitting experience that had been made on data. The arterial component was fitted onto the whole volume. This meant that in a large set of voxel where no arterial signal was actually measured, spurious data were fitted by $\Delta M_a(t)$, resulting in a nonsense arterial component. However, the arterial component estimated in this first step was inerted in a two component model only for those voxels, whose signal showed to be strongly affected by flow suppression gradients. These candidate voxels were identificated with the aid of a vascular score map, in which the degree of arteriality of each voxel was measured taking into account some appropriate indexes (see appendix B).

5.3.2 Two component model performance

The two component model for correction of vascular artifacts was fitted to data acquired without vascular crushing, exploiting the results that were obtained in the first step. The estimated arterial component was simply inserted as fixed contribution into the two component model. This procedure was a particulary safe application of two component models, as a great assistance on arterial component identification was given by the availabilty of crushed and uncrushed data both. In figure (5.16) examples of PASL two component model fit are shown. No examples of pCASL two component model are reported because other work is necessary on that model to achieve good data description (see section 6.3 for details).

The effect of two component on CBF estimation form data acquired without vascular crushing can be appreciated globally in figures (5.17, 5.18), where CBF estimate maps in three different conditions are directly compared. They are standard model CBF map form uncrushed data, two component model CBF map and standard model CBF map from crushed data.

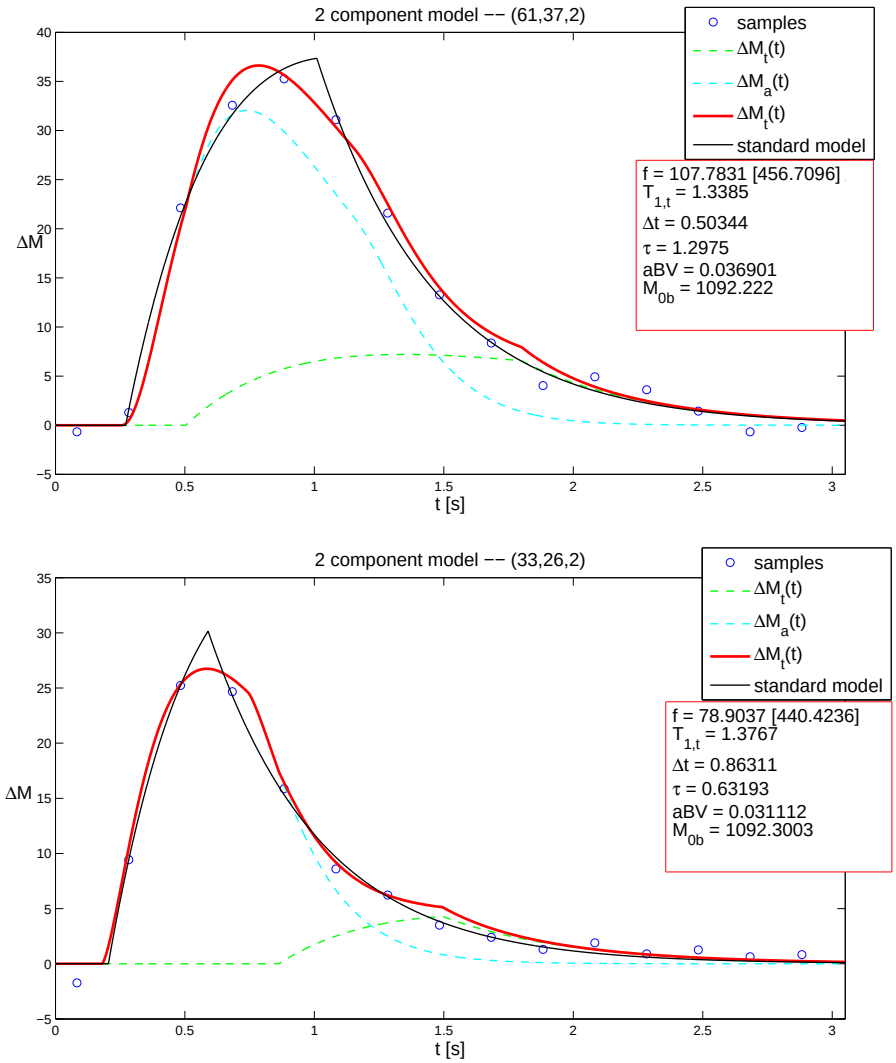

Figure 5.16: two component model fit to PASL data. The arterial component fits data in the intial portion of experimet time, whereas tissue component describe the latter part. This allows a great reduction of CBF estimate compared with single component model (standard model), whose fit is shown in black. Parameters estimate of the tissue component are listed in the box, where in bracket nearby CBF estimate, termed as f, also standard model CBF value is indicated.

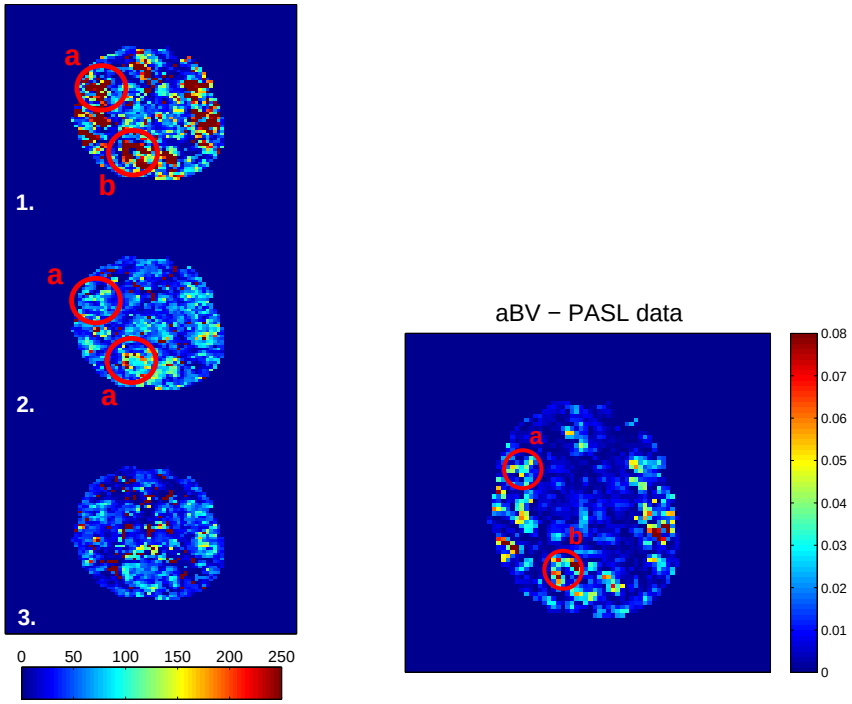

Figure 5.17: PASL data are considered (slice 2, subject 6). aBV [%] map deriving from two component model identification (right), CBF $[\frac{mL}{100g\,min}]$ map in standard model with no vascular crushing (1), in two component model (2), and in standard model with vascular crushing (3) are shown for the same slice. Red circles localize areas where aBV assumes high values, drawn approximatively around the voxels shown in in figure (5.10). In those area standard model substantially overestimates CBF (left panel,1) while two component model is able to correct this artifact due to arterial signal contamination (left panel, 2).

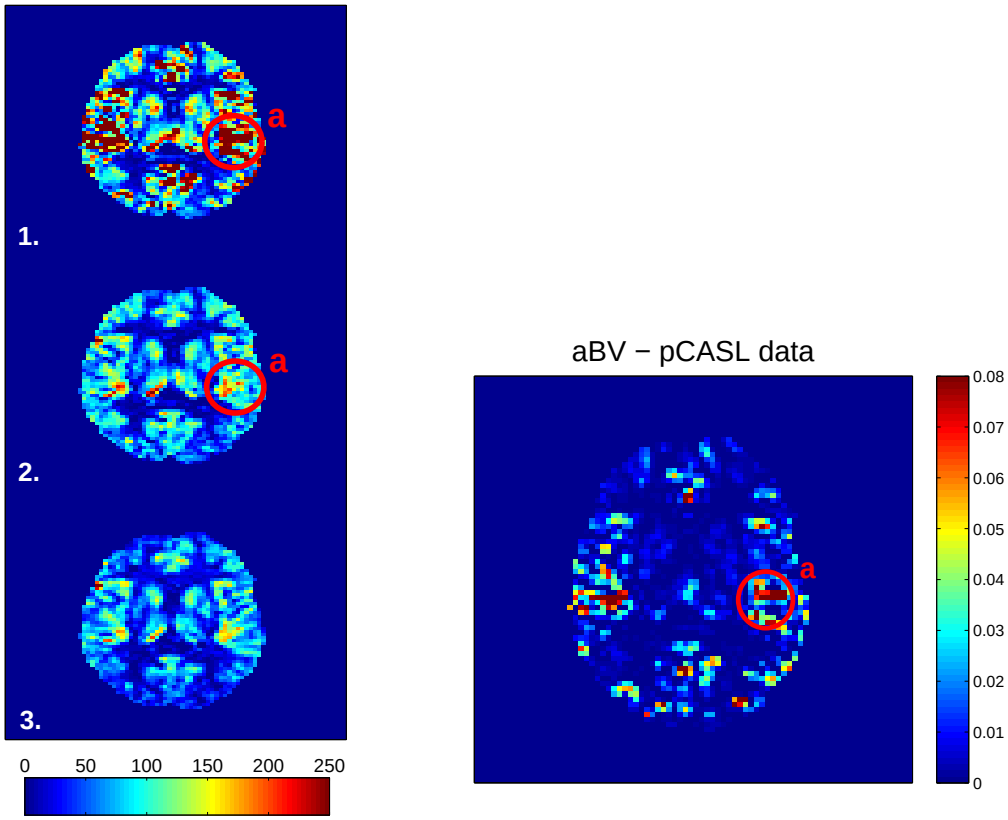

Figure 5.18: effect of two component model in pCASL data (slice 3, subject 1). See figure (5.17) for description.

Chapter 6

Discussion

In this chapter results presented previously are briefly discussed. The rationale of methods developped, limitations encountered, and clues on possible future works are given.

6.1 Bayesian approach on ASL data estimation

Quantification of ASL data through parametric models, among which standard model is the most common, usually relies on a number of fixed parameters that have to be supposed known or accurately measured, besides unknown parameters. This practice is particulary critical for some of them that can not measured with good accuracy or could vary locally from voxel to voxel. Fixing them to unique value is not best modality to proceed in ASL data quantification: this hard assignment can lead to errorrs on perfusion estimates whenever assumed values does not match data evidence.

In this work a bayesian appproach, based on MAP estimation, has been proposed to improve parameters estimation procedure. The key advantage of the bayesian approach is that prior informations about the parameters, based on physiologic knowledge, can be incorporated in estimation procedure. This is important when face with ASL data that have poor SNR since prior knowledge helps to constraint the estimation within a physiological reasonable range, leading to more robust and reliable results. Prior information thus can be used to regularize the problem, especially for time-sensitive parameters estimation.

Here, prior information has been used to better address T_{1t} and M_{0b} roles when standrad model is used in perfusion quantification from

ASL data.

6.1.1 Longitudinal relaxation time

Some methods have been considered in this work to avoid assumption of a unique fixed value on tissue longitudinal relaxation time, T_{1t}.

It has been tried to determine T_{1t} by fitting the signal from the control images obtained in the ASL experiment to a Look-Locker saturation recovery curve (see 2.1), but the absence of pre-saturation pulses in the sequence used left a variable amount of transverse magnetization that confounded T_{1t} measurement.

T_{1t} has been estimated also from data by means of WNLLS estimator, but the results has not been sucessful. The problem on doing this is that T_{1t}, being a time costant of an exponential decay, enters in the model as a nonlinear parameters, and thus several samples are required to estimate it. This is not the case of ASL signal curve at all. Standard ASL model frames the exponential decay (in which T_{1t} has the predominant role) in a temporal window usually made of a few noises samples, whose extent is moreover not well defined since it is dependent on Δt (and τ in PASL model) value, considered unknown by the model. Furthermore anatomical measurement, as T_{1t}, is required from a signal sensitized to perfusion, and thus its estimation can miserely fail in voxels showing lower perfusion levels. All these considerations are suppose to be the reasons why T_{1t} estimation with WNLLS was highly variable and so far from physiological expected range (see figure 5.3).

Then, $T_{1,t}$ estimation has been framed into a bayesian appproach to better account all its possible sources of variation, including uncertainities on actual flip angle α_{LL} value. Lognormal shape prior has been choose as prior distribution to hear tendecy shown by T_{1t} estimates to form toward high values. The resulting maps (5.4) showed that a certain degree of variability was allowed to T_{1t} without get out a reasonable range. It must keep in mind that standard model makes strong assumption on the role of T_{1t} in data description, so when model is not a good representation of system generating data, T_{1t} is likely to assumes values different form those expected. From visual inspetction of maps (5.4), it can be seen how higher T_{1t} estimates were reached right in those voxels where hyperperfusion occoured (contamined by intravascular signal), i.e. voxels where standard model was no more appropriate. Moreover it can be seen and how those values was reduced in the map estimated from crushed data where standard model

had shown to provide good results.

Prior on T_{1t} has been designed reffering to GM voxels data fitting, and modification of its mean, at least, shoud be introduced to try to properly describe also WM signal.

Procedure built for prior selection was based essentially on an empiric definition of prior variance, chosen so that a good agreement between variability of estimate distribution and prior variance was met. A more robust method for prior variance definition should be taken into account in future works. Finally, in this work T_{1t} prior distribution was calibrated on a single subject and then used for all data sets. Althought slight modification would be introduced, a better approach would require to calibrate T_{1t} prior distribution individually in each subject.

6.1.2 Equilibrium magnetizaion of arterial blood

Prior on M_{0b} is introduced to face with all the difficoulties involved in its measurement. A proved method based on CSF equilibrium magnetization value has been used to define the mean of a prior distribution for M_{0b}, instead of its unique global value. This has been done essentially to take into account the variability introduced into M_{0b} value by the indirect methods use to extract it form data. Particulary care has been imparted to these parameter as it represents the most direct scaling factor for CBF estimates in ASL.

The standard deviation assigned to M_{0b} priors was particulary small, and this is the reason why final M_{0b}estimates do not stand aside appreciably from the prior mean. The method proposed allowed the validation of a data-driven normal prior on $M_{0b}$by means of a statistical test.

Regarding implementation of method, CSF score map used for iterative thresholding, as described in section 4.2.3, was calculated form data. This means that, as a matter of principles, different priors (4.11) might be obtained for PASL and pCASL data (being different the thresholds used in the procedure), althought hypothetic M_{0b} value should be unique for subject, no matter if it is used for scale PASL or pCASL data. Therefore, the larger distribution (between PASL and pCASL) that verifyed the test was chosen as unique M_{0b} prior for whole datasets reffered to that subject. However, the strict similarity of PASL and pCASL distribution obtained is a further assurance on the reliability of the method used for M_{0b} prior design.

In table (5.1), the mean and standard deviation of the prior distribution (which derives from a intial manually selected CSF ROI) can be

compared to those deriving form a distribution of voxels extracted using a probabilistic segmentation (threshold $t_{CSF} \geq 0.95$). The apparent discrepancies between the two methods originates from the fact that CSF ROI used as initial step for M_{0b} prior definition was drawn only around ventricular CSF voxel, which showed higher values.

6.2 Standard model

Standard model estimation procedure has been redefined by adopting a bayesian approach. This new settings for standard model quantification been applied to data sets available (PASL-VC, PASL-NVC, pCASL-VC, pCASL-NVC). The bayesian approach used has allowed to improve the model fitting to data. Considering parameters estimates, standard model has shown a markedly trend of overestimate CBF when NVC data are considered, both in PASL and pCASL. The causes must be identifyied in th oversemplified description of the local tissue made by standard model. GM brain tissue is far to be a single compartement with respect to water exchanges: istantaneous and complete mixing between blood water and tissue water has been shown to not occour at all [14]. The voxel is characterized by a vascular tree that blood has to travel down before reaching capillary bed, where water exchange actually occur. The single well-mixed assumption for tissue voxel became even more critical when large arteries are enclosed by the voxel, since a vascular artifact (a non perfusion contribution) is introduced into the measured signal. This effects appear to be more prominent in pCASL labeling technique, where CBF overstimation is greater than PASL labeling technique. It is a consequene of the greater amount of blood labeled in pCASL (5.6).

Standard model CBF estimates has shown a great improvement when data acquired with vascualar crushing were considered. Both in PASL and pCASL, CBF estimates were accetably placed inside the physiological range of CBF values for healthy subjects. Vascular crushing thus permits to reduce discrepancies between the actual physiology reflected by measured signal and the assumptions made by the model. By crushing the signal for high-flowing spins, only contribution from tagged blood in capillary bed (or in proximity to capillary bed) gives rise to a detectable signal. In particular pCASL data has shown to performance very well in combination with vascular crushing application. The higher SNR of pCASL respect to PASL data has allowed to bear with the signal reduction involved by flow suppression gradients, providing

good CBF estimates map. Analysis of CBF estimates with PASL-VC has been hampered by the low SNR of these type of data. To prevent the inclusion of any misleading outcomes in the analysis, only the two lower slice of PASL volume has been considered in the comparisons. Visual inspection of the susbequent maps has suggested to discard results from higher slice.

Also Δt has been estimated from data. This important parameters, used in pathology to complement perfusion informations given by CBF, shown a relevant increase when standard model were fitted to crushed data (5.13). This underlines the different meaning assumed by these parameter, in dependance on the type of data set used. With uncrushed data, Δt reflect the transit delay from labeling creation to entrance into the tissue voxel, while with crushed data Δt gives information about the transit delay from labeling region to a level of voxel vasculature in proximity of capillaries. In pCASL data this parameter was difficult to extract since the initial part of the signal time course were not acquired (the coil was employed for long labeling blood phase), and just few samples could be used to estimated it (see figure 2.9).

Further work is also needed to better evaluate parameter τ in PASL model.

Since the main goal was to evaluate the performance in data fitting and parameters quantification of standard model, any kind of preprocessing analysis was not performed. However it can not be escluded that their application could have an impact on parameter estimated values.

6.3 Two component model

Standard model describes tissue volume as single well-mixed compartment. This quite simple system description is meantime a limitation on model ability to provide good CBF estimates. It has been largely discussed when sCBF estimates from NVC data has been shown. In briefing, the semplicity characterizing standard model makes it sensible to intra vascular tagged blood signal.

Several strategies have been developed to reduce this contamination, such as measurements at later inversion time to allow blood to pass through arterial vessels, or the use of bipolar gradient to suppress the signal form fast moving spins. Both this methods permit to improve the data fitting provided by standard model at the expense of an overall loss of signal, making SNR even more critical. In the first

case signal is reduced by the increased time allow to relaxation of magnetization tag, in the second case signal is reduced because a fraction of tagged molecules are completely crushed.

The correction of vascular artifacts by modeling approach given by (4.25) is potentially more powerful than solutions that demand to sacrify portion of perfusion signal, and in theory, it is applicable with every labeling schemes, previous a proper modeling of arterial component. The main disavantage is that estimating the extra parameters associated with the new arterial component may be detrimental to overall perfusion quantification. In particular, significant contributions from intravascular blood might only be expected in a limited number of voxels, reflecting the limited distribution of large arterial vessels in the brain. In the absence of true arterial signal, this component of the model might fit erroneously the noise or a fraction of the perfusion signal, leading to overfitting and confounding tissue perfusion estiamtion [22].

In this study the problem of best model selection has not been addressed. Effort has been made in this study to extract a plausible model for arterial component, and to show the potential ability of the two component model to eliminate vascular artifacts, restoring CBF values to those obtained from fitting of VC data. The main difficulties reside in detecting the right timing and amplitude of artetrial component to properly correct the tissue component data fitting.

Arterial component model has been derived in this study using the same strategy for PASL and pCASL data. Starting from the ideal profile of labeled bolus transit into an artery, destructives effects introduced by acquisition scheme, dispersion and magnetical property of the labeling has been modeled by means of apprpriate function of time. In particular, dispersion of labeled blood has been taking into account using a gamma shape kernel, since a previous study ([18]) indicated it as the best model for dispersion occouring in large arteries. Several assumption has been made on function descrbing LL readout effects on arterial component model. First of all, the dependance of this function from dispersion effects was nelgected. Then, the additional parameter required, δt_{min}, was fixed arbitrarly, since it could not be extracted from the data available in this study. This assumption impacted in different way on PASL and pCASL models.

Since in PASL all the infowing blood is labeled at the same time, semplifications described above resulted only in a biased scaling factor for the arterial component, but no alterations on its shape were intro-

duced. This different amplitude, were inglobed in the aBV estimated values that accounted the scaling factor lacking in $R(t)$ expression. PASL model has been applied to data, following the two step strategy described in section 4.2.5, providing hopefuls results both in data fitting and in CBF estimates correction.

In pCASL, labeling of blood is performed on time. This implies that the labeled blood bolus does not experience LL readout pulses in the same manner, but only the final part of the bouls is affected. A precise evaluation of the number of RF pulses experienced by labeld blood in time requires knowledge of trasnsit time form labeling region to imaging region, i.e. parameters δt_{min}. Taking an approximated value for δt_{min} could be very detrimental since the portion of model sensitive to δt_{min}, is just the portion sampled by acquisition scheme. Thus, a complex model requires to be fitted to a set of samples that spans the time course just partially, moreover in a temporal window where there is a strong dependence from an unknwon parameter. Finally, to keep analytical expression also for pCASL model, effect of dipersion on $R(t)$ has been discarded, resulting in a sharp transition of the modeled profile. All this considerations suggest that improvments on pCASL arterial component model are recommended.

It could be noted that a very complex arterial component model has been used in combination with a relatively basic tissue component model (standard model). The rationale of method was to correct standard model CBF estimates by adding a new component, so effort has been made on the arterial side of the model, leaving tissue component invariate. However, parameters describing dispersion could be measure more easily in large arteries than tissue, using for example ASL based angiography techniques.

Conclusion

The main goal of this work was the estimation of cerebral blood flow (CBF) from ASL data. STAR and pseudo-continuous labeling were involved in this study, as representative of the two most used approaches for ASL experiments to measure perfusion: Pulsed ASL and Continuous ASL.

Standard model, commonly known also as Buxton model [3], was adopted to describe acquired data. This model was deeply analyzed, recalling theoretical fundamentals and analytical expression derivation, and modified to accounting for the special readout used in which a Look-Locker sampling strategy was implemented.

A bayesian framework, making use of maximum a posteriori (MAP) estimator, was developped for data quantification. This alternative approach given to estimation procedure allowed a-priori knowledge to be used on some of those parameters usually treated as fixed contribution, with the aim of estimating them from data too. This approach conferred to the model more flexibility, resulting in a global improved fit.

MAP estimator was forumlated as a optimization problem, and a formalization of the procedure was given for normal and lognormal prior distributions.

Two examples of data-driven method to derive prior distribution on tissue relaxation time and blood equilibrium magnetization were shown. Improvment on those precedures should be applied in future to confer them larger robustness.

Extracting relevant consideration from results analysis required to face with the intrinsically low SNR of ASL data and with the considerable amount of data available for each subject (acquisition with vascular crushing modality was accomplished). Assistance on this work was provided by a set of MatLab routines implemented to classify results of voxel wise model fitting on the basis of appropriate indexes.

Further effort was accomplished to adapt standard model and its estimation settings into a two component model, where also the signal

of intravascular tagged blood was explicitley modelled. Mathematical formulation of the new arterial component, assumptions made and limitations encountered in the data set available was explicitely discussed. Exploiting data acquired with and without flow suppression gradients, arterial component model was fitted separately from tissue component to probe the effectivness of the two component model to reduce CBF overestimations resulting from standard model identfication onto ASL data without vascular crushing. The correct addressing of arterial component timing and amplitude was found to be fundamental for macro-vascular artifacts reduction. This last part has to be intended as a preliminary study that aim to propose two component model as a valid tool in CBF estimation with ASL data.

Appendix A

Data weights

ASL data quantifaction needs several experiment repetitions to improve SNR by means of signal averaging. Exploiting this great amount of acquisition, data weights to be used in parameters estimation procedure can be extracted. Defining $l_k^{(i)}$ and $c_k^{(i)}$ as the sample acquired at time t_k in the experiment repetition i for label and control state respectively, two types of weight model can be considered. In this work they has been termed as:

- mean of differences model
- difference of means model

First of all, it could be advantageous formalizing how voxel signal difference $\underline{\Delta}$ is obtained from the multiple experiment repetitions. Perfusion weighted signal at sampling time k is calculated as:

$$\Delta(t_k) = \Delta_k = \frac{1}{N}\sum_{i=1}^{N} l_k^{(i)} - \frac{1}{N}\sum_{i=1}^{N} c_k^{(i)} = L_k - C_k \tag{A.1}$$

$$= \frac{1}{N}\sum_{i=1}^{N} l_k^{(i)} - c_k^{(i)} = \frac{1}{N}\sum_{i}^{N} \delta_k^{(i)} \tag{A.2}$$

where L_k and C_k represent average along N repetition of label and control signals at sampling time t_k, and $\delta_k^{(i)}$ indicates pairwise subtraction of labeled and control signals from repetition i at time t_k ($i = 1,\ldots,N$ and $k = 1,\ldots,N_{LL}$). Obiouvsly, (A.1) and (A.2) provide the same values Δ_k (the observed data). However the different modeling of signal diffeence leads to a double evaluation of data weights.

A.1 Mean of differences model

Weights w_k are directly obtained by taking the inverse of the standard deviation, σ_k, of $\delta_k^{(i)}$ along all the $i = 1, \ldots, N$ repetition of the experiment:

$$\begin{aligned} w_k &= \frac{1}{\sqrt{var[\underline{\delta_k^{(i)}}]}} \\ &= \frac{1}{\sqrt{\frac{1}{N}\sum_{i=1}^{N}\left(\Delta_k - \delta_k^{(i)}\right)^2}} \\ &= \frac{1}{\sigma_{\delta_k}^2} \end{aligned}$$

A.2 Difference of means model

Weight w_k are obtained by applying variance propagation law to equation (A.1), as follows:

$$\begin{aligned} w_k &= \frac{1}{\sqrt{var\left[\underline{l_k^{(i)}}\right] + var\left[\underline{c_k^{(i)}}\right]}} \\ &= \frac{1}{\sqrt{\frac{1}{N}\sum_{i=1}^{N}\left(L_k - l_k^{(i)}\right)^2 + \frac{1}{N}\sum_{i=1}^{N}\left(C_k - c_k^{(i)}\right)^2}} \\ &= \frac{1}{\sqrt{\sigma_{l_k}^2 + \sigma_{c_k}^2}} \end{aligned}$$

Appendix B

Maps of score

To facilitate the analysis of the result, a procedure to rate voxelwise performance on the basis of some indexes has been built. This derived form a general idea of considering a weighted sum of penalities, and then has been modified to produce quantitative maps of:

- goodness of fit
- degree of CSF inclusion
- degree of arteriality

The each voxel in the volume an index of score R given by a weighted sum of penalities P_i was associated:

$$R = \frac{\sum_{i=1}^{M} w_i P_i(p_i)}{\sum_{i=1}^{M} w_i}$$

Each penality quantified the distance of voxel performance from an ideal condition, respect to a precise metric. For example, considering the goodness of fit case one of the metrics included in index R computation was the WRSS (weighted residuals sum of square), and the associated penality quantified how far was WRSS in the voxel from the ideal condition of WRSS = 0. Since metrics of different nature was considered in global indedx R, each penality should map the distance from its ideal condition into a unique domain of values, to make the weighted sum of P_i actually balanced by weights w_i and not by differences of P_i scales. To accomplish this, cumulative distribution functions of some distribution was used to restore all penality values in the range $[0 - 1]$. Figure (B.1) gives an intuitive explanation of this concept.

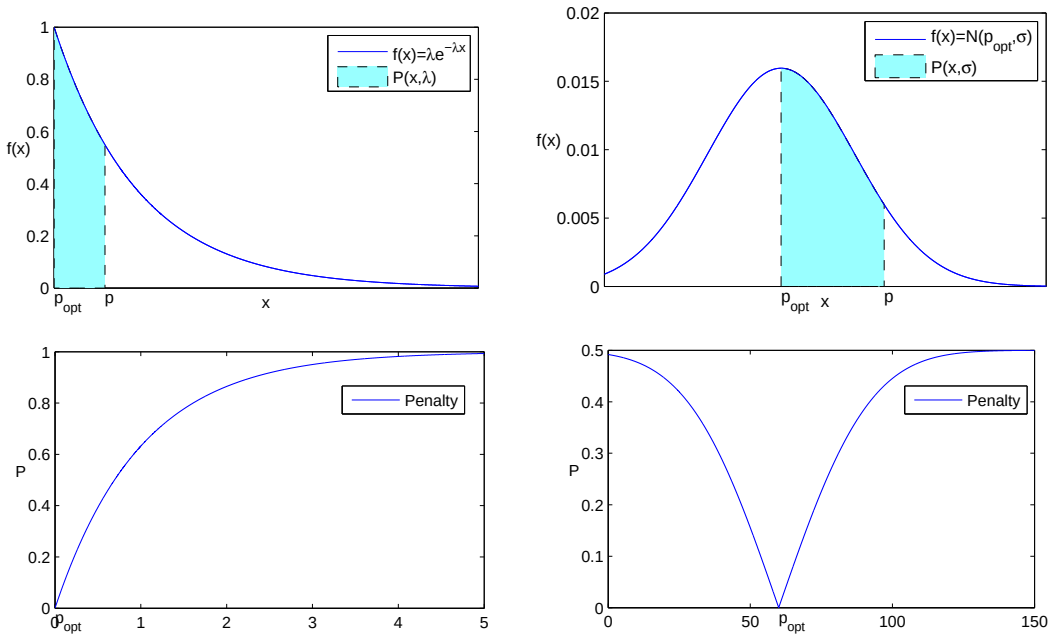

Figure B.1: example of penalities associated to exponential and normal distributions. The distance of voxel performance from an ideal condition regarding a particular metrics ($p_{opt} - p$ along x axis) is mapped into the range $[0 - 1]$ by taking the difference of the cumulative distribution function of p and p_{opt}.

The score R was highly flexible, as in the global computation weight w_i could be changed to enhance or attenuate the contribution of each penality. Moreover each of them could be calibrated varying probability distribution parameters (mean μ, and variance σ^2 for normal distribution, and λ for exponential distribution) to modify the selectivness of the penality function around certain values.

In the follows, applications of this procedure are shown.

Godness of fit

Metrics used:

- product of parametrs CV
- compatibility of parameters estimates with physiological values
- WRSS

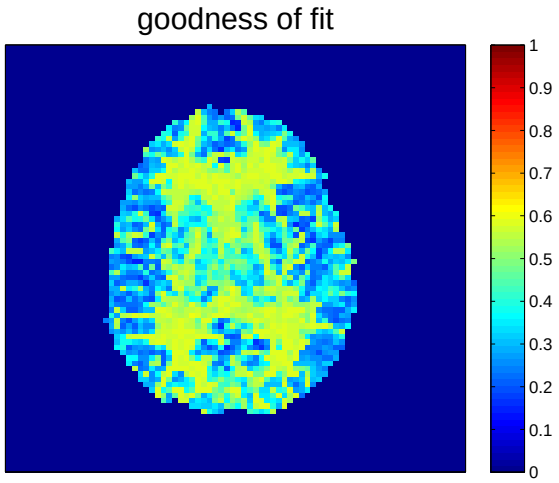

Figure B.2: R map describing the goodness of fit. Since R is defined as a sum of penalities, higher performance is associated to lower R values.

Degree of CSF inclusion Metrics used to probe the degree of CSF inclusion into the voxel was based essentially on empircal evidence of the acquired signal, that usually shows high variability coupled with low amplitude (since no tagged blood can be found in an ideal fully CSF voxel).

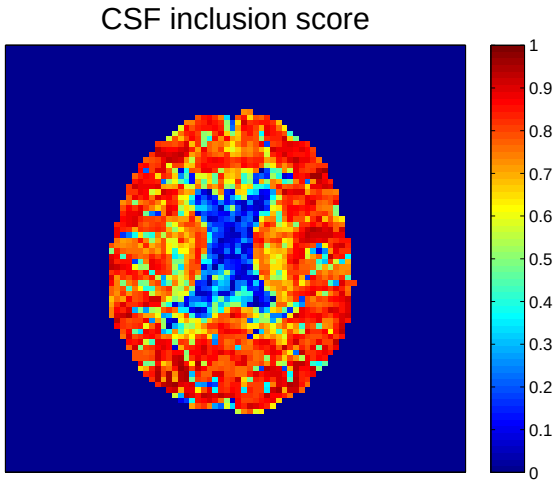

Figure B.3: R map describing the degree of CSf inclusion showed by each voxel. Since R is defined as a sum of penalities, higher performance is associated to lower R values.

Degree of arteriality

Metrics used are:

- numerical integral of signal measured in its initial part (first 5 samples were considered)
- CBF values obtained from standard model estimation
- Δt values obtained from standard model estimation

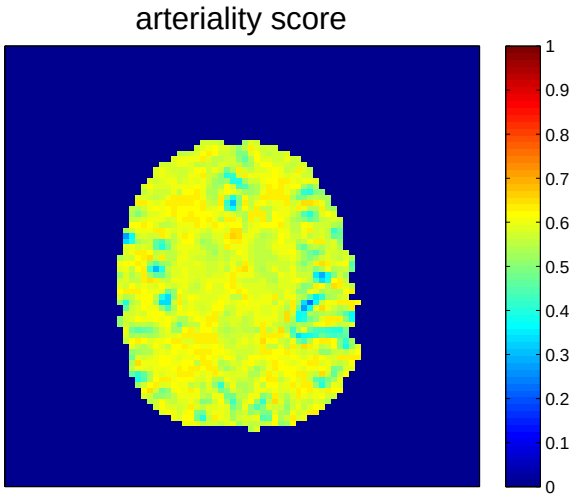

Figure B.4: R map describing degree of arteriality showed by each voxel. Since R is defined as a sum of penalities, higher performance is associated to lower R values.

Bibliography

[1] P. Tofts, *Quantitative MRI of the brain*. John Wiley and Sons, 2003.

[2] R. B. Buxton, "Quanttifying cbf with arterial spin labeling," *Journal of magnetic resonance imaging*, no. 22, pp. 723–726, 2005.

[3] E. C. W. B. S. S. W. R. R. E. Richard B Buxton, Lawrence R Frank, "A general kinetic model for quantitative perfusion imaging with arterial spin labeling," *Magnetic resonance in medicine*, vol. 40, pp. 383–396, 1998.

[4] U. G. S. P. J. Thomas W Okell, Michael A Chappel, "A kinetic model for vessel-encoded dynamic angiography with arterial spin labeling," *Magnetic resonance in medicine*, 2012.

[5] D. R. W. A. C. M. Frank Q Ye, Joseph A Frank, "Noise reduction in 3d perfusion imaging by attenuating the static signal in arterial spin tagging (assist)," *Magnetic resonance in medicine*, vol. 44, pp. 92–100, 2000.

[6] L. R. F. Eric C Wong, Richard B Buxton, "Quantitative imaging of perfusion using a single subtraction (quipss and quipss ii)," *Magnetic resonance in medicine*, vol. 39, pp. 702–7 082 500, 1998.

[7] D. C. A. Weiying Dai, Dairon Garciam Cedric de Bazelaire, "Continuous flow-driven inversion for arterial spin labeling using pulsed radio frequency and gradient fields," *Magnetic resonance in medicine*, vol. 60, pp. 1488–1497, 2008.

[8] F. H. Xavier Golay, Esben T Petersen, "Pulsed arterial spin labeling of arterial regions (pulsar): A rbust regional perfusion technique for high field imaging," *Magnetic resonance in medicine*, vol. 53, pp. 15–21, 2005.

[9] L. R. S. Matthias Gunther, Michael Bock, "Arterial spin labeling in combination with look-locker sampling strategy: inflow turbo-sampling epi-fair (its-fair)," *Magnetic resonance in medicine*, vol. 46, pp. 974–984, 2001.

[10] P. J. J. A. F. D. R. W. A. C. M. Frank Q Ye, Venkata S Mattay, "Correction for vascular artifacts in cerebral blood flow measures by using arterial spin tagging techniques," *Magnetic resonance in medicine*, vol. 37, pp. 226–235, 1997.

[11] X. G. Esben Thade Petersen, Tchoyoson Lim, "Model-free arterial spin labeling quantification approach for perfusion mri," *Magnetic Resonance in Medicine*, no. 55, pp. 219–232, 2006.

[12] P. J. Patricia M Figueiredo, Stuart Clare, "Quantitative perfusion measurements using pulsed arterial spin labelling: effects of large region-of-interest analysis," *Journal of magnetic resonance imaging*, vol. 21, pp. 676–682, 2005.

[13] J. A. D. D C Alsop, "Reduced transit-time sensivity in noninvasive magnetic resonance imaging of human cerebral blood flow," *Journal of cerebral blood flow and metabolism*, vol. 16, pp. 1236–1249, 1996.

[14] P. S. T. Laura M Parkes, "Improved accuracy of human cerebral blood perfusion measurements using arterial spin labeling: accounting for capillary water permeability," *Magnetic resonance in medicine*, vol. 48, pp. 27–41, 2002.

[15] R. B. Buxton, *Introduction to functional magnetic resonance imaging: principles and techniques*. Cambridge UK: Cambridge University press, 2002.

[16] L. M. Parkes, "Quantification of cerebral perfusion using arterial spin labeling: two-compartment models," *Journal of magnetic resonance imaging*, vol. 22, pp. 732–736, 2005.

[17] D. P. L. J Harbe, "Two analytical solutions for model of pulsed arterial spin labeling with randomized blood arrival times," *Journal of magnetic resonance imaging*, vol. 167, pp. 49–55, 2004.

[18] S. K. P. J. S. J. P. Michael A Chappell, Mark M Woolrich and B. J. MacIntosh, "Modeling dispersion in arterial spin labeling: validation using dynamic angiographic measurements," *Magnetic resonance in medicine*, 2012.

[19] K. U. K. U. Mustafa Cavusoglu, Josef Pfeuffer, "Comparison of pulsed arterual spin labeling encoding schemes and absolute perfusion quantification," *Magnetic resonance imaging*, vol. 27, pp. 1039–1045, 2009.

[20] Y. L. T F Coleman, "An interior, trust region approach for nonlinear minimization subject to bounds," *SIAM Journal on Optimization*, vol. 6, pp. 418–445, 1996.

[21] G. T. Claudio Cobelli, David Foster, *Tracer kinetics in biomedical research*. Kluwer academic publisher, 2002.

[22] M. J. D. M. G. P. J. Michael A Chappell, Bradley J MacIntosh and M. M. Woolrich, "Separation if macrovascular signal in multi-ineversion time arterial spin labeling mri," *Magnetic resonance in medicine*, vol. 63, pp. 1357–1365, 2010.

[23] C. C. Ewart Carson, *Modelling methodology for physiology and medicine*. Academic press, 2001.